

**Neutronic Studies for the Development of
A Time Dependent Monte Carlo Code**

By
Argala Srivastava
PHYS01201304017

Bhabha Atomic Research Centre, Mumbai

A thesis submitted to the
Board of Studies in Physical Sciences
In partial fulfillment of requirements
for the Degree of
DOCTOR OF PHILOSOPHY
of
HOMI BHABHA NATIONAL INSTITUTE



DECEMBER, 2019

Homi Bhabha National Institute

Recommendations of the Viva Voce Board

Members of the Viva Voce Board, we certify that we have read the dissertation prepared by **Pratibha Srivastava** entitled "Neutronic Studies for the Development of A Time Dependent Monte Carlo Code" and recommend that it may be accepted as fulfilling the dissertation requirement for the Degree of Doctor of Philosophy.

Dr. P. D. Krishnani

Date: 19-12-2019

Chairman- Dr. P. D. Krishnani

Dr. Umasankari Kannan

Date: 19/12/2019

Guide / Convener- Dr. Umasankari Kannan

Date:

Member 1- Dr. D. Devan

Dr. Amar Sinha

Date: 19/12/2019

Member 2- Dr. Amar Sinha

Date: 19/12/2019

Technical Advisor- Dr. K. P. Singh

K.P.S.

The final approval and acceptance of this dissertation is contingent upon the candidate's submission of the final copies of the dissertation to HBNI.

I hereby certify that I have read this dissertation prepared under my direction and recommend that it may be accepted as fulfilling the dissertation requirement.

Invitee: *Dr. S.B. Deogwaker*

Date:

Place:

Dr. Umasankari Kannan
19/12/2019
Dr. Umasankari Kannan
(Guide)

STATEMENT BY AUTHOR

This dissertation has been submitted in partial fulfillment of requirements for an advanced degree at Homi Bhabha National Institute (HBNI) and is deposited in the Library to be made available to borrowers under rules of the HBNI.

Brief quotations from this dissertation are allowable without special permission, provided that accurate acknowledgement of source is made. Requests for permission for extended quotation from or reproduction of this manuscript in whole or in part may be granted by the Competent Authority of HBNI when in his or her judgment the proposed use of the material is in the interests of scholarship. In all other instances, however, permission must be obtained from the author.

Argala Srivastava
Argala Srivastava

CONTENTS

SYNOPSIS	1	
LIST OF FIGURES	11	
LIST OF TABLES	16	
CHAPTER 1: Review of the Computational Methods used in Reactor Physics	18	
1.1	Neutron Transport Equation	19
1.2	Multi group Formalism of Neutron Transport Equation	21
1.3	Computational Methodology	23
1.4	Multi group Diffusion Equation	25
1.5	Time-dependent Diffusion Equations : Reactor Kinetics	27
1.5.1	Point Kinetics	28
1.5.1.1	Flux factorization & Point kinetics equation	28
1.5.1.2	Point kinetics: Step reactivity	29
1.5.1.3	Point kinetics: One group model	30
1.5.1.4	Point kinetics: prompt jump approximation	31
1.5.1.5	Numerical Methods for solution of point kinetics equations	32
1.5.2	Space time kinetics equations	33
1.5.2.1	Indirect Numerical Methods using Factorization Approach: Adiabatic and Quasi static methods	34
1.5.2.2	Direct Numerical methods	34
1.5.2.2.1	Implicit method	34
1.5.2.2.2	Alternating Direction Implicit and explicit method	35
1.6	Existing Point Kinetics and Space Time Kinetics Code	36
1.7	Limitations of the existing methods for transient analysis	38
CHAPTER 2: Monte Carlo Methods for Reactor Analysis	40	
2.1	Probability density functions	41
2.2	Random number generator	42
2.3	Random Sampling Techniques	43
2.3.1	Inversion Techniques	43
2.3.2	Rejection Technique	44
2.4	Scoring (or tallying)	46
2.4.1	Collision Estimator	47
2.4.2	Absorption Estimator	48
2.4.3	Track Length Estimator	48
2.5	Error estimation	49
2.5.1	Mean, variances and standard deviations	49
2.6	Variance Reduction Techniques	50
2.6.1	Russian Roulette and Splitting Techniques	51
2.7	Monte Carlo Simulation of Neutron Transport Equation	52
2.8	K_{eff} calculations	54
2.9	Monte Carlo Methods for Transient Analysis	55
2.9.1	Different Time Scale of prompt and delayed neutrons	56
2.9.2	Population Control	56
2.9.3	Changes in material properties/ geometry and feedback effects	57
2.10	Review of Existing Transient Monte Carlo methods	57
2.11	New Schemes Proposed and Discussed in the thesis for	58

		MC Space Time Simulations	
	2.11.1	Modeling of precursors	59
	2.11.2	Variance reduction schemes: Mean Secondary Neutrons	61
	2.11.3	Population control	63
	2.11.4	Weight control	63
2.12		Plan of the remaining Chapters of the thesis	66
CHAPTER 3: Implementation of the Simulation Schemes: Point Kinetics Model			66
3.1		Point Kinetics Model	66
3.2		Method of Simulation	67
	3.2.1	Simulation Scheme -1	68
		3.2.1.1 Numerical Results	70
	3.2.2	Simulation Scheme -2	71
		3.2.2.1 Numerical Results	74
3.3		Conclusions	82
CHAPTER 4: Diffusion Theory Monte Carlo: Model Description and Extension			96
4.1		Earlier Work	99
	4.1.1	Probability Distribution Function for Infinite Homogenous Medium	99
	4.1.2	Bare Homogenous Reactor: Method of Images	100
4.2		Further development & Extension of the method of images	101
	4.2.1	Right Circular Cylinder	101
4.3		Extension of AGF Method to Heterogeneous Media	104
	4.3.1	Heterogeneous media with uniform diffusion coefficient	104
		4.3.1.1 Single Region Medium with Fictitious Absorption	105
		4.3.1.2 Two Region Medium with different absorption but same D	108
		4.3.1.3 Two Region Medium with different Diffusion Coefficient	112
4.4		Transport Corrections to Diffusion MC	118
	4.4.1	Transient Flux Close to a Localized Source	118
	4.4.2	Transport in a strongly absorbing medium	120
	4.4.3	Transients Close to a Vacuum Boundary	121
	4.4.4	Transport Effects with Anisotropic Scattering	122
4.5		Conclusions	123
CHAPTER 5: Finite Difference Diffusion Based Space Time Monte Carlo			138
5.1		Finite Difference Kernel	138
5.2		Spatial and Temporal Modeling of Precursors	141
5.3		Numerical Validation	142
	5.3.1	Two dimensional benchmark	142
	5.3.2	Three dimensional benchmark	143
5.4		Conclusions	145
CHAPTER 6: A Diffusion Monte Carlo Based Algorithm for Estimation of Higher Modes of a Reactor			153
6.1		Methodology	156
	6.1.1	Computation of the Fission Matrix	156
	6.1.2	Eigen values and Eigenvectors of the Fission Matrix	157
	6.1.3	Estimation of Error in the Eigen values of the Fission Matrix	159
6.2		Test Problem and Result	162
	6.2.1	A Problem Description	162

6.2.2	Results	162
6.2.2.1	Standard Benchmark (near-critical case)	162
6.2.2.2	Standard Benchmark (deep sub-critical case)	163
6.3	Conclusions	163
CHAPTER 7:	Transport based Space Time Monte Carlo Code KINMC	172
7.1	Methodology	172
7.1.1	The delta tracking algorithm	172
7.1.2	Flow of the Simulation	173
7.2	Test Problem and Results	175
7.2.1	1D Benchmark	175
7.2.2	TWIGL Transient Problem	178
7.3	Conclusions	179
Chapter 8:	Summary and Conclusions	185
Appendix 1		187
References		192

List of Figures

- 1.1 Illustration of the Rejection Technique
- 3.1 Schematic representation of the MC Algorithm based on Simulation Scheme-1
- 3.2 Flow of the program for the Simulation Scheme -1
- 3.3 Variation of prompt neutron weight factor with time for step negative reactivity of -10 mk added at $t=0$.
- 3.4 Variation of prompt neutron weight factor with time for step positive reactivity of +3 mk added at $t=0$.
- 3.5 Variation of neutron power with time for step reactivity of -20 mk, -10 mk and -3 mk
- 3.6 Variation of neutron power with time of +3 mk step reactivity.
- 3.7 Variation of neutron power with time for step reactivity of -20 mk, -10 mk and -3 mk with precursor splitting model
- 3.8 Variation of neutron power with time of +3 mk step reactivity with precursor splitting model
- 3.9 Schematic Representation of the Simulation Scheme 2
- 3.10 Variation of the neutron population (neutron weight factor) with time, for $\rho = -10$ mk The solid curve shows the results obtained using the Point Kinetics code GEAR.
- 3.11 Variation of the neutron power estimated by the MC method (with six groups of delayed neutron precursors) for a step increase in reactivity by +3 mk in a critical reactor.
- 3.12 Change in the precursor concentrations with time in the MC simulation of the problem involving a step reactivity insertion of +3 mk in a critical reactor
- 3.13 A comparison of the variation of the neutron power with time as estimated by a point model MC simulation with GEAR for a ramp reactivity insertion rate of 0.1 mk/sec.
- 3.14 Variation of neutron power with time with and without fuel temperature feedback modeling for a step reactivity insertion of +3 mk
- 3.15 Fuel temperature feedback reactivity as a function of time
- 3.16 Variation in relative power for CHTR core for step reactivity

insertion of +2 mk in 5 sec.

- 4.1 Diagrammatic representation of the source and image point locations and the coordinates used in the estimation of the reduction in extrapolation distance for a bare homogeneous cylindrical reactor by method of images
- 4.2 Variation of the time integrated neutron absorption rate with distance from a point source placed at the origin in single region medium. The blue dots indicate the absorption rate obtained using the real absorption cross section $\Sigma_{ar} = 0.005 \text{ cm}^{-1}$ while the red cross indicate the absorption rate calculated with a fictitious absorption $\Sigma_{af} = 0.01 \text{ cm}^{-1}$ followed by a rejection with a 50% probability.
- 4.3 Variation of the time dependent neutron absorption rate with distance from a point source placed at the origin in single region medium. The various markers indicate the absorption rate obtained using the real absorption cross section $\Sigma_{ar} = 0.005 \text{ cm}^{-1}$ while the solid lines indicate the absorption rate calculated with a fictitious absorption $\Sigma_{af} = 0.01 \text{ cm}^{-1}$ followed by a rejection with a 50% probability.
- 4.4 Variation of the time integrated neutron flux with distance from a point source placed at the origin in a two region medium with same diffusion coefficients but different absorption cross sections viz. $\Sigma_{ar} = 0.005 \text{ cm}^{-1}$ to the left of $x=2$ and $\Sigma_{ar} = 0.01 \text{ cm}^{-1}$ to the right of the plane $x=2$. The red crosses indicate the exact results by Transport MC while the blue stands for diffusion MC.
- 4.5 Variation of the time dependent neutron flux with distance from a point source placed at the origin in a two region medium with same diffusion coefficients but different absorption cross sections viz. $\Sigma_{al} = 0.005 \text{ cm}^{-1}$ to the left of $x=2$ and $\Sigma_{ar} = 0.01 \text{ cm}^{-1}$ to the right of the plane $x=2$. The various markers indicate the flux obtained using the Diffusion MC while the corresponding black markers indicate the flux calculated with Transport MC using the rejection technique.
- 4.6 Variation of time averaged neutron absorption rate with distance

from the point source placed at the origin in two region medium with boundary at $x=2$. $\Sigma_{r1} = 0.01 \text{ cm}^{-1}$ and $D_1=0.1515$ to the left of the boundary while $\Sigma_{r2} = 0.005 \text{ cm}^{-1}$ and $D_2=0.33$ to the right. The figure shows a comparison of the absorption rate obtained with actual mean free path (mfp) and that with 4 times higher mfp. Solid curve corresponds to analytically computed neutron absorption rate.

- 4.7 Variation of time dependent neutron absorption rate with distance from the point source placed at the origin in two region medium with boundary at $x=2$. $\Sigma_{r1} = 0.01 \text{ cm}^{-1}$ and $D_1=0.1515$ to the left of the boundary while $\Sigma_{r2} = 0.005 \text{ cm}^{-1}$ and $D_2=0.33$ to the right. The figure shows a comparison of the absorption rate obtained with actual mean free path (mfp) and that with 4 times higher mfp.
- 4.8 Variation of the time averaged neutron flux with distance from a point source located at the origin in a mildly absorbing medium. The figure compares the results using transport MC and transport corrected diffusion MC.
- 4.9 Variation of the time dependent neutron flux with distance from a point source located at the origin in a mildly absorbing medium. The figure compares the results using transport MC and transport corrected diffusion MC.
- 4.10 Variation of the time averaged neutron flux with distance from a point source located at the origin in a strongly absorbing medium. The figure compares the results using transport MC and transport corrected diffusion MC.
- 4.11 Variation of the neutron flux (time averaged) with distance from the point source in a semi infinite homogeneous medium. The point source is placed at the origin and the medium-vacuum boundary is located at $x=4.5 \text{ cm}$ from the source. The figure shows a comparison of results based on transport and diffusion MC and the analytical fit.
- 4.12 Neutron Flux due to a source in an infinite homogeneous medium with mild absorption and anisotropic scattering - comparison of

results obtained using transport MC and transport corrected diffusion MC.

- 5.1 A schematic representation of the Finite Difference Diffusion MC model
- 5.2 Details of the reactor configuration in the 2D PHWR benchmark
- 5.3 Variation of the normalized thermal flux with distance in the x direction at $y=400$ cm at $t=0$ s in the 2D PHWR benchmark
- 5.4 Variation of the normalized thermal flux with distance in the x direction at $y=400$ cm at $t=2.9$ s in the 2D PHWR benchmark
- 5.5 Variation of relative average power density with time for the 2D PHWR benchmark transient
- 5.6 Vertical Cross Section at $Z=0$ for 3D PHWR benchmark
- 5.7 Vertical cross section of reactor configuration of the 3D PHWR benchmark
- 5.8 Normalized thermal flux distribution in the XY plane at 270 cm, at $t=0.0$ s for 3D PHWR Benchmark
- 5.9 Variation of relative average power density with time for the 3D PHWR benchmark transient
- 6.1 Schematic representation of the Finite Difference Diffusion MC model for estimation of the Fission Matrix
- 6.2 XY representation of PHWR test reactor
- 6.3 Shannon entropy with cycle for 3D PHWR Benchmark
- 6.4 Fundamental λ mode for PHWR Core(critical case) along X direction
- 6.5 Variation of thermal flux in fundamental λ mode obtained by KINMC for PHWR Core (near critical case)
- 6.6 Variation of thermal flux in second λ mode obtained by KINMC for PHWR Core (near critical case)
- 6.7 Variation of thermal flux in sixth λ mode obtained by KINMC for PHWR Core (near critical case)
- 6.8 Variation of thermal flux in fundamental λ mode obtained by KINMC for PHWR Core (deep subcritical case)
- 7.1 Spatial distribution of the fission sites $t=0.0$ s obtained for a critical state for Transport MC Benchmark

- 7.2 A comparison of the neutron power estimated by MC with the Transport Monte Benchmark value. A step reactivity of 2.1 mk is added to the initially critical system at $t = 10$ s and subsequently the system is brought back to the critical state at $t = 40$ s.
- 7.3 Variation of the (6 group) precursor concentrations as a function of time in the Transport MC benchmark
- 7.4 Geometry for the south-east quadrant of TWIGL
- 7.5 Comparison of the Relative Power of TWIGL Transient estimated by KINFMC with Reference Solution (Time Dependent Method of Characteristics)

List of Tables

- 3.1 Kinetics parameters for 6 groups of delayed neutron precursors
- 3.2 Comparative study of the computational time and variance estimated by simulation schemes 1 and 2 for step reactivity insertion on + 3 mk
- 3.3 Delayed neutron and cross section data used as input in the point model benchmarks (Yamoah et. al. 2013)
- 3.4 Comparison of the neutron power ($= N(t)/N(0)$) by point model MC for a -7 mk negative step reactivity insertion in athermal reactor with analytical solutions and GEAR Code.
- 3.5 Comparison of the neutron power ($= N(t)/N(0)$) by point model MC for a -7 mk negative step reactivity insertion in athermal reactor with analytical solutions and GEAR Code.
- 3.6 Feedback parameters for modeling the problem of a +3 mk step reactivity insertion with fuel temperature feedback
- 3.7 Kinetics parameters for 6 groups of delayed neutron precursors for ARCH Transient Analysis

- 4.1 Reduction in extrapolation distance d_{ex} as function of radius of the cylinder (Diffusion Length, $L=6$ cm)
- 5.1 Lattice parameters for the 2D PHWR Benchmark
- 5.2 Kinetic parameters for the 2D PHWR Benchmark
- 5.3 Comparison of the steady state K-eff values estimated by MC as a function of time with KINFIN and with Benchmark results for the 2D PHWR Benchmark
- 5.4 Lattice parameters for the 3D PHWR Benchmark
- 5.5 Kinetic parameters for the 3D PHWR Benchmark
- 5.6 Comparison of the steady state K-eff values estimated by MC as a function of time with KINFIN and with Benchmark results for the 3D PHWR Benchmark
- 5.7 Relative error in the average power density w.r.t Benchmark for Monte Carlo Simulation and KINFIN
- 6.1 Two group nuclear data Cross-section for PHWR test-case
- 6.2 Values of λ in different modes for PHWR Core (near critical case)
- 6.3 Values of λ in different modes for PHWR Core (deep subcritical case)
- 7.1 Kinetics parameters and material cross sections of the Transport MC Benchmark
- 7.2 Cross Sections and kinetics parameters for the TWIGL Transients
- 7.3 Comparison of the steady state K-eff for TWIGL Benchmark
- 7.4 Comparison of relative power as function of time for TWIGL Benchmark

Summary and Conclusions

The current methods for transient analysis, deterministic and hybrid although fast require numerous approximations e.g. homogenization. With few group approximations it is difficult to predict error in the final result and their validity for each specific case must be determined separately, which is especially difficult for new and unique reactor designs. For transient analysis, which is crucial for safety calculations it is desirable to have a higher fidelity method. Therefore Monte Carlo is an interesting option to perform reliable and accurate transient analysis.

MC simulations are quite challenging from the viewpoint of studying time-dependent reactor kinetics. One of the major challenges in such simulations is the handling of different particles of varied time scales. A related problem is controlling the vast difference in the population of neutrons and precursors. Dynamic changing of the material properties and introduction of feedback is also a challenging task. To overcome these challenges, several new techniques have been developed. These include different weights for neutrons and precursors, population and weight control, handling various precursor groups separately, forced decay of precursors without combining them together and use of mean number of secondaries per collision. The use of different weights for neutrons and precursors and the treatment of the different precursor groups explicitly is a novel approach for time dependent MC studies.

Firstly, the proposed new techniques are applied and tested in simpler models such as the Point Kinetics MC Model and the few group diffusion theory MC model as it is easier to test the proposed techniques in these simpler models. Moreover, since most space time kinetics benchmarks are based on few group diffusion equations solved by the finite difference method, the implementation in the diffusion theory MC model facilitates exact comparison with these benchmarks. The diffusion Monte Carlo model was developed earlier in the context of reactor noise simulation. A number of new developments in the theoretical basis of the diffusion Monte Carlo

model have also been carried out by us. Finally the techniques have been implemented in a transport Monte Carlo model and this has led to the development of a multi-region multi-group Monte Carlo kinetics code KINMC.

In this thesis, a new and unique dynamic Monte Carlo Method is developed which extends the possibility of the Monte Carlo Method and which enables the possibility to analyze the transient behavior of a nuclear reactor without any approximation to the geometry or any discretisation. This method can perform transient analysis on milli seconds to minutes durations and can handle changing system properties, feedback effects, delayed neutrons and prompt neutron fluctuations. This method is more accurate than the present state-of-the-art methods based on deterministic methods. This accuracy makes the method very suitable as a validation tool for other computational methods. The methods presented in this thesis are novel. The present research has shown that it is feasible to perform dynamic MC analyses on nuclear systems.

Further work in this direction would be to develop a code capable of continuous energy treatment with detailed tracking (as against the delta algorithm) and anisotropic scattering. Introduction of parallel processing would make it possible to actually carry out MC space-time kinetics calculations for realistic problems and not merely as a benchmarking tool. With these developments, realistic space-time kinetics, using the schemes discussed in the thesis, will become feasible.

SYNOPSIS

Calculation of reactivity, neutron flux, reaction rates and fission power distribution are of pivotal importance in the design of critical and sub-critical reactors. The distribution of neutrons in space, energy and direction is the basic function that governs the behavior of a nuclear reactor. The mathematical equation that governs this neutron distribution is basically a neutron balance equation known as the neutron transport equation. The transport equation is too complicated to be solved analytically, and exact solutions are obtainable only for simplified physical models. One has to take recourse to numerical methods for most cases of practical interest. The numerical methods require discretization in all variables; in particular, the energy variable is represented by a large number of groups (the multi-group method) with representative average cross sections being used in each group. Computer codes based on these numerical methods are time consuming and hence, quite often, one uses an approximation of the transport equation known as the few-group neutron diffusion equation. Since conditions for the validity of the diffusion approximation are not always satisfied, a two step procedure is employed. Multi-group transport theory is used at the lattice cell (representative unit cell) stage that yields a detailed space and energy dependent flux distribution within a lattice cell. This detailed flux distribution is used to obtain the few-group homogenized cross sections of the region, for use in the diffusion theory based core calculation for obtaining the flux and power distribution throughout the reactor. This model usually results in a reasonably good approximation to the exact solution of the transport problem. The methods based on transport theory and diffusion theory is referred to as ‘deterministic’ and several

computer codes based on these methods are in use (Sutton, 1996; Hardie, 1970; Lathrop, 1965; Casal et. al., 1991; Engle, 1967; Halsall, 1998).

The neutron population and its distribution can also vary with time and a study of its variation with time forms the subject of Reactor Kinetics. An understanding of the time dependent behavior of the neutron population in a nuclear reactor in response to either a planned change in the reactor conditions or to unplanned and abnormal conditions is of utmost importance for safe and reliable operation of nuclear reactors. For the simulation of the dynamic behavior of a nuclear system, a number of deterministic codes exist and are in current use (Rineiski, 1997; Jain et. al., 1989; Alcouffe et. al., 2008). These codes invoke all the approximations mentioned above for deterministic calculations (discretization, homogenization, diffusion theory). They may also invoke additional approximations such as adiabatic or quasi static approximations (steady state solutions in combination with point kinetics). Transport theory-based models (that do not invoke the diffusion approximation) have also been developed, but these are often restricted to two energy groups.

As opposed to the deterministic methods described above, the Monte Carlo method is a stochastic method that has been in use for a long time, but was used rather restrictively due to its large computing requirements. The radical increase in the availability of computing power in recent times permits the use of Monte Carlo (MC) methods more routinely for solving reactor physics problems. These methods have the advantage of permitting an exact treatment of the heterogeneous distribution of materials in a reactor and the rather complicated variation of cross sections with energy. A large amount of research has been carried out over the years in the area of MC methods and its use in radiation and neutron transport problems. Several general-

purpose computer codes have been developed to solve a variety of problems (MCNP, 1987; Romano et. al., 2013; MCU, 1982). Most of the well-known MC based codes, are limited to treating stationary situations involving criticality or source problems. MC methods are expected to greatly improve the accuracy of space-time kinetics calculations.

The thesis describes neutronic studies leading to the development of a time dependent MC code, for use in time dependent situations such as pulsed neutron experiments and nuclear reactor transient analysis. Several new schemes have been proposed and developed to manage variance and computing time issues associated with MC based kinetics. These include measures for neutron and precursor population and weight control, forced decay of precursors without combining them together and the use of mean number of secondaries per collision.

In this research work, the proposed new techniques are first applied to and tested in simpler models such as the Point Kinetics MC Model and the few group diffusion theory MC models, as it is easier to test new techniques in these simpler models. Moreover, since most space time kinetics benchmarks are based on few group diffusion equations solved by the finite difference method, the implementation in the diffusion theory MC model facilitates exact comparison with these benchmarks. The diffusion MC model was first proposed (Rana et. al., 2013) and studied in the context of reactor noise simulation. A number of new developments in the theoretical basis of the diffusion MC model have been carried out (Srivastava and Degweker, 2015) . Application of Diffusion based MC has been extended for transient analysis (Srivastava et. al., 2018) and for the estimation of Higher Eigenmodes (Srivastava et. al., 2018). After testing the schemes (for reduction of variance / computing time) in

these simpler models, they are implemented in a transport MC model and finally extended to the development of a multi-region multi-group MC kinetics code. These are the new results presented in this thesis.

The thesis is organized in eight chapters as elaborated below.

Chapter I is a brief introduction to the methods used in the Physics design of Nuclear reactors. It includes the neutron transport equation and its applications to lattice calculations and generation of homogenized cross sections, few group diffusion equations for core calculations. Further, the time dependent diffusion equation for the transient analysis is discussed. A brief review of the deterministic methods used for transient analysis and its limitations is presented

Chapter II gives a description of the MC Method for k eigenvalue problems. Here, the probability distribution functions for various processes associated sampling techniques and some variance reduction techniques are discussed. A survey of the literature on MC based methods for space time kinetics (including various hybrid approaches) in use for simulating transient problems is presented. Thereafter the challenges faced in the simulation of MC based space-time kinetics and the methods proposed for overcoming these is explained.

One of the major challenges in such simulations is the vastly different time scales of prompt and delayed neutrons. The average life time of a prompt neutron in a light water reactor is around 10^{-4} s while that of precursors varies roughly from 10^{-1} s to 10^2 s. The short neutron life time causes the neutron chains to decay rapidly leading to large time gaps between successive neutron chains. This results in large fluctuations in the neutron population and consequently in the estimates of neutron power in a MC simulation. A related problem is the vast difference in the neutron and precursor

populations. Another challenge is to control the varying populations of neutrons and precursors with time.

To overcome these challenges, several new techniques have been developed. These include different weights for neutrons and precursors, population and weight control, handling various precursor groups separately, forced decay of precursors without combining them together and use of mean number of secondaries per collision. While some of the techniques have been proposed earlier (Sjenitzer, 2013), others are new. These include different weights for neutrons and precursors, population and weight control, handling various precursor groups separately, forced decay of precursors without combining them together and use of mean number of secondaries per collision. The use of different weights for neutrons and precursors and the treatment of the different precursor groups explicitly is a novel approach for time dependent MC studies.

Chapter III gives a description of the application of the proposed new techniques to the simplest model viz., the Point Kinetics MC model. A number of benchmark problems are studied and the results are compared with deterministic methods. A simple feedback model is also studied. It is observed that Point Kinetics based MC simulations can be carried out with practically nil variance.

Chapter IV presents an outline of the diffusion theory MC model and the developments carried out by us in this area. The Diffusion theory MC method was developed earlier by Rana et al, 2013 for simulating reactor noise experiments. This method is further extended to demonstrate its utility in a wider class of problems involving cylindrical geometries, non-homogeneous media and some other situations.

In particular, mathematical and numerical proofs of the validity of recipes proposed for heterogeneous systems have been developed.

In Chapter V, schemes for modeling the spatial variation of neutrons and precursors are proposed and these schemes are applied in the diffusion based MC Model. The chapter also describes the space time simulations using Diffusion MC. In this method, the finite differenced form of the diffusion equation is used to estimate the probabilities of absorption, slowing down or migration to a neighboring mesh. The problem geometry is discretised in rectangular meshes and neutron history is followed as per the diffusion process across various meshes. Starting from an initial spatial distribution across meshes corresponding to a critical state, neutrons are tracked one by one.

It is observed that the computational time required for Diffusion MC is about ten times lesser than that for Transport MC. More pertinently, an exact comparison of the proposed MC simulations with several space-time kinetics benchmarks based on few-group diffusion theory is possible. This is particularly significant because there are very few space time benchmarks based on exact transport theory or transport theory MC available in literature.

Chapter VI illustrates application of the Diffusion MC Model for estimation of higher modes (eigenvalues and eigenvectors). Higher modes are of interest in flux expansion techniques for stationary as well as kinetics problems. A new MC algorithm is developed to obtain fundamental and higher eigenvalues and eigenvectors for a reactor core using the Fission Matrix Method in the Diffusion MC Model. A method for obtaining errors in the estimated eigenvalues using first order perturbation theory is also presented. The performance of the algorithm for calculating higher eigenvalues and higher eigenvectors was verified through comparison of the estimated

eigenvalues by other deterministic codes. Fundamental and higher λ eigenvalues up to six modes were compared for a Pressurized Heavy Water Reactor Benchmark. This development is of interest as it uses a simple model to understand the rather difficult problem of obtaining higher modes of the transport equation by the MC method. This can also be viewed as another method for obtaining higher modes of the diffusion equation.

Chapter VII discusses the MC Transport theory based space-time kinetics simulations. Having verified the recipes on simpler models i.e. on Point Kinetics and Diffusion Theory MC Models, they are finally implemented in Transport theory resulting in the Space Time MC Kinetics Code KINMC, developed in the course of the research work. KINMC code uses the Delta Neutron Tracking method for neutron transport. The code explicitly treats the six groups of precursors and uses population and weight control of precursors and neutrons as well as the concept of mean number of secondaries in a collision for variance reduction. It has the capability of solving multi group space time transients. The efficacy of this code is tested by comparison with results of realistic space-time kinetics benchmarks involving multi-region reactors and energy dependence. 1D Benchmark (Sjnetizer et. al., 2013) and TWIGL 2D Benchmark (Hoffman, 2013) in 2 energy groups are analysed by KINMC.

Chapter VIII gives a brief summary of the work described in the thesis. It also presents the main conclusions drawn and scope for future work which may be summarized as follows.

In this thesis a new method for the analysis of power transients in a nuclear reactor is discussed. A time-dependent MC code has been developed to solve reactor kinetics problems based on this method and is more accurate than the present state-of-the-art

methods based on deterministic tools. This accuracy makes the method very suitable as a validation tool for other computational techniques. The simulation schemes presented in this thesis are novel. Research has shown that it is feasible to perform dynamic MC analyses on nuclear systems.

Further work in this direction would be to develop a code capable of continuous energy treatment with detailed tracking and anisotropic scattering. Introduction of parallel processing would make it possible to actually carry out MC space-time kinetics calculations for realistic problems and not merely as a benchmarking tool. With these developments, realistic space-time kinetics, using the schemes discussed in the thesis, will become feasible.

Review of the Computational Methods used in Reactor Physics

Nuclear reactors are the systems which maintain controlled nuclear fission chain reactions and produce energy for the generation of electricity and for other uses. The constituent materials of a reactor are generally fuel, coolant, moderator, structural materials, and control material. In general, these materials are arranged heterogeneously to constitute a reactor core with due consideration to neutronics, thermal-hydraulics, and structural aspects. In addition, the structural arrangement and the constituents may change depending on the life-cycle of the fuel or on the mode of operation of the reactor or during accident conditions.

Although the discipline of reactor physics that deals with the design and analysis of such reactors encompasses several areas in science and engineering, the subject has matured into a well established and unique field. Reactor analysis and methods may be described as a discipline concerning determination and prediction of the states of a reactor that sustains chain reaction by balancing neutron production by fission and loss by capture and leakage.

One of the objectives of nuclear reactor physics is to determine the distribution of the neutrons in a reactor. For that we have to take into account the motion of the neutrons and their interactions with host nuclei of various kinds. Thus, we need a mathematical model or theory to describe this particle transport phenomena.

1.1 Neutron Transport Equation

The neutron transport equation is a balance equation in phase space, like the Boltzmann equation in the kinetic theory of gases. It describes the mean neutron distribution as a function of the space coordinates and the neutron velocity in a nuclear reactor. In this equation neutron-neutron collisions

are neglected and only collisions with atoms of the medium is considered which makes it linear unlike the Boltzmann equation.

The following assumptions are made in the derivation of the neutron transport equation (Lewis and Miller, 1984; Bell and Glasstone, 1970 and Weinberg and Wigner, 1958). The neutron may be considered as a point particle. The particles travel in straight line between collisions. This is true for neutrons and gamma rays since they do not carry charge and have straight trajectories as coulomb forces do not affect their paths. Neutrons interact with nuclei through collision. Neutron neutron interactions are neglected since the neutron densities in nuclear reactor are small as compared with atomic density.

The behavior of a nuclear reactor is governed by the distribution of the neutrons in the system with respect to space, energy and time. The neutron transport equation governing this distribution function considers the rates at which neutrons of different energies moving in different directions enter and leave a small phase space element $dr.d\Omega.dE$.

The neutron transport equation is derived by taking into account the terms defining gain and loss rates. The loss terms include leakage or streaming out of the volume and loss due to absorption and scattering. The gain is a result of fission, scattering and external sources. Defining each of the production and loss terms, we can write integro-differential form of the neutron transport equation as:

$$\frac{1}{v} \frac{\partial \psi}{\partial t} + \Omega \cdot \nabla \psi(r, \Omega, E, t) + \Sigma_t(r, E) \Psi(r, \Omega, E, t) = Q(r, \Omega, E, t) \quad (1.1)$$

where,

$$\psi(r, \Omega, E, t) = V \cdot N(r, \Omega, E, t) \quad (1.2)$$

is the angular flux. $\Sigma_t(r, E)$ is the total macroscopic cross section of the medium, V is the neutron velocity. The source $Q(r, E, t)$ in the right hand side of eq (1.1), consists of any external source Q^{Ext} , the scattering source Q^S and the fission source Q^F , which are given as

$$Q^S = \int dE' \int d\Omega' \Sigma_S(r, E' \rightarrow E, \Omega' \rightarrow \Omega) \Psi(r, \Omega') \quad (1.3a)$$

$$Q^F = \chi(E)4\pi \int dE' \nu \Sigma_f(r, E') \int d\Omega' \Psi(r, \Omega', E') \quad (1.3b)$$

where $\Sigma_s(r, E' \rightarrow E, \Omega' \rightarrow \Omega)$ and $\Sigma_f(r, E')$ is the scattering cross section and fission cross section of the medium respectively. $\chi(E)$ is the fission spectrum and ν is the number of neutrons produced per fission. In steady state conditions, the neutron density does not change with time and we have the equation

$$\Omega \cdot \nabla \psi(r, \Omega, E, t) + \Sigma_t(r, E) \Psi(r, \Omega, E, t) = Q(r, \Omega, E, t) \quad (1.4)$$

If the external source is absent, the steady state equation becomes an eigenvalue equation. Various eigenvalue equations are discussed later.

Since the transport equation is first order in time, an initial condition i.e. $\Psi(r, E, \Omega, t = 0)$ has to be specified. In addition, flux distribution at the surface bounding the concerned domain has to be specified. This depends upon the problem being studied and may be obtained from simple physical considerations. If we are dealing with the outermost boundary of the reactor and no neutrons can enter from outside this boundary we use the vacuum boundary condition viz., $\Psi(r, E, \Omega, t) = 0$ for $\hat{n} \cdot \Omega < 0$. Often the transport equation is solved at the lattice level and it is assumed that there is an infinite lattice of cells (such as fuel assemblies, or pin cells) and the periodic or reflective boundary conditions are used.

1.2 Multi group formalism of Neutron Transport Equation

It is not possible to obtain analytical solutions to the transport equation (except for a very limited number of simple problems) and one has to resort to numerical methods. Numerical methods involve discretisation of some or all the variables (position, energy, direction). The multi group formalism involves discretisation of the energy variable. In this formalism, neutron transport equation is made computationally suitable by dividing complete neutron energy range into G number of discrete intervals called groups. The group angular fluxes are defined as

$$\psi_g(r, \Omega) = \int_{E_g}^{E_{g-1}} dE \Psi(r, \Omega, E) \quad (1.5)$$

Now the transport equation (equation 1.1) can be expressed in its multi-group integro differential form as follows

$$\Omega \cdot \nabla \psi_g(r, \Omega) + \Sigma_{tg}(r) \Psi_g(r, \Omega) = Q^{Sg} + Q^{Fg} + Q^{Extg} \quad (1.6)$$

Where $\psi_g(r, \Omega)$ is the angular flux in group g at point r and in direction Ω . Σ_{tg} is the total macroscopic cross section for group g . Σ_{fg} is the fission cross section for group g and $\Sigma_{sg \rightarrow g'}$ is the scattering cross section for group g scattered to group g' . The scattering source Q^{Sg} contains two parts: Self scattering source Q^{Ss} and sources coming from other groups g' shown as $Q^{Sg'}$. The source terms are

$$Q^{Sg} = \int \Sigma_{sg \rightarrow g}(r, \Omega' \rightarrow \Omega) \Psi_g(r, \Omega') d\Omega' + \sum_{g' \neq g} \int \Sigma_{sg' \rightarrow g}(r, \Omega' \rightarrow \Omega) \Psi(r, \Omega') d\Omega' \quad (1.7)$$

$$Q^{Fg} = \frac{\chi_g}{4\pi} \sum_{g'} \int \Sigma_{fg'}(r) \Psi_{g'}(r, \Omega) d\Omega \quad (1.8)$$

Various group cross sections are obtained by a weighted averaging of the corresponding cross section over the energy range of each group. The weighting function is the flux spectrum within the group. The scattering cross section is generally speaking a function of the scattering angle and hence depends upon the scalar product $\Omega' \cdot \Omega$ i.e. the cosine of the scattering angle. Hence, the scattering cross section is expanded in Legendre polynomial of this quantity up to a certain number of terms. The coefficients of this expansion are the scattering matrices denoted by $\Sigma_{l, g' \rightarrow g}$. With this representation of scattering, there are as many scattering matrices as is the number of terms in the Legendre polynomial expansion. Often it is enough to retain one or two terms (isotropic or linearly anisotropic scattering) in the expansion. By making use of the addition theorem to write each of the Legendre polynomials, the scattering integral on the right hand side can be written as a sum of the product of the scattering matrices, moments of the angular flux (integrals of the product of angular flux and spherical harmonics over Ω') and spherical harmonics. Details of this procedure as well as the choice of the weighting spectrum and treatment of the scattering matrices may be found in Halsall, 1991. Codes like the GROUPR module of NJOY exist for generating multi group cross section in this way.

1.3. Computational Methodology

Various numerical methods have been devised for obtaining the quantities of interest to the reactor physicist by solving the multi group transport equation. The calculations are done by discretising some or all of the variables involved. The discretisation of the spatial variables results in what is commonly referred as the spatial mesh. The differential scattering cross sections are expressed in terms of the orthogonal Legendre polynomials.

In the spherical harmonics (P_N) method, the neutron direction variable is treated by expanding the angular flux in a series of spherical harmonics up to order N . Other methods such as the discrete ordinates (DS_N) methods and the method of characteristics discretize the direction variable also (Bell and Glasstone, 1970 and Glasstone and Edlund, 1952). The discrete directions are most often defined by a fully symmetric quadrature set where weights are chosen so as to accurately obtain the integral over the direction variables. Other methods such as collision probability methods (Sanchez, 1977) solve the integral form of the transport equation.

It is very difficult, or extremely time-consuming, to apply transport equation to full core calculations. Therefore, the neutronics calculations are usually performed in two stages; lattice calculations and full core calculations and the codes used for reactor analysis are broadly classified as lattice level codes, and core level codes (Stammler and Abbate, 1983; Cacuci, 2010). Lattice is the basic repetitive structure in a reactor core. The lattice cell is usually the fuel assembly consisting of several heterogeneities like varying fuel enrichment, burnable poison rod cells, water or control cells, inter-assembly water gaps or water slots.

A typical reactor lattice code takes as input the neutron-nuclide cross sections data from a multi group library (for example the 172 energy groups in WIMS-D format) and a description of the reactor lattice, and solves the neutron transport equation to calculate neutron flux distribution, infinite neutron multiplication factor and homogenized cross sections required for core calculations. For practical reasons, the transport equation is applied to small regions of the reactor lattice i.e. representative cells to find the detailed flux in space and energy in these cells, and to derive

homogenized properties such as cross sections, uniform over each lattice cell (spatial homogenization), which are collapsed to a very small number of energy groups say 2 or 5 groups (energy condensation), for application over full-core models based on diffusion theory. Some examples of transport theory based lattice codes are WIMSD (Askew J. R. et al., 1966), DRAGON (Marleau, Hebert and Roy, 2011), HELIOS (Villarino et. al., 1992), EXCEL (Jagannathan V. and Jain R. P., 2009), CLUB (Krishnani, P. D., 1992), LWR-BOX (Krishnani, P. D., 1987) and BOXER (Degweker, 1985). The lattice codes are used to calculate neutron flux distribution, infinite medium multiplication factor and homogenized few group cross sections.

In the second stage, the core level code uses the cell homogenized cross sections generated by the lattice code and analyses the overall behavior of the core as a function of burn-up and other reactor state variables like boron and temperatures of fuel and coolant. The analysis also includes the presence/absence of control absorbers and reflector material in estimating the flux and power distribution. An approximate form of the transport equation, viz. the diffusion equation described in the next section is used for core calculations. This is the strategy used most frequently, and successfully, in the design and analysis of nuclear reactors.

1.4 Multi group Diffusion Equation

One generally uses neutron diffusion equation for reactor core calculations. The neutron diffusion equation is an equation for the scalar flux (angular flux integrated over direction). The diffusion equation is an approximate form of the neutron transport equation, which is more amenable to calculation than the transport equation itself. It is quite simple to allow detailed calculations yet sufficiently realistic for studying many of the important concepts arising in reactor analysis. The time-dependent diffusion equation is written as:

$$\frac{1}{v_g} \frac{\partial}{\partial t} \varphi_g(r, t) - \nabla \cdot D_g \nabla \varphi_g(r, t) + \Sigma_{tg}(r) \varphi_g(r, t) = \sum_{g'=1}^G \left[\Sigma_{sg' \rightarrow g}(r) \varphi_{g'}(r, t) \right] + \chi_g \sum_{g=1}^G \left[v \Sigma_{fg}(r) \varphi_g(r, t) \right] + S_{ext_g}(r, t) \quad (1.9)$$

where $\phi_g(r, t)$ is the neutron flux in group 'g' at distance r at time t, V^g is the neutron velocity in group 'g', D_g is the diffusion co-efficient of the medium and χ_g is the fission spectrum in group 'g'.

Defining removal cross section as $\Sigma_{rg} = \Sigma_{a_g} + \sum_{g' \neq g}^G \Sigma_{sg' \rightarrow g} = \Sigma_{t_g} - \Sigma_{sg \rightarrow g}$, we get the following equation

$$\begin{aligned} \frac{1}{V_g} \frac{\partial}{\partial t} \phi_g(r, t) = \nabla \cdot D_g \nabla \phi_g(r, t) - \Sigma_{rg}(r) \phi_g(r, t) + \sum_{g' \neq g}^G \left[\Sigma_{sg' \rightarrow g}(r) \phi_{g'}(r, t) \right] \\ + \chi_g \sum_{g=1}^G \left[\nu \Sigma_{fg}(r) \phi_g(r, t) \right] + S_{extg}(r, t) \end{aligned} \quad (1.10)$$

The time dependent diffusion theory is discussed in the next section as a part of the subject of reactor kinetics. Quite often we are interested in stationary solutions such as a reactor producing steady power. The above equation (1.10) admits stationary solution when the external source does not depend upon time and the reactor is subcritical. The other stationary solutions occur in the absence of the external source, as a solution of eigenvalue problems. Two commonly studied eigenvalue problems correspond to the α eigenvalue and the λ eigenvalue. The former is obtained by writing the flux as $\phi_s(r) e^{\alpha t}$ and we get

$$\begin{aligned} \nabla \cdot D_g \nabla \phi_{sg}(r, t) - \Sigma_{rg}(r) \phi_{sg}(r, t) + \sum_{g' \neq g}^G \left[\Sigma_{sg' \rightarrow g}(r, t) \phi_{sg'}(r, t) \right] \\ + \chi_g \sum_{g=1}^G \left[\nu \Sigma_{fg}(r, t) \phi_{sg}(r, t) \right] + S_{extg}(r, t) = \frac{\alpha}{V_g} \phi \end{aligned} \quad (1.11)$$

The λ eigenvalue problem is obtained by setting the time derivative equal to zero in equation (1.9) and dividing the fission source by λ giving rise to the following eigenvalue equation (1.12). The Keff is the largest of the λ eigenvalues.

$$\nabla \cdot D_g \nabla \phi(r, t) - \Sigma_{rg}(r) \phi_g(r, t) + \sum_{g' \neq g}^G \left[\Sigma_{sg' \rightarrow g}(r) \phi_{g'}(r, t) \right] + \frac{\chi_g}{\lambda} \sum_{g=1}^G \left[\nu \Sigma_{fg}(r) \phi_g(r, t) \right] = 0 \quad (1.12)$$

The space variable is commonly discretised by writing finite difference forms for the spatial derivative terms. Details of the finite differencing of the diffusion equation are given in Cacuci, 2010; Duderstadt, J.J. and Hamilton, 1976 and Reuss, 2008. Finite differencing leads to a linear system of equations for the flux variables defined at the mesh points at each time step. The solution

of the diffusion equation is usually obtained by the inner-outer procedure (Duderstadt and Hamilton, 1976; David L. Hetrick, 1993). Over the years several other schemes for solution of multi group neutron diffusion equation have been developed and computer code packages are made based on these methods. Notable among these methods are the nodal method (Lawrence, R.D., 1986), the finite difference method (Duderstadt and Hamilton, 1976; Lewins and Ngcobo, 1996) and the finite element method (Kang and Hansen, 1973).

1.5 Time-dependent Diffusion Equations: Reactor Kinetics

One important class of problems in nuclear engineering to which computational tools must be developed and applied is the various time and space dependent phenomena that can occur within a nuclear reactor core. Such problems occur within time scales of a few seconds or less, yet may significantly affect overall reactor operations. The normal motion of control rods during reactor start-up and shutdown procedures, the abnormal motion of control rods during a rod ejection or rod drop accident, or ingress/egress of liquid during a loss-of coolant accident scenario are all situations that necessitate the development of computational tools for the analysis of space and time dependent reactor phenomena. Since core calculations are traditionally carried out using the few group diffusion approximation of the transport equation, reactor kinetics is discussed in this section in this approximation. The set of equations that describe time dependence of neutron flux are

$$\frac{1}{v_g} \frac{\partial \phi_g}{\partial t} = \nabla \cdot D_g \nabla \phi_g - \Sigma_{rg} \phi_g + (1 - \beta) \chi_g^p \sum_{g'=1}^G \nu \Sigma_{fg'} \phi_{g'} + \sum_{g' \neq g} \Sigma_{g' \rightarrow g} \phi_{g'} + \chi_g^d \sum_{i=1}^I \lambda_i C_i \quad (1.13)$$

$$\frac{\partial C_i}{\partial t} = \beta_i \sum_{g'=1}^G \nu \Sigma_{fg'} \phi_{g'} - \lambda_i C_i \quad (1.14)$$

where β is the delayed neutron fraction, χ_g^p is the prompt neutron fission spectrum, χ_g^d is the delayed neutron spectrum, λ_i is the decay constant for the i^{th} precursor group and C_i is the precursor concentration for the i^{th} precursor group. The first equation (1.13) is the usual time dependent multi group diffusion equation with the difference that the prompt fission neutron source is shown separately from the contribution due to decay of delayed neutron precursors in 6 groups. The second

equation (1.14) shows the evolution of the precursor concentrations as a function of time (Keepin, 1965). Various methods have been devised to solve the above set of equations. They are discussed below.

1.5.1 Point Kinetics

1.5.1.1 Flux factorization & Point kinetics equation

In the flux factorization method developed by Yasinsky and Henry, 1965, the flux distribution is first factorized into a time dependent factor and a space dependent factor which depends weakly on time as follows

$$\varphi_g(r, t) = n(t)\psi_g(r, t) \quad (1.15)$$

where $n(t)$ is the amplitude function and describes the rapid variation in power/neutron population in the reactor. $\psi_g(r, t)$ is known as the shape function and it is assumed that it is a slowly varying function of time. The shape function $\psi_g(r, t)$ essentially describes the spatial variation of neutron flux in the reactor. Different ways of treating the function $\psi_g(r, t)$ give rise to different approximations. We can assume that $\psi_g(r, t)$ is completely independent of time and the flux shape continues to be the same as that of the critical reactor. This is the **point kinetics approximation**. This model assumes that the power /flux distribution does not change with time throughout the transient period. Moreover, we assume that the form of the flux is the same as that in the critical reactor which has been perturbed to make it depart from criticality. More generally the shape function must be treated as a slowly varying function of time. Substituting the factorized form of the flux in the time dependent equations (1.13) and after some complicated manipulations (described in detail in text books such as as Bell and Glasstone, 1970 and Stacy, 2001), the following coupled set of equations for n and C are obtained.

$$\frac{dn}{dt} = \frac{\rho - \beta}{\Lambda} n + \sum_i \lambda_i C_i \frac{dn}{dt} = \frac{\rho - \beta}{\Lambda} n + \sum_i \lambda_i C_i \quad (1.16)$$

$$\frac{dC_i}{dt} = -\lambda_i C_i + \frac{\beta_i}{\Lambda} n \frac{dC_i}{dt} = -\lambda_i C_i + \frac{\beta_i}{\Lambda} n \quad (1.17)$$

where ρ is the reactivity and Λ is the prompt neutron generation time. It is possible to get analytical solution of the point kinetic equations for the step input of the reactivity without any feedback. However, in general analytical solutions are difficult to obtain but numerical solution is possible and number of codes like SASIA (J. C. Carter, 1970), ADEP (Denning R. S., 1971), MRIF (Balaraman and Trasi., 1981), GEAR (Podar et. al., 1989), PATH (Dwivedi et. al., 2014), PEARL (Singh A. and Gupta H. P., 2013) have been developed for this purpose. Point kinetics works fairly well for small reactors or when the departure from criticality is small. It is also interesting because simple analytical solutions are obtainable in some cases that enable the understanding of reactor kinetics behavior

1.5.1.2 Point kinetics: Step reactivity

In the case when the reactivity is changed suddenly, from one value to another, the point kinetic equations reduce to equations with constant coefficients and are easily solvable. We consider this situation in this section. A case of special interest is when the reactor is critical ($\rho = 0$) and has been operating at a constant power for a long time and suddenly through some control action, a reactivity is introduced which may be positive or negative.

The equations are easily solvable and the solution can be written as sum of exponentials as follows:

$$n(t) = \sum_k n_k \exp(w_k t) \quad (1.18)$$

where w_k are the roots of the in hour equation

$$s\Lambda + \sum_i \frac{\beta_i s}{s + \lambda_i} - \rho = 0 \quad s\Lambda + \sum_j \frac{\beta_j s}{s + \lambda_j} - \rho = 0 \quad (1.19)$$

For positive ρ , the above equation has six negative roots and one positive root. Thus, in the absence of a source, after all the negative exponentials have died out, the reactor power increases with a time period given by the positive root. For negative ρ , on the other hand, all roots are negative and the reactor power goes to zero. The main results (without temperature feedback) that can be obtained from solutions of this model are: small positive step reactivity input introduced, ($\rho < \beta$) called a sub prompt critical system, there is a rapid (limited) rise in power called the prompt jump

followed by a slower power rise which after some time grows as a single exponential with time. For a positive step reactivity input ($\rho > \beta$) called super prompt critical state, there is a rapid unlimited rise in power which is difficult to control. For a negative step reactivity input, there is a rapid fall in power called the prompt drop, followed by slower fall in power which ultimately is a single exponential.

1.5.1.3 Point kinetics: One group model

A particular case is when there is a single group of delayed neutrons. This can be obtained by clubbing all the delayed neutron groups together into a single group. The equation for the single group of precursors can be obtained by summing the equations for the individual precursors.

$$\frac{dC}{dt} = -\sum_i \lambda_i C_i + \frac{\sum_i \beta_i}{\Lambda} n = -\lambda C + \frac{\beta}{\Lambda} n \quad (1.20)$$

For systems close to critical we see that the rate of decay of the i^{th} precursor is approximately proportional to the precursor yield of that precursor. Making this approximation we can obtain the average delayed neutron precursor decay constant as

$$\lambda = \frac{\beta}{\sum_i \frac{\beta_i}{\lambda_i}} \quad \lambda = \frac{\beta}{\sum_i \frac{\beta_i}{\lambda_i}} \quad (1.21a)$$

The equation for the neutrons becomes

$$\frac{dn}{dt} = \frac{\rho - \beta}{\Lambda} n + \lambda C \quad \frac{dn}{dt} = \frac{\rho - \beta}{\Lambda} n + \lambda C \quad (1.21b)$$

The one group model is interesting primarily because of its simplicity and it captures (in a qualitative manner) most of the physics associated with reactor transients. The simplicity permits solution of the equations even when the reactivity is time dependent.

For the case of step reactivity discussed earlier we get a simple expression for the flux (neutron population) variation with time given below

$$n(t) = n_0 \left[\frac{\beta}{\beta - \rho} \exp\left(\frac{\lambda \rho t}{\beta - \rho}\right) - \frac{\rho}{\beta - \rho} \exp\left(-\frac{\beta - \rho}{\ell} t\right) \right] = n_0 \left[\frac{\beta}{\beta - \rho} \exp\left(\frac{\lambda \rho}{\beta - \rho} t\right) - \frac{\rho}{\beta - \rho} \exp\left(\frac{-\beta - \rho}{\ell} t\right) \right] \quad (1.22)$$

where ℓ is the prompt neutron life time.

1.5.1.4 Point kinetics: prompt jump approximation

In most reactors (except heavy water reactors) the prompt lifetimes are indeed very short compared to reactivity insertion rates, delayed precursors, actuation of feedback and control mechanisms. Since the prompt neutron lifetime is much shorter than the delayed precursor decay times, we can assume that the neutron population is always in equilibrium with the precursor concentration. In other words, we set $\frac{dn}{dt} = 0$ in the first equation and solve for n and introduce the same in the precursor equation. We thus obtain

$$\frac{dC}{dt} = \frac{\rho\lambda}{\beta-\rho} C \quad \frac{dc}{dt} = \frac{\rho\lambda}{\beta-\rho} C \quad (1.23)$$

which gives

$$\frac{dn}{dt} = \frac{\rho+\rho\lambda}{\beta-\rho} n \quad \frac{dn}{dt} = \frac{\rho+\rho\lambda}{\beta-\rho} n \quad (1.24)$$

The equation is fairly tractable and the following solution is easily written down as

$$n = n_0 \exp\left(\int_0^t \frac{\rho+\rho\lambda}{\beta-\rho} dt'\right) \quad (1.25)$$

We have used this equation to explain the (apparently anomalous) observed behavior of the flux in Chapter 3. With this approximation it is possible to write down fairly simple solutions for linear, step and sinusoidal reactivity insertions.

1.5.1.5 Numerical Methods for solution of point kinetics equations

The set of point kinetics equation describes a “stiff” problem meaning that the various time constants involved (delayed neutron precursor lifetimes, neutron lifetime, etc), are very different sometimes by several orders of magnitude. Thus, what is a short time step relative to one may not be relative to another.

Point kinetic equations are coupled ordinary differential equations. Various numerical schemes like Euler implicit schemes, Euler explicit schemes, higher order schemes and backward difference schemes are used (Weaver, 1963). The explicit schemes are stable for small time step sizes but not

for the large ones i.e. they are conditionally stable. The various explicit schemes require time steps comparable to the shortest time constant involved for their stability. The implicit schemes have more stability regions than the comparable explicit methods and are the preferred choice. The backward difference schemes are unconditionally stable for any positive step size and therefore score over the forward (explicit) schemes. MRIF-Fuel (Jain V. K. and Yadav R.D.S., 1989), NARD (Trasi et.al., 1976), PATH (Dwivedi et. al., 2014) are based on implicit Euler's method. GEAR's method (Poddar et.al., 1989) of solving a system of ODE such as the equations of point kinetics is based on higher order backward difference schemes.

1.5.2 Space Time Kinetics

Point kinetics method is suitable for small tightly coupled reactors where spatial flux distribution is insensitive to local changes in material properties. But, for large, neutronic loosely coupled reactors, the study of the neutronic transient behavior under accidental conditions requires accurate methods of solution of systems of coupled three dimensional multi group time dependent neutron diffusion equations. We will discuss various numerical methods that are used to solve space time kinetic equations to varying degrees of approximations (Ott, 1985).

The solution techniques for Space time kinetics equations are broadly categorized as: direct methods and space-time factorization methods. In direct methods, neutron diffusion equations are converted to a set of first-order differential equations in each volume element and that can be solved by the finite difference method over small time interval for all volume elements and energy groups. During each of the time steps certain parameters are kept constant enabling the time dependent diffusion equation to be transformed into steady state equation. (Sutton and Aviles, 1996, Stacey, 2001) Indirect methods involve a factorization of the flux into space and time parts. They are described in the subsequent sub sections.

1.5.2.1 Indirect Numerical Methods using Factorization Approach: Adiabatic and Quasi static methods

These methods are based on the flux factorization described in Section 1.5.1.1. In Adiabatic approximation, the flux shape changes as various sources of reactivity are introduced but it is assumed that the flux shape at different instants of time is given by the (stationary) k eigenvalue solution at that time. In the **quasi static method** we divide the time of interest into relatively long time steps and the flux distribution is recalculated at the end of each of these time steps using Eq. (1.15) as a source problem (with the derivative of the shape function set to zero). This shape function is used to obtain the kinetics parameters that go as input into the point kinetic equations (1.16 and 1.17) for the length of the next long time step. A further improvement is to replace the time derivative of the shape function by a finite difference expression.

1.5.2.2 Direct Numerical methods

1.5.2.2.1 Implicit Method

Fully implicit (backward differencing) method is used for solving the time derivative of space time kinetics equation. The first order backward differencing for the time derivative in the time dependent equation is given by

$$\frac{1}{V_g} \frac{\phi^{n+1} - \phi^n}{\Delta t} = D_g \phi_g^{n+1} - \Sigma_{ag} \phi_g^{n+1} + S_{ext}^{n+1} + \lambda_g^{(p)} C^{n+1} - \Sigma_{g \rightarrow h} \phi_g^{n+1} + \Sigma_{h \rightarrow g} \phi_h^{n+1} + \lambda_g^{(p)} (1 - \beta) \Sigma_{fh} \phi_h^{n+1} \quad (1.26)$$

The left hand side can be interpreted as a time derivative at the time n^{th} time step or the $(n+1)^{\text{th}}$ time step. In the former case the flux on the RHS would be the flux at the n^{th} time step and would correspond to the usual forward differencing and lead to an explicit solution for the flux at the $(n+1)^{\text{th}}$ time step. In the latter case, as is written in Eq. (1.26), the flux on the RHS is at the $(n+1)^{\text{th}}$ time step corresponding to backward differencing and leads to an implicit equation for the flux at the $(n+1)^{\text{th}}$ time step. The RHS of Eq. (1.26) contains spatial derivatives that are treated by the finite difference method outlined in an earlier section.

While the implicit method has the advantage of guaranteed stability and permits the use of long time steps when the flux evolution is slow, the iterative solution of the implicit equations gets more and more time consuming as the flux evolution gets slower. Two alternative methods to the fully implicit method have been reported (Weaver, 1963) with success. These are outlined below.

1.5.2.2.2 Alternating Direction Implicit and explicit method

In the Alternating Direction Implicit method (Weaver, 1963; Ash M., 1965) the derivative is treated as being implicit over a single direction. The advantage is that in one dimension, the solution involves a tri diagonal matrix which can be solved by the forward elimination and backward substitution in two sweeps. The solution is carried out by alternating each of the three directions to be implicit in successive time steps.

The Alternating Direction Explicit Method (Weaver, 1963; Ash M., 1965) uses the fact that in any iteration scheme, while calculating the flux in any mesh, the flux of three of the neighbors is already known. Thus, by reversing the direction of iterations in alternate steps it may be possible to ensure stability.

1.6 Existing Point Kinetics and Space Time Kinetics Code

Some of the existing Point Kinetics and Space Time Kinetics Code that are used at present for transient analysis are

NARD : Point Kinetics code NARD (Trasi M.S. et. al, 1976) solves the point reactor kinetics equations with temperature feedback by Cohen's modified Runge Kutta method.

MRIF: Point Kinetics code MRIF (Balaraman and Trasi M S., 1981) solves point kinetics code based on Method of Real Integrating Factors.

MRIF-FUEL: MRIF-FUEL (Jain V. K. and Yadav R. D. S., 1989) is the modified MRIF Code which includes one-dimensional (radial) heat conduction equations to treat temperature variation in fuel, sheath and coolant.

GEAR: GEAR (Poddar et. al., 1989) solves point kinetics code based on backward difference schemes.

PATH: PATH (Dwivedi et. al., 2014) solves the point kinetics equation with fourth order Runge Kutta as well as Implicit Euler method. This code has been augmented as point kinetics code which uses lumped parameters for coupled point kinetics and thermal-hydraulics with fuel and coolant temperature reactivity feedback.

ADEP: Two-dimensional space time kinetics code, ADEP (Denning R.S., 1971) is based on alternating direction explicit method with fuel and coolant temperature feedback.

3D-FAST: A multidimensional code 3D-Fast (Jain V. K. and Gupta H. P., 1986) based on IQS or adiabatic approach. The spatial part uses centre-mesh finite difference scheme. Various acceleration schemes have also been incorporated to accelerate the convergence. Provision is there to get space dependent average fuel temperature and core average coolant temperature.

ARCH: ARCH code (Analysis of Reactor Transients in Cartesian and Hexagonal Geometries) (Gupta A., 2012) solves the neutron diffusion equation in 3D Cartesian and triangular geometry. The solution is performed in few neutron energy groups using Finite Difference Method (FDM). The discretised diffusion equation results in a large linear system of equations in the form of $AX = B$, which is solved by conventional as well as advanced Krylov Subspace algorithm based schemes. It is based on IQS approach

KINFIN: KINFIN (Singh K. P., 2013) is finite difference based reactor kinetics code written in FORTRAN. It is based on direct integration method. The code can be used for analyzing transients

in PHWRs, LWR and sub-critical reactors. It can take variable meshes in X-Y-Z direction and also can simulate prompt and delayed neutrons in any group. One, two and three dimensional core models can be easily represented by using appropriate boundary conditions. Few group nuclear data generally computed by transport theory code WIMS, reactor core dimensional description mostly in the form of mesh width in X-Y-Z direction are major input data of the software.

TRIKIN : TRIKIN (Triangular meshes based kinetics code with thermal hydraulic feedback) is a Space Time Kinetics Code. It employs methodologies of the existing kinetics code NEUT and core physics code TRIHEXFA. TRIKIN model includes multichannel thermal hydraulics module to address reactivity feedback and determine the thermal safety parameters.

1.7 Limitations of the existing methods for transient analysis

Till recent times the neutronic part of the reactor transient is treated using deterministic methods. Currently many state of the art deterministic methods are based on the improved quasi static method (Ikeda et. al., 2001; Zachary et. al., 2016) but this method relies on the factorization of the neutron flux in a shape and an amplitude function. Factorization is not always a good approximation especially when a positive or negative reactivity is larger than a dollar and when the flux profile changes.

Also direct methods are used for transient analysis but they depend on simplified transport models e.g. diffusion theory (Boer et. al., 2010) and S_N methods (Alcouffe et.al., 2008). More advanced methods model the neutron transport itself. These methods need to discretise the angular dependence of the neutron flux. The neutrons will be transported along discrete angles, defined by spherical harmonics (P_N theory) or discrete ordinates (S_N theory). Also the MOC which solves the integral transport equation uses discrete angles. These methods describe the anisotropic behavior of the neutron transport better than diffusion theory, but it becomes difficult to use enough angles to describe neutron transport. If too few angles are used, ray effects can occur (Cho Chang, 2009). Stability and accuracy demands finer time steps. The main limitations of these direct deterministic

methods are the required discretisation. To deal with larger number of unknowns is computationally difficult. Therefore stochastic methods can be an more accurate option for the transient analysis. Since the neutron balance can be treated in a probabilistic manner, the corresponding time dependent behavior also can be tracked through these processes. The challenging part is the treatment of the neutron from the delayed neutron precursors.

Monte Carlo Methods for Reactor Analysis

Monte Carlo is a mathematical method of solving deterministic problem in stochastic way by the use of random number. Monte Carlo (MC) methods have been used for centuries, but only in the past several decades the technique has gained the status of a full fledged numerical method capable of addressing the most complex applications.

MC simulations are widely used in reactor physics problems, for their exact treatment of the heterogeneous distribution of materials in a nuclear reactor and the rather complicated variation of cross-sections with energy. MC Methods are very different from deterministic transport methods. Deterministic methods solve the transport equation for the average particle behavior. By contrast, MC does not solve an explicit equation but simulates a larger number of individual particle histories by treating process of production, collision, scattering, fission in form of probability distributions and recording some aspects (tallies) of their average behavior. The average behavior of particles in the physical system is then inferred from the average behavior of the simulated particles. Deterministic methods typically give fairly complete information (for example flux) throughout the phase space of the problem. MC supplies information only about tallies requested by the user. The MC method poses no limitations with regard to treatment of geometrical and nuclear cross section complexity in all its exactitude (Pal, 1958; Stephen Dupree et.al., 2001). The only uncertainties are those associated with statistics and errors in nuclear data. With growing computing power, the method is increasingly being used for day to day reactor calculations. The major component of a MC Algorithm is explained in the subsequent sections.

2.1 Probability density functions

The physical (or mathematical) system must be described by a set of probability distribution function (pdfs) (Sobol, 1994). Each stochastic process related to a random variable x is

characterized by a probability distribution $f(x)$, which is defined in such a way that the probability of the event occurring between x and $x + dx$ is given by:

$$dP = f(x) dx \quad (2.1)$$

The distribution function $f(x)$ is also called probability density function, or PDF. Consequently, the probability of the event occurring in an interval $[a, b]$ of the variable is

$$P(a < x < b) = \int_a^b f(x) dx \quad (2.2)$$

A natural requirement for the PDF is that the integration yields non negative and finite values. Assuming that the behavior of physical system can be described by probability density functions, then the MC simulation can proceed by sampling from these probability density functions. Sampling from a desired distribution is carried out by first drawing random numbers from a uniform distribution between 0 and 1 and then transforming to the desired distribution as explained in subsequent sections. Thus there is a requirement of a fast and effective way to generate random numbers uniformly distributed on the interval $[0, 1]$.

2.2 Random number generator

The success of a computation utilizing MC methods depends, mainly upon the quality of random numbers used. MC methods make extensive use of random numbers to control the decision making when a physical event has a number of possible results (Sobol, 1994; Stephen Dupree et. al., 2001; Anderson, 1990, Murthy K. P.N., 2000). The random number generator (RNG) is always one of the most crucial subroutines in any MC based simulation code. RNG are based upon specific mathematical algorithms, which are repeatable. As such, the numbers are not truly random and are referred to as pseudo random numbers. Reproducibility, generation of uncorrelated sequences, long period or cycle length, uniformity, and speed are some of the desirable properties of any RNG.

A larger number of generators are readily available. The most widely used technique of generating uniformly distributed random numbers on computers is by use of some recurrence relation where

each successive number U_{n+1} is found by using the preceding number U_n since it may satisfy some of the various statistical criteria of randomness. The most commonly used generator is the linear Congruential RNG (LCRNG). The LCRNG has the form

$$U_{n+1} = a(U_n + C) \text{ mod}(m) \quad (2.3)$$

Where m is the modulus and is the largest number available on the computer, a is the multiplier and c is the additive constant or addend. These parameters of the RNG must be chosen carefully to meet the requirements mentioned above. A typical MC simulation uses from 10^7 to 10^{12} random numbers and hence the period must be longer than this. Several combinations of these numbers have been tried and tested (Marsaglia, 1985). Pseudo Random numbers R_n (0, 1) can be generated by defining,

$R_n = U_n / m$. Pseudo Random numbers (E. D., Everett C. J., 1959) can be obtained by setting

$$m=2^{31}-1, a=65539 \text{ and seed}=3115$$

Since non uniformity and correlations between these numbers could lead to significant errors, a number of tests have been devised for this purpose. We mention some of the simple tests that may be used. Uniformity may be tested by the chi square test (Murthy K. P. N., 2000; Stephen Dupree et. al, 2001). On the other hand, randomness may be tested by calculating correlation coefficients between successive numbers or numbers separated by two, three, four or more numbers. Other tests include the n tuple test in which successive pairs of numbers are plotted in two dimensional space to check if the entire space in the unit rectangle is filled or whether patterns are seen (Stephen Dupree, 2001).

2.3 Random Sampling Techniques

The random sampling techniques help us to convert a sequence of random numbers (R_i), uniformly distributed in the interval (0, 1) to a sequence (x_i) having the desired density, say $f(x)$. There are several techniques that do this conversion. Two important techniques namely direct inversion and rejection method are described below to illustrate how a desired probability density function $f(x)$

can be simulated by use of random numbers (Hammersley and Handscomb. C., 1967; Lux et. al, 1991).

2.3.1 Inversion Technique

The simplest technique is based on the direct inversion of the cumulative density function of the random variable X. Consider the sampling of the exponential distribution. The distance to the next collision of the particle in a uniform infinite medium follows exponential distribution and is given by

$$p(x)dx = \Sigma e^{-\Sigma x} dx \quad (2.4)$$

This probability distribution is positive for all x and its integral is unity. Let ξ be the random numbers produced by the random number generator. ξ is uniformly distributed in the interval (0-1).

The distribution can be written as

$$P(\xi)d\xi = 1.d\xi \quad (2.5)$$

Suppose a transformation $x=f(\xi)$ takes the number ξ to x and $\xi+d\xi$ to x + dx. Then

$$p(x)dx = P(\xi)d\xi \quad (2.6)$$

Integrating the above equation we obtain

$$-e^{-\Sigma x} = \xi + c \quad (2.7)$$

On inverting (solving for x) the equation (2.7), we get

$$x = -\frac{1}{\Sigma} \ln(1 - \xi) \quad (2.8)$$

Since $1-\xi$ has the same distribution as ξ

$$x = -\frac{1}{\Sigma} \ln(\xi) \quad (2.9)$$

The inversion technique is also usable for discrete distributions that frequently occur in neutron transport.

2.3.2 Rejection Technique

Rejection Techniques are frequently used to improve the efficiency of the Monte Carlo computation in cases where the pdf cannot be easily integrated or inversion (solution) of the equation is difficult and time consuming. This method is fast and no approximation is involved. Define Random Number R as

$$R = \int_0^x f(x)dx \quad (2.10)$$

With $\int_a^b f(x)dx = 1$

Let $f(x)$ be the probability density function defined in the interval a and b from which the sampling is needed and let M be the upper limit of $f(x)$ (Fig. 1.1)

The steps for sampling x from $f(x)$ are

1. Select two independent random numbers R_1 and R_2 .
2. Compute $x = a + (b-a)R_1$ which is uniformly distributed over $[a, b]$.
3. Accept this value as the sampled value of x

If $R_2 \leq [f(x)/M]$, where $x = a + (b-a)R_1$; and M is the maximum value of the pdf

Otherwise x is rejected and one selects two fresh random numbers and repeats steps 2 and 3. The above procedure results in generating a uniformly distributed point $(a + (b-a)R_1, MR_2)$ in a rectangle of area $M(b-a)$. The third step accepts the selected value of x if it falls within the area under the curve otherwise the point is rejected. The probability of obtaining a satisfactory value of x in the first trial, which is also the efficiency (E) of the techniques, is given by

$$E = \frac{1}{M(b-a)} \int_a^b f(x)dx = \frac{1}{M(b-a)} \quad (2.11)$$

Where $\int_a^b f(x)dx = 1$

Fig. 1.1 Illustration of the Rejection Technique

A number of other methods have been devised for generating specific distributions that occur in the simulation of neutron transport such as energy distributions of elastically or inelastically scattered neutrons, fission neutrons, isotropic and anisotropic distributions and so on (Stephen Dupree et. al., 2001; Williams, 1974).

2.4 Scoring (or tallying)

Unlike deterministic methods MC method does not give the solution of neutron transport equation (e.g. flux and K for Eigenmode simulation of transport equation) on its own. In this method user has to specify each and every quantity which has to be tallied. The specific formula used to obtain the estimates is called an estimator of the quantity. Estimators should be unbiased i.e. the expectation value of the estimator should be equal to the theoretically exact value of the quantity. Estimation should be efficient which means how precise the estimate for a given effort at simulation is. In the following sub sections we describe some of the commonly used estimators for obtaining the K_{eff} and the flux in a given region (MCNP Manual, 2003).

2.4.1 Collision Estimator

The collision estimate for K_{eff} for any active cycle is

$$k_{\text{eff}}^c = \frac{1}{N} \sum_i W_i \left[\frac{\sum_k f_k \bar{v}_k \sigma_{fk}}{\sum_k f_k \sigma_{Tk}} \right] \quad (2.12)$$

Where i is summed over all collisions in a cycle where fission is possible

k is summed over all nuclides of the material involved in the i^{th} collision

σ_{Tk} = total macroscopic cross section

\bar{v}_k = average number of prompt or total neutrons produced per fission by the collision nuclide at the incident energy

f_k = atomic fraction for nuclide k

N = nominal source size for cycle

W_i Weight of particle entering collision

The flux in a given region of volume V is obtained using

$$\frac{1}{NV} \sum_{i,k} \frac{W_i}{f_k \sigma_{\text{Tk}}} \quad (2.13)$$

2.4.2 Absorption Estimator

The absorption estimator for k_{eff} for any cycle is made when a neutron interacts with a fissionable material. The estimator differs for analog and implicit absorption. For analog absorption,

$$k_{\text{eff}}^A = \frac{1}{N} \sum_i W_i \bar{v}_k \frac{\sigma_{\text{fk}}}{\sigma_{\text{ck}} + \sigma_{\text{fk}}} \quad (2.14)$$

where i is summed over each analog absorption event in the k^{th} nuclide. In analog absorption, the weight is the same both before and after collision. Because analog absorption includes fission in criticality calculations, the frequency of analog absorption at each collision with nuclide k is $\sigma_{\text{ck}} + \sigma_{\text{fk}} / \sigma_{\text{Tk}}$.

2.4.3 Track length Estimator

The track length estimator of k_{eff} is accumulated every time neutron traverses d in a fissionable material cell. It is given by

$$k_{\text{eff}}^{\text{TL}} = \frac{1}{N} \sum_i W_i \rho d \sum_k f_k \bar{v}_k \sigma_{\text{fk}} \quad (2.15)$$

where i is summed over all neutron trajectories

ρ is the atomic density in the cell

d is the trajectory track length from last event

The flux in a given region of volume V is obtained using

$$\frac{1}{NV} \sum_{i,k} W_i d \quad (2.16)$$

2.5 Error estimation

It is important in MC simulations, to estimate the statistical error (variance) as a function of the number of trials and other quantities. MC results represent an average of the contributions from many sampled histories and the tallied quantities have the statistical error or uncertainty associated with the result.

2.5.1 Means, Variances, and Standard Deviations

MC results are obtained by sampling possible random walks and assigning a score x_i (contributed by the i^{th} random walk) to each random walk. Random walks typically will produce a range of scores depending on the tally selected (Murthy K. P. N., 2000; Stephen Dupree, 2001, Bielgiew, 1998).

Assume that x is a quantity to be estimated (tallied) by MC simulation. Let there be N particle histories that are simulated. Assign and accumulate the value x_i and x_i^2 for the score associated with the i^{th} history where $1 \leq i \leq N$. Then the mean value of x is given as

$$x_{\text{avg}} = \frac{1}{N} \sum_i^N x_i \quad (2.17)$$

The estimated variance associated with the distribution of the x_i is given by

$$\begin{aligned} & x_i \\ & x_i^2 \end{aligned} \quad (2.18)$$

$$S_x^2 = \frac{1}{N-1} \sum_i^N$$

The estimated variance of x_{avg} is the standard variance of the mean given by

$$S_{x_{\text{avg}}}^2 = \frac{S_x^2}{N} \quad (2.19)$$

The square root of the variance is σ , which is called the standard deviation of the population of scores. The estimated mean in x_{avg} in equation (2.19) is the estimate for the true mean μ and the estimated variance is an estimate of the true variance σ_x^2 .

These formulae do not depend on any restriction on the distribution of x or x_{avg} beyond requiring that the expectation value of x and σ_x^2 exist and are finite. The estimated standard deviation of the mean x_{avg} is given by $S_{x_{\text{avg}}}$. It is important to note that $S_{x_{\text{avg}}}$ is inversely proportional to \sqrt{N} which is an inherent drawback to the Monte Carlo method. To have $S_{x_{\text{avg}}}$ reduced by half, four times the original number of histories must be calculated, making the calculation rather expensive. The quantity $S_{x_{\text{avg}}}$ can also be reduced for a specified N by making S smaller. This can be accomplished by using variance reduction techniques.

2.6 Variance reduction techniques

There are methods for reducing the variance in the estimated solution to reduce the computational time for MC simulation (Stephen Dupree, 2001). There are several methods to reduce variance in the tallied quantities. The type of variance reduction technique to be used depends on specific problems studied and the quantities to be estimated. The simplest and commonest approach to variance reduction is to introduce a particle weight. The particle histories begin with the statistical weight of the particle set to unity. Upon collision the particle always survives with its weight multiplied by the non absorption probability. In the event of fission, along with coordinates the weight of the particle is also stored. In the next generation, the particle begins its history with the stored weight. The multiplication factor is now estimated as the ratio of the total weight of the particles of the particular generation to that of the previous generation. For a large number of histories simulated, the total weight of the particles generated will be almost equal to the total number of particles generated in the analogue simulation.

However, introducing statistical weight also has certain disadvantages. One might end up simulating long histories with small statistical weights, which is not required. Also there is a lot of fluctuations in weight which tends to increase the statistical error. To avoid these problems two techniques known as Russian Roulette and splitting are introduced.

2.6.1 Russian roulette and Splitting Techniques

This is most probably the most widely used and safest of the variance reduction schemes. Whenever a particle goes from a region of lower importance to a region of higher importance, it is split into a number of particles. The average number of particles is usually kept equal to the ratio of the importance of the two regions. Suppose a particle goes from a region with importance equal to one to a region with importance equal to two. It is then split into two particles with both the split particles having the same coordinates as the particle just before splitting. At the same time, their weights will be reduced by a factor of two (Stephen Dupree, 2001).

Russian roulette is a complementary procedure to splitting. This is used whenever a particle crosses from a region of higher importance I_1 to one of lower importance I_2 . A random number R is chosen and the particle is killed if R is less than $1 - I_2/I_1$. If the particle survives, its weight is increased by a factor I_1/I_2 so that, on average, the total weight of the surviving particles is the same as that before the procedure was applied.

The combined use of Russian and splitting ensures that the weight of a single particle in any region remains within a limited range. It may be noted here that splitting always reduces the variance, whereas Russian roulette increases it.

2.7 Monte Carlo Simulation of Neutron Transport Equation

For simulation we need (1) a description of the geometrical shapes or boundaries of various regions in a space fixed co-ordinate system (2) description of the material composition within each region and (3) the cross sections as a function of energy for all materials in the regions. Particle histories

are simulated from birth to absorption (death) or leakage as follows (Jerome Spanier and Gelbard, 1969; Williams, 1974).

The simulation of the particle history begins with random sampling of the neutron position, energy and direction from the source distribution $S(r, \Omega, E)$. Depending on the position co-ordinate (x, y, z) of the source particle, the region is identified and the corresponding cross section at energy E are selected. Let the direction cosines of the source particle be (u, v, w) with respect to the (x, y, z) directions. The distance to the next collision is sampled from the exponential distribution as described above.

Let the inter collision distance be ' λ '. Then the new position of the particle is given by $(x+u\lambda, y+v\lambda, z+w\lambda)$. One checks whether any boundary crossing has occurred. If no boundary crossing has occurred, then the collision co-ordinates lie within the same region. Otherwise the position coordinates are updated to the point at which boundary crossing occurs. The new region is identified and the corresponding cross sections are selected. The distance traversed in the new medium is re-calculated and the new collision coordinates are computed. Again a check is made for a region boundary crossing and the procedure is repeated till the collision point is found.

The neutron can either induce fission, or undergo absorption/scattering reaction on collision with the nucleus of the material. The normalized probabilities for these processes can be deduced from the interaction cross sections as follows. The probability for absorption for a neutron energy E is the ratio of absorption cross section to total cross section at energy E . Similarly, the probability for fission for a neutron of energy E is the ratio of fission cross section to a total cross section at energy E . The probability for scattering for a neutron of energy E is the ratio of scattering cross section to total cross section at a neutron of energy E .

If this happens to be an absorption event, the particle history comes to an end. The particle history is also terminated when the particle leaks out of the system. In the case of scattering event, the energy of the scattered neutron is randomly sampled from the density function for the type of scattering (elastic/inelastic) constructed from the double differential scattering cross section data. As regards

direction, if the scattering is isotropic, μ , cosine of the polar angle θ is chosen from a uniform density function in the range -1 to +1. The azimuthal angle φ is chosen from a uniform density function in the range 0 to 2π . The direction cosines of the scattered particle are easily obtainable from these angles. If scattering is anisotropic μ is then the cosine of the angle of scattering and must be sampled from the given distribution of scattering angle. The angle φ is the azimuthal angle in a transformed coordinate system whose z axis is aligned with the direction of motion, and is chosen from a uniform density function in the range 0 to 2π . Then the direction cosines of the scattered particle are obtained after transforming back to the fixed coordinate system and are given by

$$u' = u \cos \theta - \frac{v^2 + w^2}{1/2} \sin \theta \cos \varphi$$

$$v' = v \cos \theta + D(uv \sin \theta \cos \varphi - w \sin \theta \sin \varphi)$$

$$w' = w \cos \theta + D(uw \sin \theta \cos \varphi + v \sin \theta \sin \varphi)$$

Where $D = 1 / \sqrt{v^2 + w^2}$

With the new phase space coordinates of the particle, the particle history is continued as described earlier.

If the collision results in fission, it is treated as absorption and the history ends (for that cycle) in case of the K_{eff} calculations described below. Else new neutrons produced in the fission are tracked till their absorption or leakage. Neutrons produced in fission are isotropic and their energy is sampled from the fission spectrum distribution.

The simulation described above is normally called as the analogue simulation. Analog Monte Carlo simulates the neutron transport problem by tracing each of the neutron histories as they would occur in the actual reactor. In other words all neutrons are tracked using the actual probability distributions (i.e. without modifying them in any way) and without using weights etc until they are lost by leakage or absorption.

2.8 K_{eff} calculations

For the estimation of K_{eff} , calculations are carried out in cycles (Jerome Spanier and Gelbard, 1969). Neutrons of a given cycle are followed from birth to absorption (including fission) or leakage. The locations and number of fission neutrons that may be produced due to these source neutrons is recorded and is used in the next cycle. However, neutrons produced as a result of (n,2n) (n,3n) reactions are tracked from their production to absorption or leakage. When all neutrons of a cycle have been tracked, we reach the end of the cycle. A new cycle begins with the fission neutrons produced at the end of the previous cycle being treated as the new source for the new cycle. At the end of each cycle one or more estimates of the k_{eff} are calculated and is (are) used to divide the fission neutron source by the k_{eff} . Thus the number of source neutrons is kept approximately constant from one cycle to the next. As the cycles proceed, the fission source distribution approaches the fundamental mode. Each individual cycle source distribution may depart considerably from the fundamental mode but an average of several cycles is close to the fundamental mode which depends on the dominance ratio and the number of neutron histories used per cycle. Some number of cycles are required for the fission source to converge to the fundamental mode (these cycles are called passive cycles). These cycles are continued after this point, and are called active cycles. The k_{eff} and all other tallies are then averaged over these active cycles.

2.9. Monte Carlo Methods for Transient Analysis

Most of the well-known MC based codes (X-5 MNCP, 2005; Leppanen et. al , 2015; Paul K. Roamno et. al., 2013; Gupta H. C., 1991; MCU Code, 1982), are limited to treating stationary situations involving criticality or source problems. MCNP6 (MCNP 6.2 , 2018) code can treat some limited time dependent problems including delayed neutrons, but not in a way usable for the kinetic problems discussed in the thesis.. Deterministic methods are most often used for the space-time analyses that are required for the study of the transients under normal operating or accidental

conditions. Among the presently available deterministic codes for space-time kinetics problems, (Rineski, 1997; Jain et. al., 1986; Alcouuffe et. al., 2008). few-group diffusion theory (preceded by lattice homogenization for obtaining few-group cross sections) is almost universally employed. The approximations involved in this procedure could result in significant errors in the estimation of the reactor power and its variation with time. MC methods are expected to greatly improve the accuracy of space-time kinetics calculations.

In this section, we present a literature survey of the MC based methods for space time kinetics and various hybrid approaches in use for simulating transient problems. We also discuss the challenges faced in the simulation of MC based space time kinetics and the methods proposed for overcoming these.

2.9.1. Different time scale of prompt and delayed neutrons

One of the major challenges in such simulations is the vastly different time scales of prompt and delayed neutrons. The average life time of a neutron in a light water reactor is around 10^{-4} sec while that of precursors varies roughly from 10^{-1} sec to 10^2 sec. The short neutron life time causes the prompt neutron chains, initiated by decay of a precursor, to die away rapidly leading to large time gaps between successive neutron chains. This results in large fluctuations in the neutron population and consequently in the estimates of neutron power in a MC simulation (Sjenitzer et. al., 2013). A related problem is the large ratio of the number of precursors to the number of neutrons at any instant making it difficult to handle the precursors individually.

2.9.2 Population control

Another challenge is to control the varying populations of neutrons and precursors with time. For the subcritical state, as a function of time, the neutron population decreases with time which leads to

a large variance in the estimates of power. In case of a super critical state, there will be an increase in the neutron population with time which results in large computing time. As stated above, the number of precursors and neutrons are vastly different and it is not possible to treat all the precursors (due to memory limitations) individually. Instead, it is necessary to reduce the precursor population and increase their weights. The problem then reduces to handling the particles of vastly different weights in the course of the simulation which is also quite challenging.

2.9.3 Changes in material properties / geometry and feedback effects

A reactor transient will usually involve changes in material properties such as density of the coolant, or geometrical changes due to introduction / removal of a control rod. In addition changes in power on account of the transient introduce reactivity changes due to temperature and density related feedback effects. For realistic reactor kinetics simulations, therefore, the capability to model changes in geometry, material properties and fuel temperature and power dependent feedbacks need to be incorporated in the MC simulation code in the course of the transient.

2.10 Review of Existing Transient Monte Carlo methods

Theoretical models for MC based reactor kinetics were first proposed by Kaplan (Kaplan et. al.,1958) wherein he proposed the concept of weight windows for controlling the number of particles in the simulation. He also proposed the concept of population control at the time boundaries and collision biasing.

Later the concept of hybrid time-dependent MC simulations was proposed (Wadell et. al.,1993). In this method a MC Code is embedded within a quasi-static kinetics framework. The time- dependent flux amplitude is computed deterministically by a conventional point kinetics algorithm. The point kinetics parameters, reactivity and generation time as well as flux shape which is slowly varying in time are computed stochastically by the MC calculation.

There are also other methods in which the time-dependent neutronic parameters are calculated using MC methods and delayed neutrons are treated as a source in the point model (Shayesteh et. al., 2009). Yun et. al., 2008 proposed to use the fission source shape iteration as a means to solve the shape function equation by MC. The point kinetics parameters are obtained during the MC solution process and the point kinetic solutions are solved by standard ODE solvers. Continuous energy Transient Analysis based on Predictor-Corrector Quasi method is carried out by YuGwan Jo et.al., 2016. The transport based MC code GEANT-4 (Russell et. al., 2014) uses the concept of instantaneous production of delayed neutrons i.e. average generation time to reflect the presence of delayed neutrons for time-dependent simulations.

In 2011, Sjenitzer and Hoogenboom developed a Dynamic MC Method of modeling neutron and precursors in space and time and implemented the same in the code TRIPOLI (Petit O. et.al., 2008).

2.11 New Schemes Proposed and Discussed in the thesis for MC Space Time Simulations

Various simulation schemes are developed to deal with the challenges mentioned above. These schemes are described below and discussed in detail in the subsequent chapters of the thesis. While some of the techniques have been proposed earlier (Sjenitzer et. al., 2013), others are new. These include different weights for neutrons and precursors, population and weight control, handling various precursor groups separately, forced decay of precursors without combining them together and use of mean number of secondaries per collision.

2.11.1. Modeling of precursors

In MC simulations there are two different types of particles - neutrons and precursors that on decay produce delayed neutrons and act as a source of neutrons. Neutrons have a life time of ~ 0.0001 sec (in LWRs) and the fission chain of neutrons lasts for a time (inverse of the prompt neutron decay constant α) that is typically about 0.01 sec. Delayed neutrons are produced by the decay of the

precursors. Precursors are categorized into 6 groups on the basis of their life time which varies from ~0.18 to 55 sec.

The starting point for the most of the kinetics simulations is a stationary critical state. In stationary critical conditions, the precursors come into equilibrium with the neutron population. This may be used to obtain the relation between the number of neutrons and the number of precursors, which serves as an initial condition. For a stationary situation, the number C_{i0} of precursors of delayed group i is given by

$$C_{i0} = \frac{\beta_i n_0}{\Lambda \lambda_i} \quad (2.20)$$

where, n_0 is the stationary number of neutrons, β_i is the delayed neutron fraction of group i , λ_i are the precursor decay constants and Λ is the neutron generation time. Thus, for a population of 10^5 neutrons, there will be 10^9 precursors. A population of 10^5 neutrons is probably the minimum that would be required to get any statistically meaningful results whereas modeling 10^9 precursors explicitly is virtually impossible on current desktops. Hence, these precursors are lumped into a more manageable number say 10^5 and assign a weight 10^4 to each.

In time-dependent MC simulations, the total time span over which the solution is required is divided into short time bins. One reason for doing this is that MC methods are developed for stationary systems whereas the system is evolving with time. During the course of a time bin, the geometry, composition and cross sections are kept constant. These are changed at the end of the time bin (which may be due the action of a control rod movement or feedback effects). The binning also serves the purpose of obtaining the average power during the time bin. Another purpose served is related to the way the precursor decay is treated and is discussed later. The width of the time bin will clearly be determined by these factors and is typically of the order of the average life time of the prompt neutron chain i.e. 0.01 sec in case of light water reactor systems. Thus, there will be certain time bins in the simulations, in which the chains due to neutrons at the beginning of a time bin have ended and the delayed neutrons produced by the decay of the precursors within a time bin are very few (about 10, each of weight 10^4) since the life time of the precursors has the decay time

of ~ 0.18 to 55 sec. Thus, very few source particles are sampled in the time bin and this will lead to fluctuations in the tallied quantities like neutron power and neutron flux. To overcome this problem in the time-dependent simulations, the decay of precursors is modified such that each of the 10^5 precursors is forced to decay within each time bin. The weight must be adjusted so as to have the correct average delayed neutron source strength in the bin. The time distribution of the delayed neutron appearances within a bin is chosen to be uniform which may be an approximation but is acceptable considering the small size of the bin compared to the decay lifetime of the precursors. Thus, at every time step, enough delayed neutrons are produced in each time step of the simulation. Precursors produced as a result of neutron induced fissions within a time bin are introduced in the system at the end of the the bin. It is a simplification and represents an approximation of the same order as that of causing decay of precursors uniformly distributed within a time bin. These approximations have negligible effect on the results since the time bin is much smaller than any precursor decay time. They help to simplify the algorithm but are not strictly necessary.

The concept of forced decay was also used by Sjenitzer and Hoogenboom, 2013. They have used the concept of combined precursor decay in which all the precursor families are combined into one MC particle and then a weight adjustment is carried out to correct the precursor decay since the combined precursor no longer has an exponential decay. In this simulation, each precursor group is explicitly treated and each group has its exponential decay. This is done since there is no unique way in which to assign weights to the different groups of precursors. Two extreme cases have been suggested by Hoogenboom viz the respective delayed neutron fractions or the equilibrium precursor concentrations. In kinetics simulations, it is obvious that both these represent approximations that could introduce an unknown and undesirable uncertainty in the simulations.

2.11.2 Variance reduction schemes: Mean Secondary Neutrons

In order to minimize variance in any MC simulation, wherever possible (i.e. where no bias results) one should use average numbers instead of statistically distributed numbers that are obtained by sampling. This may appear odd considering that MC is about using probability distributions for

sampling various events that form a neutron history. There is no way avoiding the use of sampling for determining points of collision, and the energy and angular distributions of neutron. However, in a collision with any given material one may choose to find the reaction that occurred and sample the number of neutrons produced in that reaction. Alternatively, the average number of neutrons may be obtained that would be produced if each of the reactions were to occur with a probability proportional to the macroscopic reaction cross section.

The number of neutrons that will be produced by v_i secondary neutrons generated at a point in the i^{th} reaction having probability α_i of occurrence and energy angle distributions $p_i(E, \Omega)$ is

$$T = \int \sum_i v_i \alpha_i p_i(E, \Omega) I(E, \Omega) dE d\Omega \quad (2.21)$$

The weight is changed to $W' = cW$, where W is the weight of the ingoing particle and c is the mean number of secondaries, given by

$$c = \sum_i v_i \alpha_i \quad (2.22)$$

Hence T can be rewritten as follows

$$T = c \int P(E, \Omega) I(E, \Omega) dE d\Omega \quad (2.23)$$

where,

$$P(E, \Omega) = \frac{v_i \alpha_i}{c} p_i(E, \Omega) \quad (2.24)$$

In view of the above, the energy angle distribution is sampled from that of any one of the energy angle distributions with a probability proportional to the product of the number of secondaries in that reaction and the reaction probability (the latter being proportional to the macroscopic reaction cross section). This is equivalent to using a combined energy angle distribution given by the above equation.

In the time-dependent simulation of sub prompt critical systems, the number of neutrons produced in a chain initiated by a delayed neutron can have a very large variance. So, to reduce variance, average number of neutrons that would be produced at each collision point is estimated. Average number of neutrons produced is proportional to the macroscopic reaction cross section of the

system. The total weight of the delayed neutrons thus produced is adjusted by the deterministic value.

2.11.3 Population control

In a time-dependent simulation of a super critical system, the neutron population increases with time. As time passes, more neutrons need to be sampled per bin which results in more computation time. To reduce the computation time, the neutron population is normalized to its initial value and the weight of each neutron is altered in the ratio of current to initial neutron population.

Simulation of sub critical (or sub prompt critical transients) for a few seconds or even tens of seconds does not cause substantial change in precursor population and precursor population control may not be necessary. For longer simulations, the precursor population is also substantially altered and it would be necessary to implement precursor population control as well.

2.11.4 Weight control

Use of the average number of particles per collision for the particle weight can lead to increased variance if the particle weight may become too small or too large causing large weight related fluctuations. For example in case the weight becomes too large, leakage of a large weight particle causes a sudden decrease in the total weight and is undesirable. Following the particles having a very small weight also increases computation time. To keep the weights comparable in magnitude, the particle weight is maintained within a narrow window. If the particle weight is beyond the upper limit of the weight window, the particle is split in two equal weights and if the particle weight is below the lower limit of the weight window, particle is killed by Russian roulette criteria.

2.12 Plan of the remaining Chapters of the thesis

The remaining chapters describe neutronic studies leading to the development of a time dependent MC code, for use in time dependent situations such as pulsed neutron experiments, reactor noise

simulation and nuclear reactor transient analysis. The studies also include MC methods for computation of higher modes that are of interest in flux expansion methods in statics as well as kinetics problems. The schemes outlined above to manage variance and computing time issues in MC based kinetics are applied to simpler models before applying them in transport MC kinetics, as it is easier to test new techniques in these simpler models.

In Chapter 3 the proposed new techniques are first applied to and tested in the simplest model viz. the Point Kinetics MC Model.

For space dependent problems, the diffusion Monte Carlo model is explored. The diffusion MC model was first proposed (Rana and Degweker, 2013) and studied in the context of reactor noise simulation that requires analog Monte Carlo and is therefore time consuming. The simpler diffusion Monte Carlo helps in reducing computing time in such simulations and is sufficiently realistic for such studies. A number of new developments in the theoretical basis of the diffusion MC model have been carried out (Srivastava and Degweker, 2015) and these are described in Chapter 4.

Another reason for studying the Diffusion Monte Carlo model is that there are very few transport theory or transport theory equivalent Monte Carlo benchmarks and most space time kinetics benchmarks are based on few group diffusion equations solved by the finite difference method. Thus, the implementation of the MC schemes in the diffusion theory MC model facilitates exact comparison with these benchmarks. This is discussed in Chapter 5.

In recent years there has been interest in developing methods for obtaining higher modes using Monte Carlo. Here again a simple model like the diffusion Monte Carlo model can help in gaining insight into various problems associated with various methods developed for this purpose. One of the specific problems of developing a method for obtaining error estimates in the higher eigenvalues is addressed. This is discussed in Chapter 6.

After testing the schemes (for reduction of variance / computing time) in these simpler models, they are implemented in a transport MC model and finally extended to the development of a multi-region multi-group MC kinetics code KINMC. This is discussed in Chapter 7.

Chapter 8 presents conclusions and scope for further work.

Implementation of the Simulation Schemes: Point Kinetics Model

Some of the proposed new simulation techniques discussed in Chapter 2 are applied to Point Kinetics MC. The point kinetics equation is characterized by stiff ordinary differential equations which pose severe problems of stability. To overcome these, either very short time steps are required or special techniques such as backward differencing schemes that have guaranteed stability (Podar et. al., 1989) properties must be used. This problem is not found in time dependent MC simulations since in MC methods, there is no discretisation of time as the time of event is directly sampled. In this chapter, time dependent MC studies based on point kinetics model is presented. The study includes the sampling of prompt and delayed neutrons, modeling of six groups of precursors, neutron population control using weights and modeling of power dependent feedbacks.

3.1 Point Kinetics Model

The multi group delayed neutrons point kinetics equations without the effect of extraneous source are given by

$$\frac{dn(t)}{dt} = \frac{\rho(t)-\beta}{\Lambda} n(t) + \sum_{i=1}^K \lambda_i C_i(t) \quad (3.1a)$$

$$\frac{dC_i(t)}{dt} = \frac{\beta_i}{\Lambda} n(t) - \lambda_i C_i(t), \quad i = 1, 2, \dots, K \quad (3.1b)$$

Where $n(t)$ is the neutron density, $\rho(t)$ is the reactivity, λ_i is the decay constant of i -group of delayed neutron precursors, $C_i(t)$ is the density of i -group of delayed neutron precursors, β_i is the fraction of delayed neutrons for i -group, β is the total fraction of delayed neutrons, Λ is the prompt neutron generation time, and t is the time.

In the criticality calculation the delayed neutron precursors do not play a role. Hence, from the total number of N particles resulting from criticality calculation the number of prompt neutrons and

delayed neutron precursors must be determined to start the time dependent simulation. For a stationary situation the number C_{i0} of precursors of delayed group i is given by

$$C_{i0} = \frac{\beta_i n_0}{\Lambda \lambda_i} \quad (3.2)$$

With n_0 the stationary number of prompt neutrons, β_i is the delayed neutron fraction of group i , λ_i is the decay constants and Λ is the neutron generation time.

3.2 Method of Simulation

For applying these simulation schemes on point kinetics model, an infinite homogeneous medium in one energy group is considered. The medium has an absorption cross section Σ_a and a fission cross section Σ_f . The time domain is divided into discrete time bins. These time steps are created for simulation control and for possible geometry changes, feedback effects etc. In the simulations, kinetics of a reactor is modeled initially in a critical state with equilibrium condition between neutrons and delayed neutrons precursors. Two simulation schemes for the point kinetic modeling are developed.

3.2.1 Simulation Scheme -1

Schematic representation of the algorithm for the simulation scheme 1 is shown in Fig. 3.1. Each neutron is tracked one by one and assigned weight 1.0. The capture cross section of the medium is subsequently adjusted to introduce the required reactivity (or K_∞ , infinite multiplication factor) the medium as given by

$$K_\infty = \frac{v \Sigma_f}{\Sigma_a} \quad (3.3)$$

To start with, the time of event of the neutron is estimated as given by

$$t = -\frac{1}{(v \Sigma_a)} \ln \xi \quad (3.4)$$

Where, v is the velocity of the neutron, Σ_a is the absorption cross section of the medium and ξ is a random number. If the time of event lies outside the time bin, neutron is stored in an array to be simulated for next time bin and all such neutrons will be tracked with their initial time being the

next time boundary. If the neutron event lies in that time bin, it is checked for the probability for fission or capture. If the capture occurs then the neutron chain dies out. If fission occurs then the number of neutrons produced in the fission is estimated and their time of production is also noted. Likewise all neutrons are tracked and their daughter neutrons are stored with their respective production time. Next, all the daughter neutrons produced are tracked in the same time bin. This process is continued until the neutron dies out due to capture or if the time of event lies outside the time bin such that there are no neutrons left in the subsequent generation. Also the precursors formed in each fission event are also recorded.

As discussed in Chapter 2, section 2.11.1, for a MC calculation it is important to have enough statistics per tally bin, and therefore, it is required that there should be enough delayed neutrons in each time bin. This can be achieved by allowing the natural decay of the precursors in each time bin. The probability that the precursors decay in the time bin of time width Δt is given by

$$P(t) = \lambda e^{-\lambda \Delta t} \quad (3.5)$$

Where λ is an isotope specific decay constant. At $t = 0.0$ s, there are neutrons (n_0) and delayed neutron precursors (C_0) corresponding to the equilibrium condition. A fixed fraction $f (=e^{-\lambda \Delta t})$ of the precursor population is allowed to deterministically decay in the time bin of size Δt . The balance $1 - f$ is carried over to the next time bin, where λ is the group specific decay constant. So, $C_0 f$ delayed neutrons are produced in the bin in addition to the neutrons at $t = 0.0$ s.

Delayed neutrons are then tracked in the similar way as prompt neutrons. At the end of the time bin, total number of neutrons and precursors formed are added to the undecayed precursors.

The neutron population is maintained to its initial value with weights reduced in the ratio of current to initial as per the following equation

$$W_{pi} = W_{pi-1} \frac{n_i}{n_0} \quad (3.6)$$

Where, W_{pi} is the current weight of the neutron, W_{pi-1} is the previous weight of the neutron, n_i is the current neutron population and n_0 is the initial neutron population. If the weights of the prompt

neutrons become less than the delayed neutron weights, renormalisation is not done. The precursors formed due to the fission of prompt neutrons carry the same weights.

Neutron weights given by equation (3.6) contributes to the neutron power as a function of time for a given reactivity. Flow chart of the calculation is shown in Fig. 3.2.

3.2.1.1 Numerical Results:

Firstly the simulation results of only with prompt neutrons are discussed. 10^4 neutrons are considered for simulation. Fig. 3.3 shows the variation of weight factor (given by equation (3.6)) with time in a medium with negative reactivity of 10 mk. It is observed that prompt neutron decay time constant, α estimated by the exponential fitting, is 109 sec^{-1} . It implies that prompt neutron population falls to its $1/e$ values in 10^{-2} sec and the neutron chain dies out in 10^{-1} s which is quite small as compared to the decay time of precursors. Also with rapid fall in neutron population lesser prompt neutrons are available for the simulation in the subsequent steps and it leads to large relative variance. This is controlled by the renormalising the prompt neutron population to 10^4 at each time step and reducing its weight in the same ratio as given by equation (3.6). Simulation is carried out for two different time widths, 3 msec and 4 msec. The value of α is same for the two time widths and agrees well with its analytical value of 109 sec^{-1} . Similarly, in Fig. 3.4 it is observed that for $\rho = +3 \text{ mk}$ neutron decay time constant is 16 sec^{-1} which means that neutron chain will rise to its $1/e$ value in 0.06 sec which implies that with time number of prompt neutrons to be simulated increases which will increase the computational time. This is reduced by renormalizing the neutron population at the end of each time bin to its value of 10^4 and reducing the weight of the neutrons by the expression given in equation 3.6.

Next simulation was carried out with 10^6 prompt neutrons and equilibrium concentration of precursors. Six group of precursors were considered and the corresponding kinetics parameters used are given in Table 3.1. Prompt neutron life time, $\ell_p = 1.8 \times 10^{-4} \text{ sec}$. Fig. 3.5 and 3.6 shows the variation of neutron power with time for different values of reactivity for the time step of 1 msec.

Equilibrium concentrations of precursors are considered and all the six group of precursors are allowed a natural decay in each time bin. It is observed for the step negative reactivity addition, there is prompt drop, slope of which is dictated by the prompt neutron decay time. Even though the prompt neutron chain dies out in 0.1sec as in case of $\rho = -10$ mk, but due the constant decay of the precursor in each time bin, there are enough delayed neutrons present in each time bin to maintain the neutron population. It is seen that after the decay time of the prompt neutron chain, neutron population within a time bin reduces to a very low value which leads to large relative variance of the order of 0.01. To overcome this, it is assumed that each precursor is splitted into 500 precursors and produces on decay delayed neutrons with reduced weight of 0.002. The precursors formed due to the fission of delayed neutrons will have same weight of 0.002. It is observed that with the precursor splitting, relative variance in the estimated power is reduced to ~ 0.001 as shown in Figs. 3.7 & 3.8.

3.2.2 Simulation Scheme -2

It is observed that in simulation scheme 1, by precursors splitting within a time bin, computational time is increased. To overcome this, the concept of mean sceondary neutrons, as discussed in chapter 2, was introduced in the simulation. Schematic representation of the algorithm for simulation scheme 2 is shown in Fig. 3.9.

Each neutron is tracked as follows. Initially (i.e. at $t=0$) a neutron carries a weight, $w = 1.0$. The time of the absorption event (t) of the neutron is given by the equation (3.4)

If the neutron event lies within the time bin, its weight is multiplied by the mean number of neutrons produced in the event which is given by,

$$w_{n_i} = w_{n_{i-1}} \nu \Sigma_f / \Sigma_a \quad (3.7)$$

Where, $w_{n_{i-1}}$ is the weight of the neutron entering the collision (in this case the absorption event) and w_{n_i} is the weight of the emerging neutron from the collision event. In the general case this is the mean number of secondaries per collision including prompt fission neutrons. In the point model,

this is simply the prompt K_{eff} and is selected with a probability proportional to $(1-\beta)$. With a probability β the neutron history is terminated and with a probability β_k/β a k^{th} group precursor is created at that time (and place) of the event with weight given by

$$w_{\text{ck}} = w_{n_{i-1}} v \Sigma_f / \Sigma_a \quad (3.8)$$

In case a precursor is not formed, the neutron history is continued further till the time of the absorption event falls outside the time bin. Once the time goes beyond the bin limit, the history is terminated and the weight of the neutron is stored in an array to be simulated for next time bin. The initial time of this resumed history is the time boundary of the next time bin.

The precursor modeling is similar to simulation scheme 1. The instantaneous neutron power at the time boundaries of each time step can be estimated using the estimator

$$P(t) = \varepsilon \sum_i w_i V_i \Sigma_{\text{fi}} \quad (3.9)$$

where ε is the energy per fission, w_i is the neutron weight of the i^{th} neutron, V_i is velocity of neutrons and Σ_{fi} is the fission cross section. The summation is over all neutrons at that instant. While this estimator has the advantage of giving the instantaneous power, the statistics depends upon the total neutron number and will be poor. Alternatively, the power by averaging it over a time bin by the usual collision or track length estimators may be obtained. While averaging the power over time bins may have advantage in terms of statistics, the bins must be small compared to the instantaneous period and correlations in temporal fluctuations might give estimates of errors lower than they actually are.

Binning serves the twin purposes of obtaining (average) power tally during the time period of a bin and that of making changes in the system (geometry, cross sections) at the end of a time bin. Clearly the bin size will be determined by two considerations (i) the rate of rise of power (ii) the rate at which the system itself changes. Ideally the aim would be to obtain results that have an accuracy that is independent of the bin size and free from bias. Practically speaking this may not be possible in all situations.

For sub prompt critical transients, the power is governed primarily by the delayed neutron source that changes slowly with time. The device of forced decay of precursors injects the same number of delayed neutrons in each bin and hence the variance is expected to be practically independent of the bin size.

For super prompt critical transients, the precursors play very little role and hence the neutron population at the beginning of a bin (which is fixed) will primarily determine the number of particles available for producing tracks during the time bin. The number of tracks actually produced will depend upon the size of the time bin and will be larger for longer time bins. Even though the tracks produced by the progeny of a given starting particle are not independent of one another, the variance will be lower for more tracks than for fewer tracks. This is expected to be true for total power, and most certainly so for the power distributions. Thus, in this situation, one would expect the statistics to deteriorate with decreasing size of the time bins. Collision estimators would be fare worse. The instantaneous estimator described in Eq. (3.9) is the limit of the track length estimator for short time bins.

At the end of each time bin, the number of neutrons that have crossed the time boundary are summed up. Neutron population at the next time boundary can be more or less than the initial neutron population depending upon the reactivity inserted in the system. At this instant, the scheme proposed for population control is applied. The neutron population at the time boundary is maintained as its initial value and the weight of each neutron is altered as per equation (3.6). The precursors formed due to the fission of neutrons carry the same weights as the neutron that produced them.

3.2.2.1 Numerical Results

A number of problems were studied in this category. These are (i) a neutron pulse introduced in a sub critical reactor; (ii) introduction of a positive step reactivity ($< \beta$) in a critical reactor; (iii) validation with analytical benchmark; (iv) positive ramp reactivity in an initially critical reactor; (v)

positive step reactivity with feedback; (vi) transient analysis of Compact High Temperature Reactor (CHTR) (vii) transport equivalent simulations. A comparison of results obtained by MC scheme with those based on analytical solutions or a point kinetics code is described.

(i) *Sub critical reactor transients*

Two problems are studied in this category. In the first of these, only neutrons are present initially (at $t=0$) in a subcritical system (reactivity -10 mk) and the decay of the neutron population together with the build up and decay of precursors is simulated. In the second simulation, the transient is produced by introducing a step reactivity of -10 mk in a critical reactor in which neutrons and delayed neutron precursors have reached equilibrium. The prompt neutron lifetime is taken to be 1.7×10^{-4} sec. The macroscopic cross sections, neutron lifetime and six group delayed neutron precursor yields and decay constants used in these simulations are given in Table 3.1.

The calculation procedure follows the scheme described in Section 3.2.2. A fixed fraction of precursors is allowed to decay in each time bin. The neutron power at the end of each time bin is calculated using the instantaneous power estimator. The neutron population and the time bin width are chosen to be 10^5 and 1 msec respectively. Variation of the weight factor (corresponding to the neutron power and given in equation (3.6)) with time for the two simulations are plotted in Fig. 3.10. It is observed that, in the first simulation with only neutrons at $t=0$, the neutron decay time, $\alpha(\alpha = (k-1)/\ell)$ estimated by the exponential fitting, is 59 sec^{-1} . It implies that neutron population falls to its $1/e$ values in 10^{-2} sec and the neutron chain dies out in 10^{-1} sec which is quite small as compared to the decay time of precursors to form delayed neutrons. It implies there are very few neutrons that are sampled at a given time and this will lead to fluctuations in the tallied quantities like neutron power and neutron flux.

In the simulation start with neutrons together with the equilibrium concentration of precursors (as given by eq. (3.2)). There is a prompt drop, the slope of which is dictated by the neutron decay

constant α , followed by a slower decay of power. Even though the initial neutron population dies out rapidly (in about 0.1 sec), the constant source due to decay of the precursors in each time bin maintains the neutron population to a sufficiently high level. Additionally, the use of the mean number of secondary neutrons produced in each neutron (absorption) event, keeps the relative variance in the simulation extremely low. The simulation is in excellent agreement with results obtained using the GEAR (Podar et. al, 1989). The simulations confirm the proposed precursor modeling in which a fixed fraction of precursors is allowed to decay within each time bin. This helps to maintain a fairly constant neutron population within a bin and thereby reduces population fluctuations and hence the relative variance.

(ii) Positive step reactivity in a critical reactor

In another simulation, the neutron power is estimated till 6 reactor periods after insertion of positive step reactivity of +3 mk as shown in Fig. 3.11. Prompt neutron life time, $\ell_p = 1.8 \times 10^{-4}$ sec. Other kinetic parameters used are the same as in the previous simulation and are given in Table 3.1. The estimated relative variance and computational time obtained for this simulation for the simulation scheme 1 and 2 are compared in Table 3.2. It is seen the relative variance estimated in the simulation with concept of mean secondary is lesser and also it is faster than the simulation scheme 1. The simulated neutron power by simulation scheme 2 is compared with that obtained by the GEAR code. This demonstrates the validity of the method for the longer times. For the same simulation, the growth of the precursor concentration for each group as a function of time is plotted in Fig. 3.12 and is compared with the corresponding point kinetics code values. They are found to have similar trend.

(iii) Validation with Analytical Benchmarks

This method is also validated against reactor kinetics benchmarks. Kinetic parameters given in Table 3.3 are used and neutron life time, $\ell = 2 \times 10^{-5}$ sec. Table 3.4 and 3.5 gives the values of

neutron power with time obtained by the GEAR code and available analytical solutions (Yamoah et. al., 2013) and are compared with the MC simulations for step reactivity of +3 mk and -7 mk. Results obtained by MC simulation are found to compare within the standard deviation with that estimated by point kinetics code GEAR and reported by analytical solution.

(iv) Positive ramp reactivity in a critical reactor

The insertion of ramp reactivity is also tested by MC simulation method. Fig. 3.13 shows the variation of neutron power with time for a ramp reactivity of 0.1 mk /sec. 10^5 neutrons and 10^9 precursors are considered at $t=0$. Kinetic parameters given in Table 3.1 are used. The figure also shows a comparison with results obtained using the GEAR code. It is seen that the agreement between the two is excellent.

(v) Positive step reactivity (with feedback) in a critical reactor

Power reactors generally have a reactivity feedback due to temperature changes of fuel, moderator, coolant etc as a result of power changes. Negative feedback helps to stabilize the reactor operation and also limits the power rise in case of an accidental increase in reactivity. The fastest response is due to temperature change of the fuel which is prompt and this is most important in stable operation of reactor. The negative temperature coefficients also limit the power rise in supercritical transients. The reactivity feedback coefficients are of three or four types. The most important of these is the fuel temperature coefficient and arises primarily due to the Doppler broadening of resonances. A smaller contribution is due to expansion of the fuel elements / reactor core and is particularly important in fast reactors. The fuel temperature feedback is the fastest acting and is also called the prompt temperature coefficient and must be negative. Slower acting effects are due to temperature changes of the coolant / moderator and due to changes in the density due to boiling (called voiding) of the coolant. A simple model in this case is the lumped parameter model. Simple equations are written down for the average fuel temperature, coolant temperature and density as follows:

$$\frac{dT_f}{dt} = -h(T_f - T_c) + \alpha n$$

$$\frac{dT_c}{dt} = h(T_f - T_c) + b(T_c - T)$$

T_f is the fuel temperature

T_c is the average coolant temperature

$$h = \frac{P_0}{T_{fo} - \bar{T}_c}$$

The last of the problems studied introduces a simple reactivity feedback based on the fuel temperature reactivity coefficient. The rise of neutron power with time with and without fuel temperature feedback was estimated for a step reactivity insertion of +3 mk. The fuel temperature at each point on the time grid is calculated using the equation

$$T_{fn+1} = \left[\frac{(\gamma P(t) + d)\Delta t}{1 + a_{11}\Delta t} \right] + T_{fn} \quad (3.10)$$

that is a discretised version of the following equation representing nuclear heating and Newtonian cooling by a coolant at a fixed temperature.

$$M_f C_f \frac{dT_f}{dt} = P(t) - h_f(\bar{T}_f - \bar{T}_c) \quad (3.11)$$

Where,

M_f is the mass of the fuel

C_f is the specific heat capacity of the fuel

T_f is the fuel temperature

\bar{T}_c is the average coolant temperature

$$\gamma = 1/M_f C_f$$

$$d = h_f \bar{T}_c / (M_f C_f)$$

$$a_{11} = -h_f / M_f C_f$$

$$h_f = \frac{P_0}{T_{fo} - \bar{T}_c} = 0.658545 \text{ MW}/^\circ\text{C}$$

The feedback reactivity is calculated using the equation

$$\rho_{\text{feed}} = \rho_0 + \alpha_f \Delta T_f \quad (3.12)$$

where,

ρ_{feed} is the feedback reactivity

ρ_0 is the external reactivity

α_f = fuel temperature co-efficient = $-1 \times 10^{-7} \text{ } ^\circ\text{C}$

Other input data used in the calculation are given in Table 3.6.

Fig. 3.14 shows the variation of the feedback reactivity with time. Feedback reactivity is estimated using the equation (3.12). Initially at $t = 0.0$ s, feedback is zero so the positive reactivity added to the system is +3 mk but, at the next time step, feedback reactivity is estimated by equation (3.12). Negative feedback reactivity increases with time and accordingly the weight factor also decreases with time for simulation with negative feedback as shown in Fig. 3.14. The variation of power with time is plotted in Fig. 3.15. It is seen from Fig. 3.15 that without fuel temperature feedback, the weight factor, which is measure of neutron power rises to 1000 times its initial value, but with feedback it is restricted to less than 10 times the initial value.

The power reaches a maximum at 23.2 seconds and starts falling thereafter well before the reactivity becomes negative (at about 39.1 seconds). This is due to the fact that in sub prompt critical transients, the power is essentially determined by the neutron source due to decay of the precursor population and the prompt reactivity. Since the precursor population changes slowly over time scales of the order of the precursor decay constant, a rapid fall of reactivity can cause the power to fall even though the reactivity is positive. A solution of the one delayed-neutron-group kinetics equations in the prompt jump approximation discussed in section 1.5.1.4 gives the following expression for the variation of the neutron population with time

$$n(t) = n_0 \left(\frac{\beta}{\beta - \rho(t)} \right) \exp \left(\int_0^t \frac{\lambda \rho(t')}{\beta - \rho(t')} dt' \right) \quad (3.13)$$

On differentiating w.r.t. t , the following condition for the derivative of $n(t)$ to be negative is obtained

$$\frac{1}{\rho} \frac{d\rho}{dt} < -\lambda \quad (3.14)$$

In the present case the power starts falling when the rate of relative reactivity decrease exceeds 0.07, which is fairly close to the average precursor decay constant value of 0.078. Fig. 3.15 also shows a comparison with the results obtained using the deterministic point kinetics code and the agreement is seen to be very good. Sjenitzer et. al, 2011 has reported that the results of non linear kinetics in case of thermal hydraulics feedback produces a bias in the mean if the number of particles per batch is very small. In the above involving feedback the results do not show any bias (at least the comparison with the deterministic results shows good agreement). However, in this case batch size was quite large (10^4) and hence the bias observed in the above work is not observed.

(vi) Transient analysis of Compact High Temperature Reactor (CHTR) with temperature feedback reactivity

A reactivity transient analysis of CHTR core was simulated with the feedback modeling. Kinetic parameters used are mentioned in Table 3.7. In the study of transient, the rising power (neutron density) in CHTR core due to positive reactivity insertion has been arrested with negative feedback from fuel temperature rise (1000 °C to 1300 °C) only. For comparison, a case has been studied when +2 mk reactivity inserted in the core in 5.0 sec and variation of relative power (neutron density) and feedback reactivity has been followed up to 10 min. Fuel temperature coefficient $\alpha_f = -0.0001 \text{ } ^\circ\text{C}$ and prompt neutron life time, ℓ_p in the analysis is taken to be 0.0015 sec. Simulated power was compared with ARCH Code (Dwivedi et. al., 2014) as shown in Fig. 3.16. It is seen that the agreement between the two is good and is within the standard deviation of ± 0.001 .

3.3 Conclusions

Time dependent MC method to solve point kinetics equations has been developed. The method includes the sampling of prompt and delayed neutrons, modeling of six groups of precursors, neutron population control using weights. Two simulation schemes were studied. It was found that with the use of mean secondary concept in simulation scheme 2, relative variance is reduced and computational speed is faster. Variations of neutron power for different reactor states are compared with the analytical solution and with other point kinetics code. Results are also validated against the benchmark problems and are found to be in good agreement. Fuel temperature feedback model was also implemented and was tested for transient analysis. It is observed that Point Kinetics based MC simulations can be carried out with minimum variance. Actual time dependent transport MC would however show much larger variance.

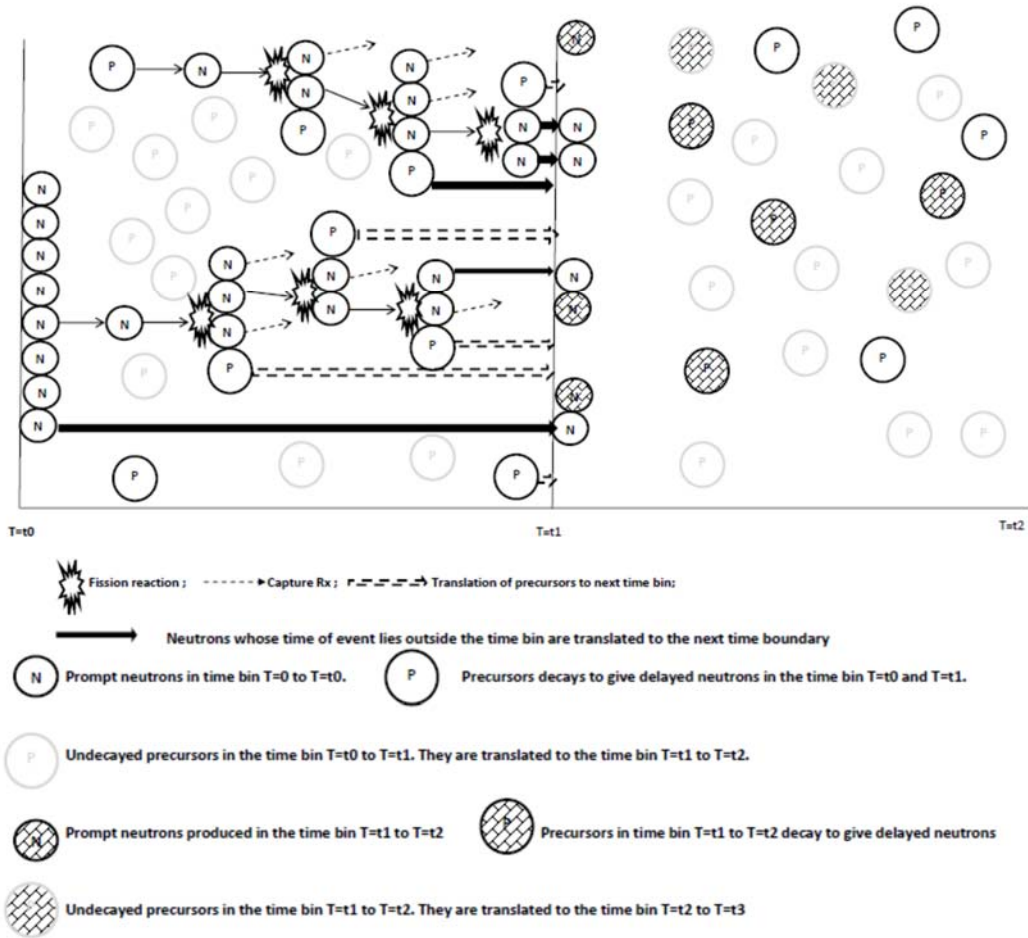


Fig. 3.1 Schematic representation of the MC Algorithm based on Simulation Scheme-1

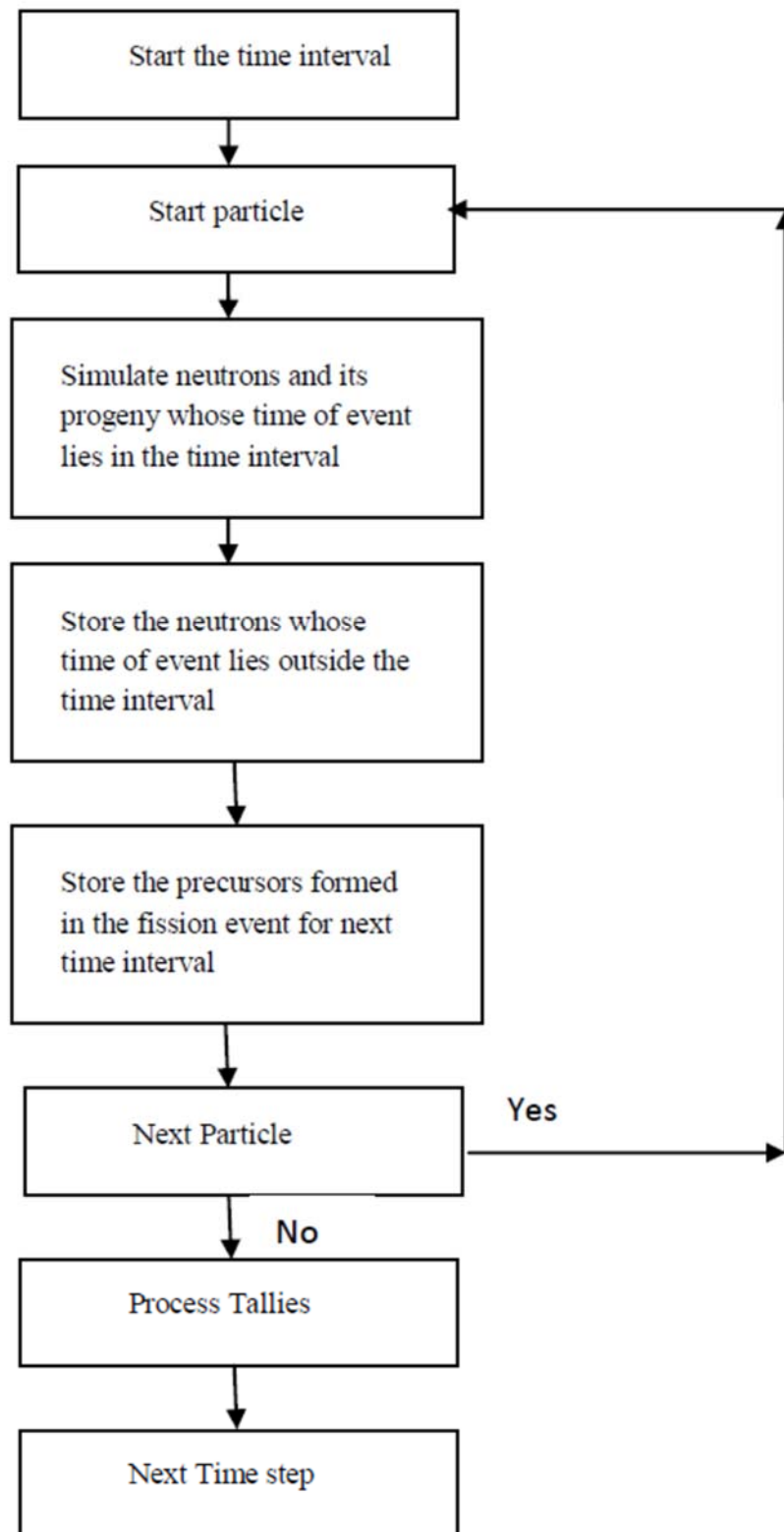


Fig. 3.2 Flow of the program for the Simulation Scheme -1

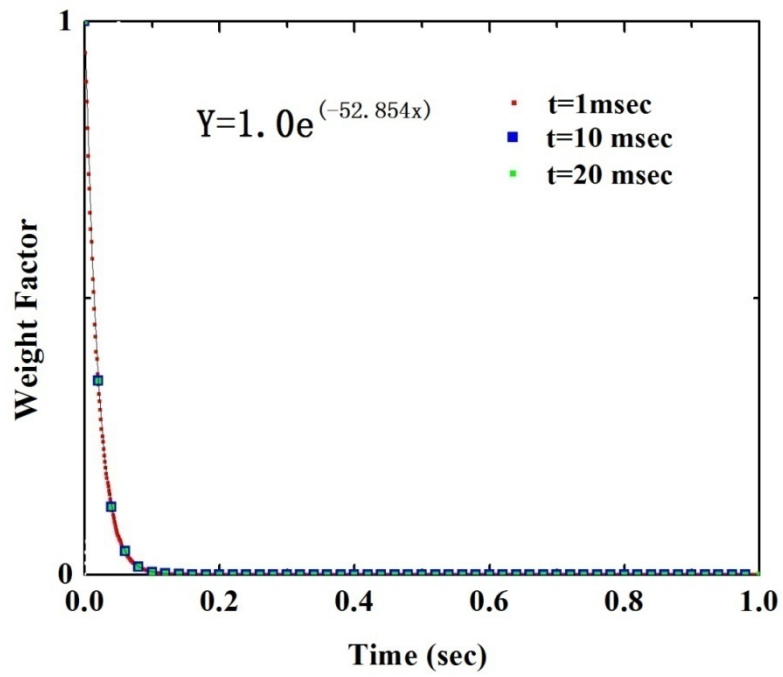


Fig. 3.3 Variation of prompt neutron weight factor with time for step negative reactivity of -10 mk added at t=0.

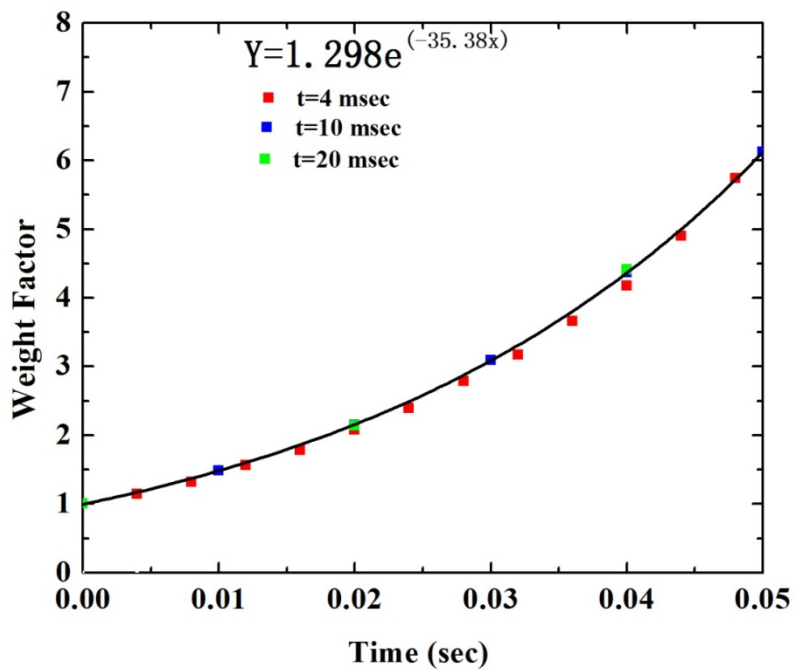


Fig. 3.4 Variation of prompt neutron weight factor with time for step positive reactivity of +3 mk added at t=0.

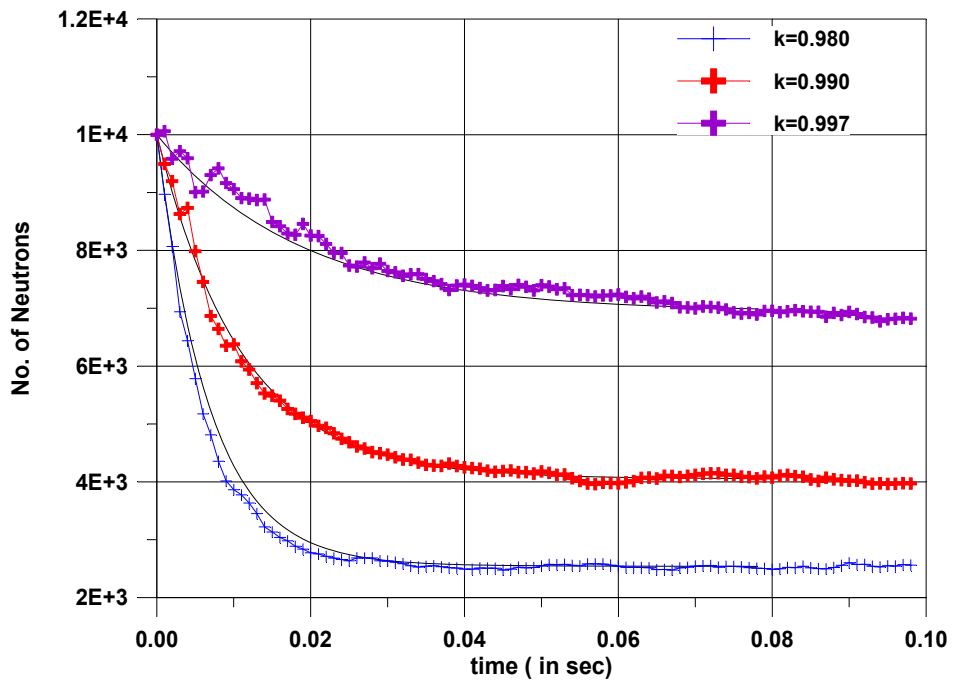


Fig. 3.5 Variation of neutron power with time for step reactivity of -20 mk, -10 mk and -3 mk

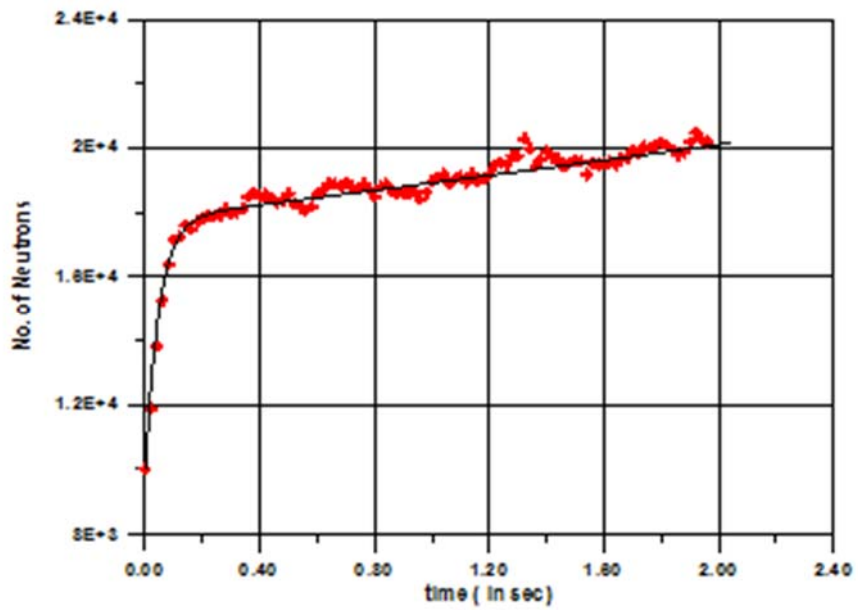


Fig. 3.6 Variation of neutron power with time of +3 mk step reactivity.

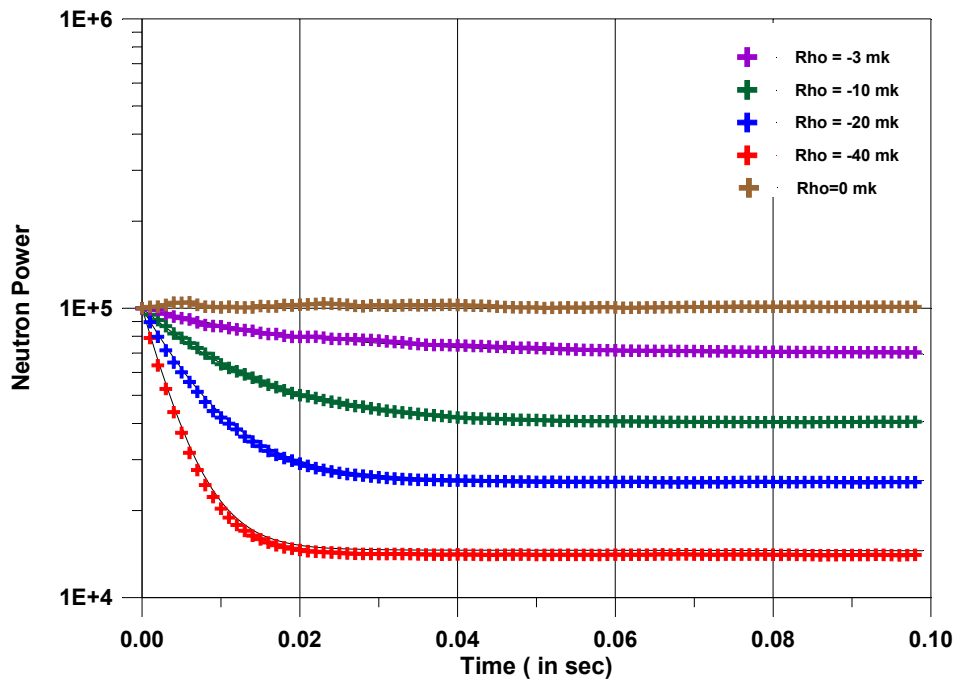


Fig. 3.7 Variation of neutron power with time for step reactivity of -20 mk, -10 mk and -3 mk with precursor splitting model

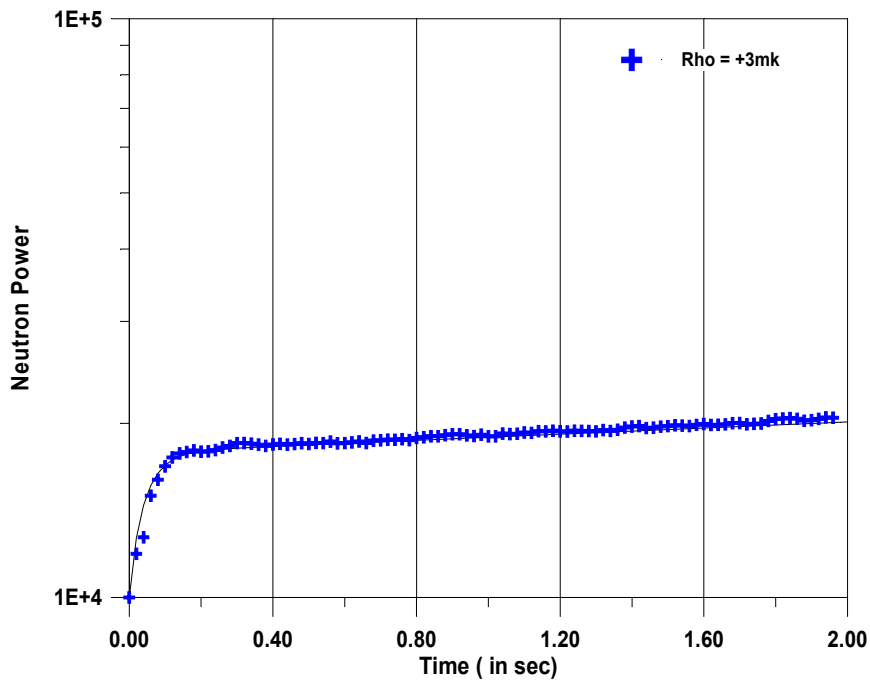


Fig. 3.8 Variation of neutron power with time of +3 mk step reactivity with precursor splitting model

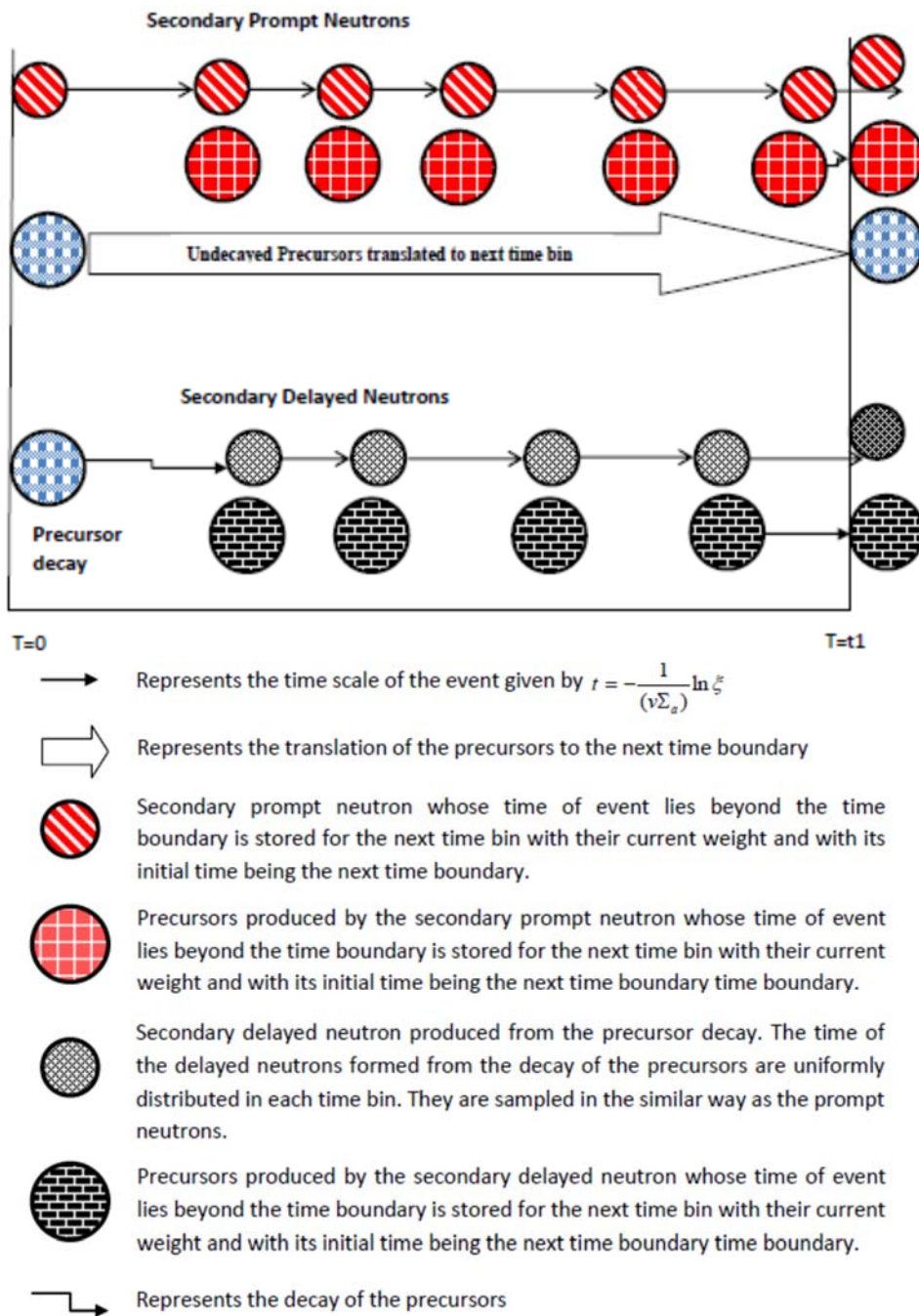


Fig. 3.9 Schematic Representation of the Simulation Scheme 2

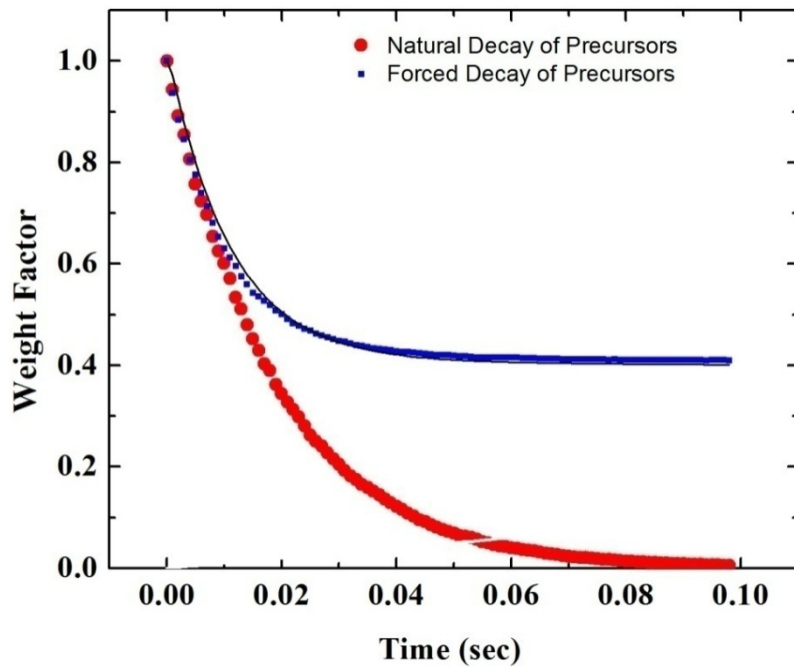


Fig .3.10 Variation of the neutron population (neutron weight factor) with time, for $\rho = -10$ mk The solid curve shows the results obtained using the Point Kinetics code GEAR.

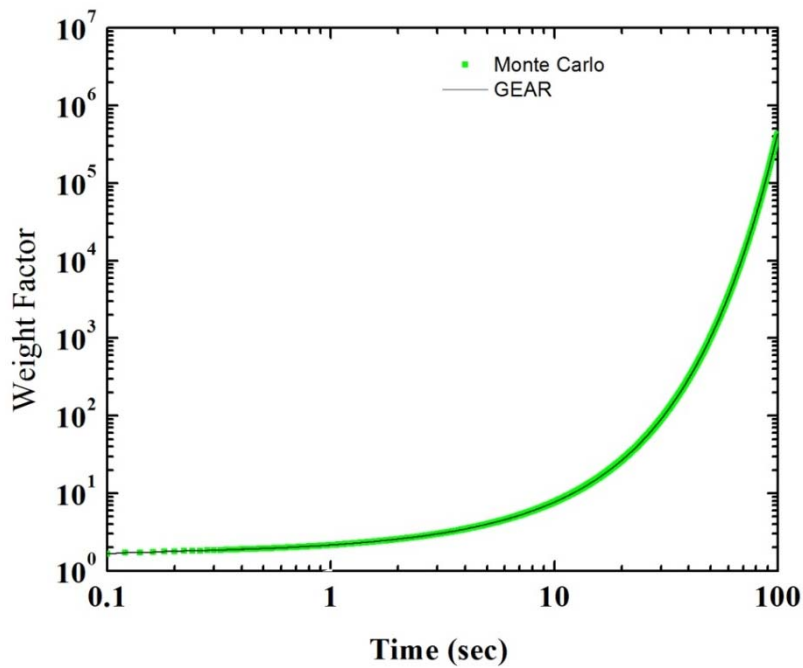


Fig 3.11 Variation of the neutron power estimated by the MC method (with six groups of delayed neutron precursors) for a step increase in reactivity by +3 mk in a critical reactor.

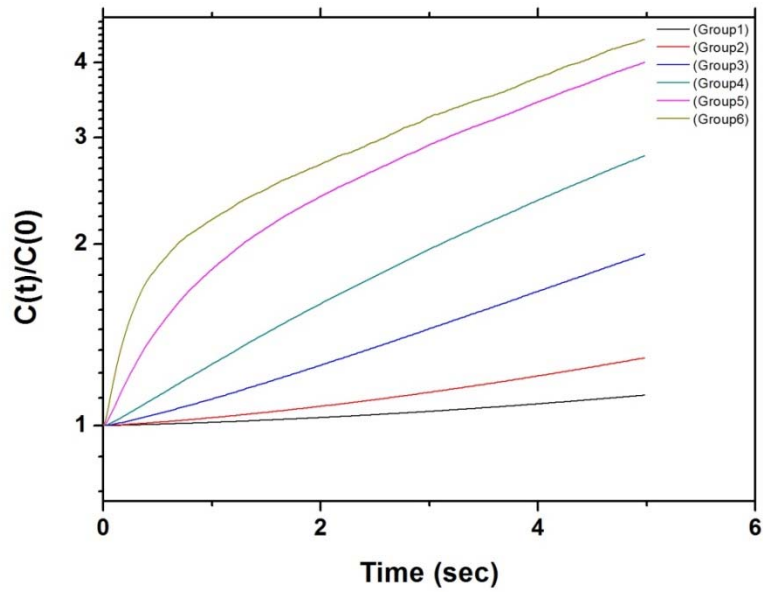


Fig 3.12 Change in the precursor concentrations with time in the MC simulation of the problem involving a step reactivity insertion of +3 mk in a critical reactor

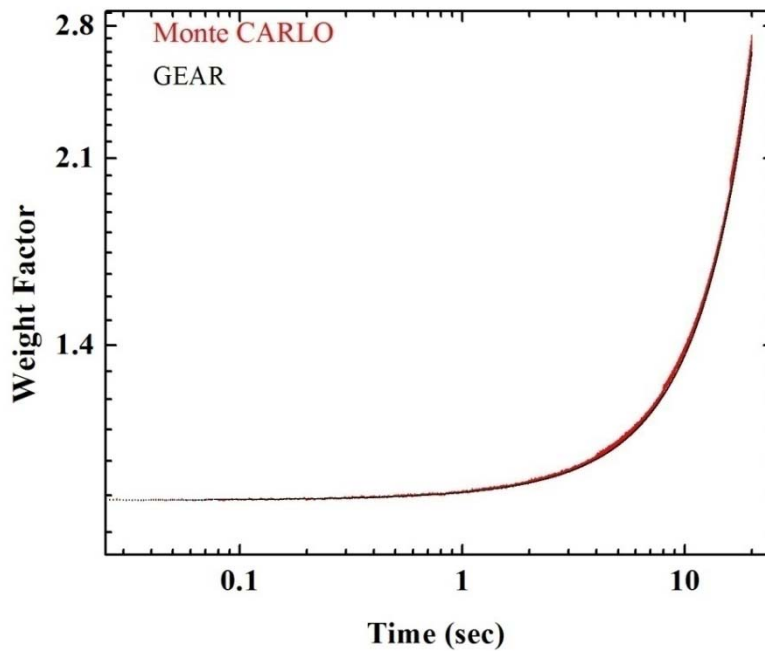


Fig 3.13 A comparison of the variation of the neutron power with time as estimated by a point model MC simulation with GEAR for a ramp reactivity insertion rate of 0.1 mk/sec.

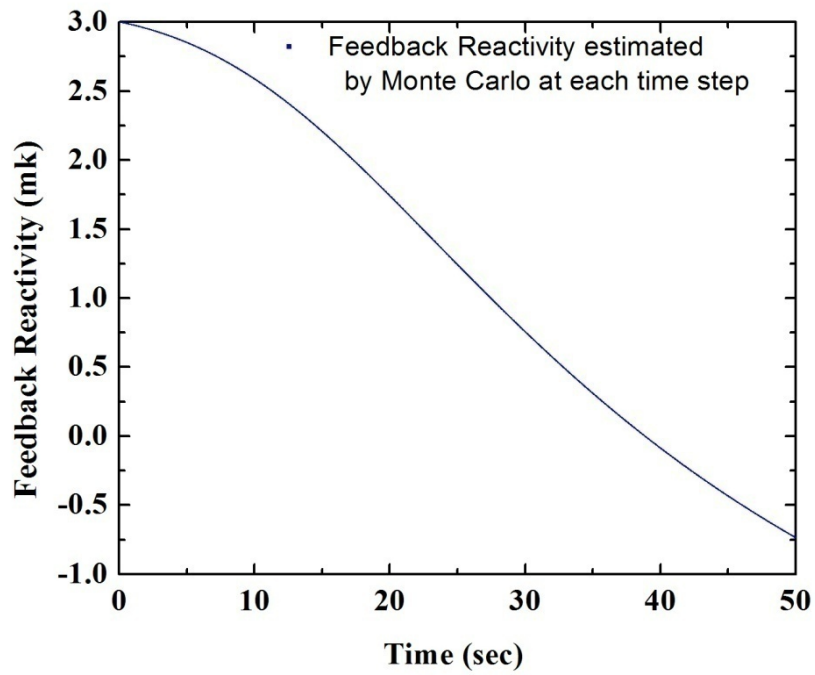


Fig. 3.14 Variation of neutron power with time with and without fuel temperature feedback modeling for a step reactivity insertion of +3 mk.

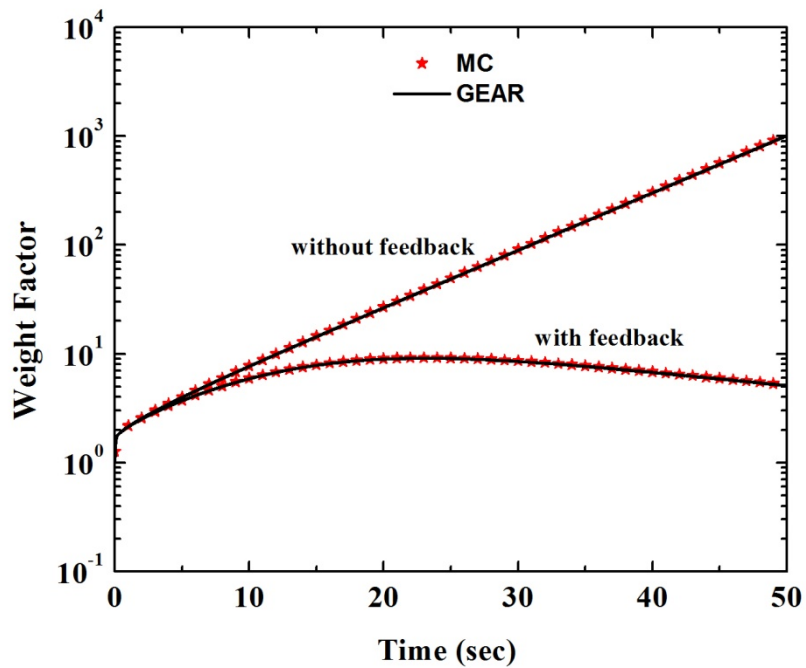


Fig. 3.15 The fuel temperature feedback reactivity as a function of time

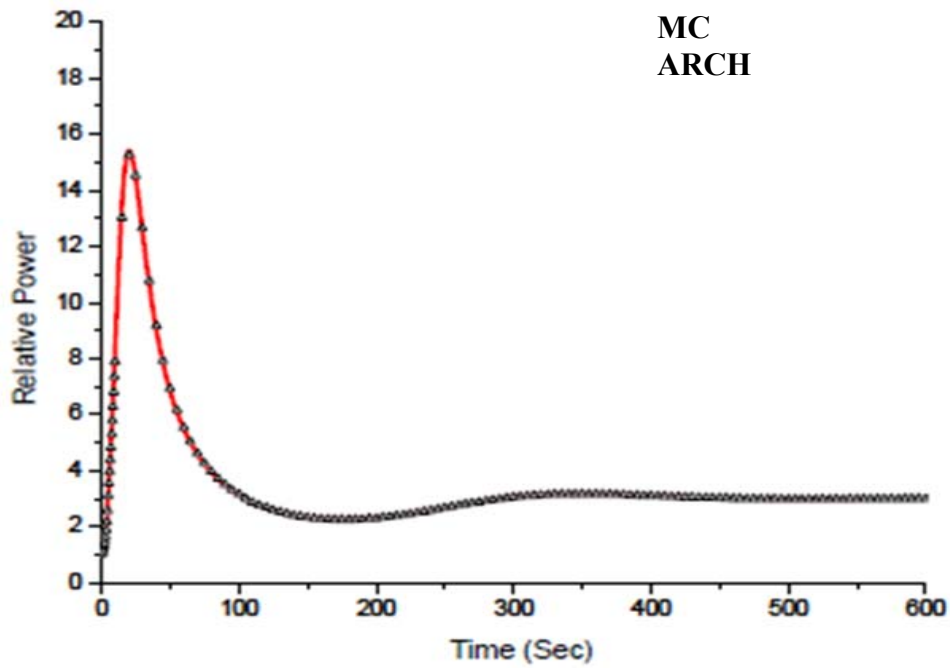


Fig. 3.16 Variation in relative power for CHTR core for step reactivity insertion of +2 mk in 5 sec.

Table 3.1 Kinetics parameters for 6 groups of delayed neutron precursors

$\lambda_d(s^{-1})$	0.0127	0.0317	0.115	0.311	1.40	3.87
β_d	0.000266	0.001491	0.001316	0.002849	0.000896	0.000182
λ						β_{eff}
= 0.0784sec ⁻¹						= 0.00685

Table 3.2 Comparative study of the computational time and variance estimated by simulation schemes 1 and 2 for step reactivity insertion on + 3 mk

Model	Computational Time	Standard Deviation
Simulation Scheme - 1	~ 30 sec	± 0.03
Simulation Scheme - 2	~ 3 sec	± 0.004

Table 3.3 Delayed neutron and cross section data used as input in the point model benchmarks (Yamoah et. al. 2013)

$\beta_i/\beta_{\text{eff}}$	0.038	0.213	0.188	0.407	0.128	0.026
λ_i (s ⁻¹)	0.0127	0.0317	0.1156	0.311	1.4	3.87
β_{eff}				0.007		
λ_{avg} (s ⁻¹)				0.0784		
ν				3.24		
Σ_f (cm ⁻¹)				0.007530		
Σ_a (cm ⁻¹)				0.02681		
ℓ_p (s)				1.7 x 10 ⁻⁴		
V(cm/s)				220000		

Table 3.4 Comparison of the neutron power (= N(t)/N(0) by point model MC for a -7 mk negative step reactivity insertion in a thermal reactor with analytical solutions and GEAR Code.

Time (s)	Analytical Solution	GEAR Code	Monte Carlo
0.0	1.0000	1.0000	1.0000
0.2	1.8513	1.8513	1.8473 ± 0.0035
0.4	1.9476	1.9476	1.9408 ± 0.0041
0.6	2.0379	2.0379	2.0372 ± 0.0048
0.8	2.1248	2.1248	2.1194 ± 0.0090
1.0	2.2098	2.2098	2.1938 ± 0.0066

Table 3.5 Comparison of the neutron power (= N(t)/N(0) by point model MC for a -7 mk negative step reactivity insertion in a thermal reactor with analytical solutions (Yamoah et. al, 2011) and GEAR Code.

Time (s)	Analytical	GEAR Code	Monte Carlo
----------	------------	-----------	-------------

Solution			
0.0	1.0000	1.0000	1.0000
0.2	0.4807	0.4810	0.4812 ± 0.0044
0.4	0.4653	0.4653	0.4623 ± 0.0022
0.6	0.4519	0.4520	0.45153 ± 0.0043
0.8	0.4402	0.4403	0.4346 ± 0.0046
1.0	0.4297	0.4298	0.4301 ± 0.0028

Table 3.6 Feedback parameters for modeling the problem of a +3 mk step reactivity insertion with fuel temperature feedback

Parameter	Value
Power P_0	90 MW
M_f	2680 kg
\overline{T}_{fo}	390 °C
\overline{T}_C	253.335 °C
C_f	7.4×10^{-2} cal/gm °C
γ	5.0423×10^{-6} °C/cal
d	200.885 °C/s
a_{11}	-0.7929636 / s
h_f	0.658545 MW/°C

Table 3.7 Kinetics parameters for 6 groups of delayed neutron precursors for ARCH Transient Analysis

$\lambda_d (s^{-1})$	0.00031	0.00087	0.00063	0.00127	0.00051	0.00094
β_d	0.01527	0.03862	0.13614	0.34111	0.92435	2.76407

 β_{eff} 0.00454

Diffusion Theory Monte Carlo: Model Description and Extension

In the previous Chapter the application of some of the ideas regarding Monte Carlo Kinetics to the simplest model viz. the point kinetics model is discussed. In this chapter another model for studying Monte Carlo space time kinetics viz. the Diffusion theory Monte Carlo Model is introduced.

Monte Carlo Methods for solving problems in Diffusion Theory have been studied by Booth, 1981; Sadiku, 2006. Rana and Degweker, 2013 developed the analytical Green's function approach as well as the finite difference based numerical approach for diffusion theory Monte Carlo. The present chapter is based on and is an extension of their work..

For full Space-Time Space Time Monte Carlo Simulations, both spatial as well as temporal variation of the neutron and precursor concentrations has to be modeled. The model discussed in this chapter allows to apply the schemes for modeling the spatial variation of neutrons and precursors. Besides providing a simple model for testing these ideas regarding Monte Carlo space time Kinetics, the diffusion theory MC model permits an exact comparison of the results of MC simulation with the large number of kinetics benchmarks that have been solved using deterministic diffusion theory methods. This is particularly important since there are very few 'exact' benchmarks that are based on transport theory MC

There is another reason for interest in the study of this model. MC calculations are mostly performed by the non analog technique for the purpose of computational efficiency. However, for simulation of noise experiments for measurement of reactor kinetics parameters such as reactivity, the analog MC is more appropriate. There has been a lot of theoretical and experimental interest (Pazsit et. al., 2005; Degweker et. al., 2003; Munoz Cobo et. al. 2001) in recent times in the noise methods for sub criticality measurement of accelerator driven systems. This also includes noise simulation using standard MC codes after removing all non analog features (Yamamoto et. al., 2011). While there have been suggestions (Szeiberth et. al., 2010) that non analog methods can be

used for this purpose, they will have limitations such as being applicable for the specific stochastic descriptor for which the tallies have been corrected and would certainly not be suitable for estimating errors due to statistics or dead time effects. Since analog MC is highly computational time consuming, the concept of the diffusion theory based analog MC technique to reduce the computing time was proposed by Rana and Degweker, 2013. This is based on the observation that in a variety of situations, diffusion theory, an approximate form of transport theory is very successful in giving quick results which may be fairly close to transport theory. It was shown that the methods of Diffusion MC developed are quite successful in simulating noise experiments.

Two approaches - viz., the analytical Green's function method and the finite difference method - were developed by Rana and Degweker, 2013. In analytical Green's function method they use analytical solutions of diffusion equation to construct probability distribution function for neutron absorption in a medium. The analytical Greens function approach has several advantages such as speed and exactitude, but was applicable to a rather restricted class of problems, such as the bare homogeneous reactor. A number of developments in this approach have been carried out and these form the subject of the present chapter.

With the developments discussed in this chapter the Analytical Greens Function MC becomes a useful tool of stochastic space time kinetics primarily for simulating noise experiments. On the other hand the finite difference diffusion MC is useful for exact comparison with diffusion theory benchmarks and forms the subject for the next chapter.

It was mentioned in earlier works (Rana and Degweker, 2013) that analytical Greens function method can be used for (a) infinite homogeneous medium and (b) bare homogeneous reactor of the rectangular geometry. Some recipes were proposed (without proof) for treating other situations like cylindrical geometry and non homogenous media.

The analytical Greens function (AGF) approach is further developed, to demonstrate its utility in a wider class of problems including homogeneous cylinders and heterogeneous reactors. In this Chapter, mathematical and numerical proofs of the validity of these recipes which were proposed

for such systems is provided. Other limitations of Diffusion MC Methods and means to overcome these are also discussed. It is well known that diffusion theory is not valid (a) close to localized sources (b) close to vacuum boundary (c) inside and close to strong absorbers (d) highly anisotropic scattering. In all such cases, the flux gradients are very sharp and the angular distribution of the flux is highly anisotropic causing the diffusion approximation to break down. Corrections to diffusion MC methods to overcome these limitations is applied.

With these developments, the Analytical Greens Function MC becomes a useful tool of stochastic space time kinetics primarily for simulating noise experiments. On the other hand, the finite difference diffusion MC is useful for exact comparison with diffusion theory benchmarks and forms the subject for the next chapter.

4.1 Earlier Work

4.1.1 Probability Distribution Function for Infinite Homogenous Medium

The probability distribution function (pdf) for simulating infinite homogeneous medium with Diffusion MC was derived by solving the one group time dependent diffusion equation using Fourier and Laplace transforms (Rana et. al., 2013).

It was shown (Rana et. al., 2013) that for a single source neutron initially (at $t=0$) located at the origin in an infinite homogeneous medium, the flux is given by

$$\varphi(\vec{r}, t) = \frac{v}{4\pi Dvt} e^{-\frac{r^2}{4Dt}} e^{-\lambda t} \quad (4.1)$$

where v is the velocity of the neutron and D is the diffusion coefficient. The neutron life-time in an infinite medium is given by $l=1/\nu\Sigma_r$. The probability that a neutron will be removed in the small space time interval $dx dy dz dt$ is obtained by multiplying the flux with the macroscopic removal cross section Σ_r to give

$$P(x, y, z, t) = \frac{1}{4\pi Dvt} \exp(-t/l) \frac{1}{l} \quad (4.2)$$

The marginal distribution for the removal time is obtained by integrating equation (4.2) over the space variables and $\int \frac{1}{l} \exp(-t/l) dt$ is obtained. The conditional distribution for the space variables for a given value of time is obtained by dividing equation (4.2) by the marginal distribution. The conditional distribution is given by

$$\frac{1}{4\pi Dvt} \exp(-t/l) \quad (4.3)$$

The conditional distribution can be written as a product of the three Gaussians for the three coordinates, each having zero mean and $\frac{2Dvt}{3}$ as variance. Therefore the position and time of absorption of a neutron in an infinite medium with Diffusion MC using pdf given in equation (4.2) with the following scheme can be sampled. First the time as an exponential distribution (with mean as l) is sampled. Then the position coordinates as three independent Gaussians, each with zero mean and $\frac{2Dvt}{3}$ as the variance (for the sampled value of time) is sampled. In what follows, variants of the above sampling scheme for finite and multi-region medium (with same or different diffusion coefficients and absorption cross-sections) is employed.

4.1.2 Bare Homogenous Reactor: Method of Images

For a point source in an infinite medium, pdf described in the previous section can be used. To use these pdfs for bare homogeneous reactor of rectangular and cylindrical geometry, the method of images was developed (Rana et. al., 2013) to reproduce zero flux boundary condition.

Rectangular Parallelepiped

Rana et. al. (2013) also showed that the zero flux boundary condition for a bare homogeneous reactor can be simulated by locating suitably placed image sources outside the reactor, for one, two

and three dimensional rectangular geometries. Unlike the case of electrostatics where an infinite number of images are required, one, three or seven images (depending upon whether the source is near a face, edge or corner) placed outside the reactor volume suffice to reproduce the zero flux boundary condition (Jackson, 1958). This makes the problem fairly tractable.

4.2 Further development & Extension of the method of images

4.2.1 Right Circular Cylinder

It is difficult to reproduce the zero flux boundary condition on the curved surface exactly using the method of images. Since the problem is not exactly solvable in terms of simple function, a simplifying argument is used. The crux of this argument is that the use of the image point at an equal distance is equivalent to using the tangent plane as the boundary. Hence, the material between the tangent plane and the curved cylindrical surface can scatter neutrons back into the cylinder (i.e. act as a reflector) and this is incorrect. To correct this we try to estimate this effect in the form of the reflector savings of this material and subtract this from the extrapolation distance (that is used for a vacuum boundary). Since the reflector material in this situation has a thickness that varies from point to point along the curved surface, (being larger for points away from the line joining the source and the image and smaller otherwise), it is not immediately clear what thickness (and corresponding reflector saving value) should be used. We proceed as follows. We obtain the reflector thickness from the geometry of the situation in the plane P' and use it to estimate the reflector saving. We use the expression for the flux in this plane due to a point source (in an infinite medium) as a weighting function to find the average reflector saving.

We place an image source in a transverse plane containing the source along the diameter joining the centre (axis) and the source point and at an equal distance outside the cylinder as shown in Fig. 4.1 and applying a small correction to the extrapolation distance. In what follows, an analytical expression for this correction is obtained.

The image causes the flux to be zero at the tangent plane rather than at the circular boundary. A reflector causes the flux to go to zero at a distance beyond the usual extrapolated boundary. To compensate for this the usual extrapolated length ($0.71 \lambda_{tr}$) by an amount which will give the correct buckling or K_{eff} is reduced. This was done numerically in works of Rana et. al, 2013. In this section an approximate analytical formula for this reduction in extrapolation distance is attempted.

Since the problem is not exactly solvable in terms of simple function, a simplifying argument is used. The crux of this argument is that the reflector thickness varies from point to point along the curved surface, being larger for points away from the line joining the source and the image and smaller otherwise. If it is assumed that the radius is large compared to a diffusion length, the extra reflector thickness can be shown to be small. This effect can be compensated by reducing the extrapolation distance by a suitable amount obtained, in a heuristic manner, below.

As shown in Fig. 4.1, an image source is placed in a transverse plane containing the source along the diameter joining the center axis and the source point and at an equal distance outside the cylinder represented by axial plane P. A vertical plane P' parallel to the axial plane P (which contains the source point) is drawn and at a distance x away from it. The total flux at the plane P' due to the source is easily calculated to be

$$\begin{aligned} \phi(x) &= \int_0^R \frac{1}{4\pi D} \frac{\exp(-\sqrt{x^2+r^2}/L)}{\sqrt{x^2+r^2}} 2\pi r dr \\ &= \frac{L}{2D} \exp(-x/L) \end{aligned} \tag{4.4}$$

where L is the diffusion length. It is not merely a coincidence that this turns out to be the same as the flux due to a plane source. In fact this would be expected on the basis of the reciprocity as well. The flux at any point Q on P' is same as the flux at the source point due to source at Q. Integrating over all points in the plane P', the flux due to source in plane P' at the original source point is obtained.

Neutrons in this plane see an extra reflector thickness (between the tangent plane T and the circle)

$$y = R - \sqrt{R^2 - x^2} \approx \frac{x^2}{2R}$$

given by . The approximation is justified since neutrons travel a distance

typically to a distance of a few diffusion lengths and since R is assumed to be small compared to L , it is clear that x is also small compared to R . For a thin reflector, this extra thickness can be treated as the added extrapolation distance (reflector saving) for neutrons at the plane P'. Using the number of neutrons (removed) absorbed at the plane P' as a weighting function, the average value of the additional extrapolation due to the extra reflector is calculated as

$$d_{ex} = \int \frac{x^2}{2RL} \exp(-x/L) dx = \frac{L^2}{R} \quad (4.5)$$

For systems with smaller radii, the assumption of a thin reflector is not correct and the expression

$$L \tanh \left(\frac{x^2}{2RL} \right)$$

for the extrapolation distance (Glasstone and Edlund, 1953) must be used. With this,

$$d_{ex} = \int_0^\infty \tanh \left(\frac{x^2}{2RL} \right) \exp(-x/L) dx \quad (4.6)$$

The integration is not easy and so it is substituted with approximation $\tanh(x) = 1 - \exp(-ax)$.

The following result is obtained as

$$d_{ex} = L \left[\sqrt{\frac{2\pi R}{aL}} \exp\left(-\frac{R}{aL}\right) - \operatorname{erf}\left(\frac{R}{aL}\right) \right] \quad (4.7)$$

In Table 4.1 a comparison is shown for d_{ex} obtained using the expressions in Eq. (4.5), (4.7) and by exact numerical integration of (4.6) with the value required to get the correct k_{eff} with diffusion MC based on infinite medium kernel and a single image. It is seen that with, $a=1.2$ practically indistinguishable result is obtained from the MC calculation down to radii about 5 times the diffusion length. Exact numerical evaluation of the integral gives similar results. Even the simple formula in equation (4.5) is in error by about 2 mm in a reactor of radius 30 cm. The corresponding error in the estimated geometrical buckling amounts to less than 2%.

This shows that, for cylindrical geometries, the approximate boundary condition described in this section can be used together with a reduction in the extrapolation distance by an amount d_{ex} . The latter is small enough (few mm up to about 1 cm) to be treated as a correction and may be obtained using the simple expressions derived above.

4.3 Extension of AGF Method to Heterogeneous Media

It might appear that the diffusion theory kernel derived for an infinite homogeneous medium could be extended to situations involving interfaces between two media through the use of the familiar interface conditions of continuity of flux and current. While the general three dimensional problems are clearly unsolvable, even the time dependent problem involving a single planar interface between two media presents insurmountable difficulties. It was suggested (Rana et. al., 2013) that the probabilities derived for the infinite homogeneous medium can be applied not only to bare homogeneous reactors but also to multi-region reactors including reflected reactors. A number of recipes were described earlier without any mathematical or numerical proof. One by one these recipes are examined and the necessary mathematical and numerical justification is provided in this section.

4.3.1 Heterogeneous media with uniform diffusion coefficient

Two different cases of heterogeneous media with uniform diffusion coefficient is considered. First case is a single region medium with actual absorption cross section and a fictitious absorption cross section. In the second case, two regions medium with different absorption cross sections but with same diffusion coefficient is considered. In the following section the recipes to simulate these cases with Diffusion MC Methods and provide mathematical and numerical proofs for the recipes is described.

4.3.1.1 Single Region Medium with Fictitious Absorption

Consider a single region with actual absorption cross section. Introduce a fictitious absorption in the medium, fictitious absorption being larger than the actual one. The time of removal neutron using the usual probability distribution function of the infinite homogeneous medium [as given eq. (4.2)] is sampled but with a 'fictitious' removal cross section (lifetime) which is the highest (shortest) among the two. Then the position using the Gaussian corresponding to this time is sampled and

accept the point with a probability equal to the ratio of the actual absorption cross section of the region in which the selected point lies and the maximum absorption cross section. Else the point is rejected. In the latter case another point is selected starting from the rejected point. The process is repeated till a point is accepted.

Mathematical proof of the recipe goes as follows. The demonstration given below shows that if there is a single medium having some absorption cross section and sampling from infinite medium kernels is chosen but with a fictitious absorption cross section which is larger than the actual absorption cross section, the above recipe gives the same results as that with the actual cross section.

Start with a neutron at the origin at time $t=0$. Let $P(\vec{r}, t)$ be the probability of real absorption at point \vec{r} and time t . Then $P(\vec{r}, t)$ in terms of infinite medium diffusion kernel as given by (4.2), is given by

$$P(\vec{r}, t) = \frac{1}{4\pi Dvt} \exp\left(-\frac{r^2}{4Dt} - \frac{t}{l}\right) \quad (4.8)$$

Where,

D- Diffusion coefficient of the medium

l- Neutron lifetime

t- Time of absorption

Consider a fictitious absorption in the medium. Let Σ_{ar} be the absorption cross section of the medium, called the real absorption cross section, such that $l = 1/\nu\Sigma_{ar}$. Let Σ_{af} ($>\Sigma_{ar}$) denote a fictitious absorption cross section and define a corresponding fictitious neutron lifetime $l_0 = 1/\nu\Sigma_{af}$. Then, the probability (p) of non absorption event following (or after) one fictitious absorption and the probability ($1-p$) of real absorption event following one fictitious absorption, are given by

$$1 - p = \frac{\Sigma_{ar}}{\Sigma_{af}} = \frac{l_0}{l} \quad (4.9)$$

$$p = 1 - \frac{\Sigma_{ar}}{\Sigma_{af}} = 1 - \frac{l_0}{l}$$

If $P_0(\vec{r}, t)$, is written for the probability corresponding to the fictitious absorption at point \vec{r} and time t , i.e.

$$4\pi Dvt \quad 1/2$$

$$l_0 \quad (4.10)$$

$$P_0(\vec{r}, t) = \frac{1}{l_0}$$

Then as per the above recipe, the actual probability $P(\vec{r}, t)$ for absorption at point \vec{r} and at time t can be expressed as,

$$P(\vec{r}, t) = (1-p)P_0(\vec{r}, t) + \int p P_0(\vec{r}, t)(1-p)P_0(\vec{r} - \vec{r}_1, t - t_1) d\vec{r}_1 dt + \int (1-p)p^2 P_0(\vec{r}_1, t_1)P_0(\vec{r}_2 - \vec{r}_1, t_2 - t_1) \dots \quad (4.11)$$

Where, the 1st term indicates that in the first collision itself, the neutron undergoes a real absorption, 2nd term indicates that neutron suffers in the first collision a fictitious absorption at $r-r_1$ and time $t-t_1$ and real absorption at r and time t in the 2nd collision. 3rd term is for the real absorption after 3 collisions and so on. It can be seen that each of the terms is a convolution. Hence if a Fourier transform of the equation (4.11) is performed in the position variables ' \vec{r} ' and a Laplace Transform in time ' t ' then,

$$\mathcal{P}(\vec{k}, s) = \mathcal{P}_0(\vec{k}, s)(1-p) + p\mathcal{P}_0(\vec{k}, s)(1-p)\mathcal{P}_0(\vec{k}, s) + p\mathcal{P}_0(\vec{k}, s)(1-p)\mathcal{P}_0(\vec{k}, s)p\mathcal{P}_0(\vec{k}, s) + \dots \quad (4.12)$$

Equation (4.12) is an infinite geometric series. The sum of the series is easily written as

$$\mathcal{P}(\vec{k}, s) = \frac{(1-p)\mathcal{P}_0(\vec{k}, s)}{1-p\mathcal{P}_0(\vec{k}, s)} \quad (4.13)$$

The expression (4.13) is the (transformed) probability for real absorption as per the recipe. To proceed further, take the Fourier-Laplace transform of the expression for the probability of fictitious absorption viz. that of equation (4.10) and then

$$\int_{-\infty}^{+\infty} P_0(\vec{r}, t) \exp(-i2\pi\vec{k} \cdot \vec{r}) d\vec{r} = \frac{1}{l_0} \exp\left(-\frac{t}{l_0}\right) \exp\left(-\frac{\pi^2 k^2}{a}\right) \quad (4.14)$$

Laplace Transformation of equation (4.14) over the time variable gives

$$\tilde{P}_0(\vec{k}, s) = \int_0^\infty P_0(\vec{k}, t) \exp(-st) dt = \frac{1}{1 + (4\pi^2 k^2 Dv + s)l_0} \quad (4.15)$$

Substituting equation (4.15) in (4.13)

$$\tilde{P}(\vec{k}, s) = \frac{(1-p)}{1 + (4\pi^2 k^2 Dv + s)l_0 / (1-p)} \quad (4.16)$$

Since the functional forms of $\tilde{P}(\vec{k}, s)$ and $\tilde{P}(\vec{k}, s)$, are the same it follows that $P(\vec{r}, t)$ should also have the same form as $P_0(\vec{r}, t)$ but with the increased neutron lifetime $\frac{(1-p)}{l_0}$, which is the same as the actual lifetime of the medium as given by equation (4.9). This proves the correctness of proposed recipe.

Numerical Validation

Numerical simulation of the recipe was carried out using a fictitious absorption cross section twice as large as the real absorption. Another simulation was carried out using only the real absorption cross section. For both the simulation pdfs [given in eq. (4.2)] derived for infinite homogeneous medium for Diffusion MC Method was used. A point source placed at the origin in single region medium with real absorption cross section $\Sigma_{ar} = 0.005 \text{ cm}^{-1}$ and a fictitious absorption section $\Sigma_{af} = 0.01 \text{ cm}^{-1}$ is considered. 10^7 neutrons are considered for simulation. Fig. 4.2 shows a comparison of the time integrated neutron flux for the two cases. Maximum deviation of the absorption rate estimated for the case with fictitious absorption w.r.t. case with only real absorption is about 0.5%. Associated statistical error is about $\pm 0.03 \%$.

Fig. 4.3 gives comparison of time dependent neutron absorption rate at different times. It is seen that the absorption rate decreases with the distance away from the source and this rate of decrease becomes less effective with longer collision time. Maximum deviation of 1% is observed in absorption rate for time bin of 0-0.1 msec for the case with fictitious absorption w.r.t. that with only

real absorption with statistical error of $\pm 0.2\%$. Thus, in all cases the two sets of results are found to be in good agreement confirming the correctness of the recipe for a single region.

4.3.1.2 Two Region Medium with different absorption but same Diffusion

Coefficient

Here the probabilities derived in section 4.1.1 to the two-region medium with different absorption cross sections (Σ_{r1}, Σ_{r2}) in the two regions are applied, but having a uniform diffusion coefficient. The two region medium assumed here is akin to regions having different enrichments or burn ups in different assemblies which give rise to a varying absorption cross sections but almost same diffusion coefficient throughout the core.

If a neutron is produced in a region close to the interface of the regions, it may be absorbed in one of the two regions. Assuming the larger value of the cross-sections let say in region 1 and using equations (4.1) and (4.2) to evaluate probability of absorption in an infinite medium, the probability of absorption in either of the two regions is calculated. If this event occurs in the region 2, accept it with $\frac{\Sigma_{r1}-\Sigma_{r2}}{\Sigma_{r1}}$ probability. In the region 1, the probability of the neutron absorption is always one. Σ_{r1} is called the fictitious absorption cross section as used in section 4.3.1.1

Mathematical proof of the above recipe goes as follows. Let us consider two region medium with ($x < a$ being region I and $x > a$ being region II) different absorption cross-sections (Σ_{r1}, Σ_{r2} with $\Sigma_{r1} > \Sigma_{r2}$) and a constant diffusion coefficient D . The diffusion equation can be written as

$$\nabla \cdot D \nabla \varphi - \Sigma_r \varphi + \delta(r) \delta(t) = \frac{1}{v} \frac{\partial \varphi}{\partial t} \quad (4.17)$$

where

$\Sigma_r = \Sigma_{r1} + (\Sigma - \Sigma)H(x - a)$ and the diffusion co-efficient D is a constant, Hence forth referred to as D_1 . $H(x - a)$ is the Heavyside function. By substituting the above forms for the removal cross section and diffusion coefficient, rewrite the diffusion equation in the form

$$\frac{1}{v} \frac{\partial \varphi}{\partial t} - D_1 \nabla^2 \varphi + \Sigma_{r1} \varphi = \delta(r) \delta(t) - (\Sigma - \Sigma)H(x - a)\varphi \quad (4.18)$$

consider the equation

$$\frac{1}{v} \frac{\partial \varphi}{\partial t} - D_1 \nabla^2 \varphi + \Sigma_{r1} \varphi = \delta(r - r') \delta(t - t') \quad (4.19)$$

and denote its solution (the Green's function) by $G(r,t,r',t')$. Then the solution of (4.18) can be written formally as

$$\varphi(r, t) = G(r, t) + \int G(r - r', t - t') S(r', t') dr' dt'$$

where the source $S(r', t') = (\Sigma - \Sigma) H(x - a) \varphi$. Inserting this expression for the source we get

$$\varphi(r, t) = G(r, t) + \int G(r - r', t - t') [(\Sigma - \Sigma) H(x - a) \varphi] dr' dt' + \int_2 G(r - r', t - t') [(\Sigma - \Sigma) \varphi(r')] dr' dt' \quad (4.20)$$

Expanding in a Von Neumann series we get,

$$\begin{aligned} \varphi(r, t) = & G(r, t) + \int_2 G(r - r', t - t') [(\Sigma - \Sigma) \varphi(r', t')] dr' dt' \\ & G(r, t) + (\Sigma - \Sigma) \int_2 G(r - r', t - t') G(r', t') dr' dt' \quad (4.21) \\ & \Sigma - \Sigma \int_2 \int_2 G(r - r', t - t') G(r' - r'', t' - t'') G(r'', t'') dr'' dt'' dr' dt' + \dots \\ & + \end{aligned}$$

Rewrite the above equation in terms of the probability of absorption instead of flux. Using the same notation as before write $P(\vec{r}, t) = \Sigma_r \varphi(\vec{r}, t)$ and $P_0(\vec{r} - \vec{r}', t - t') = \Sigma_{r1} G(\vec{r} - \vec{r}', t - t')$ Then the above equation becomes

$$\begin{aligned} P(r, t) = & \frac{\Sigma}{\Sigma} P_0(r, t) + \frac{\Sigma}{\Sigma} \left(1 - \frac{\Sigma}{\Sigma}\right) \int_2 P_0(r - r', t - t') P_0(r', t') dr' dt' \quad (4.22) \\ & \frac{+\Sigma}{\Sigma} \left(1 - \frac{\Sigma}{\Sigma}\right)^2 \int_2 \int_2 P_0(r - r', t - t') P_0(r' - r'', t' - t'') P_0(r'', t'') dr'' dt'' dr' dt' + \dots \end{aligned}$$

The Von Neumann series on the RHS of the above equation can be interpreted as being equivalent to the MC recipe described above.

Numerical Validation

A Diffusion MC simulation based on the above recipe was carried out using the pdf of the infinite medium [as given in eq. (4.2)]. Consider a two region infinite medium with the inter region boundary 2 cm away from the origin at $x=2$, and a source placed at the origin. The total cross sections and diffusion coefficient in the two regions are 2.2 cm^{-1} and 0.1515 . Absorption cross

sections are $\Sigma_{al} = 0.005 \text{ cm}^{-1}$ to the left of $x=2$ and $\Sigma_{ar} = 0.01 \text{ cm}^{-1}$ to the right of the plane $x=2$. 10^7 neutrons are used in the simulation.

Transport MC was also carried out for the same problem for the purpose of comparison with Diffusion MC. In Transport MC method each particle is tracked collision by collision through the problem geometry. The flight of the particle is along + X axis and a first collision point is sampled using the equation, $\lambda = -1/\Sigma_t \ln(\xi)$ (where ξ is a random number and λ is the mean free path). Direction of flight of the particle is sampled using the random number. The random point is found by first calculating a random cosine for the polar angle over the range (0, 1) assuming forward scattering, after which a random azimuthal angle φ is selected over the range (0, 2π). Following this collision direction for the second flight path is obtained by selecting fresh random number. The length of this second flight is obtained and by equation, $x = x_0 + \lambda \Omega$, (λ is sampled with new random number for every collision) the second collision point is determined.

Each collision is scored by testing the distance of the collision point from the source, finding the spatial bin (with bin width of 0.1 cm) that contains this point and incrementing a counter for that bin. Flux of the particle for each bin is obtained by dividing by the total cross sections. First collision of the particle is not tallied to remove the transient due to source.

The neutron flux distribution obtained by the Diffusion MC is compared with exact transport MC. Fig. 4.4 shows a comparison of the time integrated flux by the two methods. Flux distribution obtained by Diffusion MC agrees with that obtained by Transport MC within statistical error of $\pm 2\%$. Fig. 4.5 shows a comparison of the flux distributions at different times. Maximum deviation of 1% is observed in absorption rate for time bin of 0-0.1 msec which is within the statistical error. First collision was neglected in Transport MC to mitigate the effect of transients. Deviation of 1% shows that transients are not fully eliminated in the 0-0.1 msec interval. It was found that to simulate 10^7 particles with Transport MC, CPU time is ~ 6 min while for the same simulation, Diffusion MC takes only ~ 6 sec.

4.3.1.3 Two Region Medium with different Diffusion Coefficient

Consider a two region medium as before but with significantly different diffusion coefficients

$D_1 \neq D_2$ and removal cross sections $\Sigma_{r1} \neq \Sigma_{r2}$

In this case, the diffusion co-efficient D and the absorption cross sections can be written in terms of

Heavy side function as follows

$$\Sigma_r = \Sigma_{r1} + (\Sigma - \Sigma_{r1})H(x - a)$$

$$D = D_1 + (D_2 - D_1)H(x - a)$$

The diffusion equation

$$\nabla \cdot D \nabla \varphi - \Sigma_r \varphi + \delta(r) \delta(t) - \frac{1}{v} \frac{\partial \varphi}{\partial t} = 0 \quad (4.23)$$

can be written as

$$\begin{aligned} \frac{1}{v} \frac{\partial \varphi}{\partial t} - D_1 \nabla^2 \varphi + \Sigma_{r1} \varphi &= \nabla \cdot (D \nabla \varphi) - D_1 \nabla^2 \varphi + (\Sigma_{r1} - \Sigma) \varphi + \delta(r) \delta(t) \\ \nabla D \cdot \nabla \varphi + (D - D_1) \nabla^2 \varphi + (\Sigma_{r1} - \Sigma) \varphi &+ \delta(r) \delta(t) \end{aligned} \quad (4.24)$$

and the equation for the Green's Function is

$$\frac{1}{v} \frac{\partial G}{\partial t} - D_1 \nabla^2 G + \Sigma_{r1} G = \delta(r - r') \delta(t - t')$$

By the method of Green's function, solution of the above equation is

$$G(r - r', t - t') [\nabla D \cdot \nabla \varphi(r', t') + (D - D_1) \nabla^2 \varphi(r', t') + (\Sigma_{r1} - \Sigma_r) \varphi(r', t')] dr' dt'$$

$$\varphi(r, t) = G(r, t) + \int G(r - r', t - t') [\nabla D \cdot \nabla \varphi(r', t') + (D_2 - D_1) \nabla^2 \varphi(r', t') + (\Sigma_{r1} - \Sigma_{r2}) \varphi(r', t')] dr' dt' \quad (4.25)$$

Since, $\nabla \cdot D \nabla \varphi = D \nabla^2 \varphi + \nabla D \cdot \nabla \varphi$, so equation (4.25) becomes

$$\begin{aligned} & (D_2 - D_1) \\ [& \nabla^2 G(r - r', t - t') - \nabla D \cdot \nabla G(r - r', t - t') + (\Sigma_{r1} - \Sigma_{r2}) \varphi(r', t') dr' dt' \end{aligned} \quad (4.26)$$

$$\varphi(r, t) = G(r, t) + \int$$

By explicitly evaluating the $\nabla D \cdot \nabla G$ term, equation (4.25) is further simplified as

$$\begin{aligned}
& r - r' \quad ^2 \\
& +(\Sigma_{r1} - \Sigma_{r2}) \\
& \text{righ} \quad (4.27)
\end{aligned}$$

$$\frac{(D_2 - D_1)}{\sigma^2}$$

Rewrite the above equation so that the contributions of the delta function and the distributed sources are seen distinctly.

$$\begin{aligned}
& r - r' \quad ^2 \\
& (\sigma^2 - 3| \) + (\Sigma_{r1} - \Sigma_{r2}) \\
& G(r - r', t - t')\varphi(r', t') \\
& \frac{+(x-x')}{\sigma} G(r - r', t - t')\sigma\delta(x' - a)\varphi(r', t') \quad (4.28) \\
& \text{righ}
\end{aligned}$$

$$\frac{(D_2 - D_1)}{\sigma^2}$$

$$\varphi(r, t) = G(r, t) +$$

$$\text{where } \sigma^2 = \frac{1}{2D_1 v(t-t')}$$

Like before rewrite the equation in terms of the probability of absorption $P(\vec{r}, t) = \Sigma_r \varphi(\vec{r}, t)$ and

$$P_0(\vec{r} - \vec{r}', t - t') = \Sigma_{r1} G(\vec{r} - \vec{r}', t - t'), \text{ rather than the fluxes, to get}$$

$$r - r' \quad 2$$

$$(\sigma^2 - 3| \) + (\Sigma_{r1} - \Sigma_{r2})$$

$$P_0(r - r', t - t')P'(r', t')$$

$$\frac{+(D_2 - D_1)(x - x')}{\sigma^2 \Sigma_r} \frac{1}{\sigma} P_0(r - r', t - t') \sigma \delta(x' - a) P(r', t') \quad (4.29)$$

ri gh

$$\frac{(D_2 - D_1)}{\sigma^2 \Sigma_r}$$

$$P(r, t) = \frac{\Sigma_r}{\Sigma_{r1}} P_0(r, t) +$$

Finally the solution of the integral equation in a Neuman series is developed to obtain

$$\begin{aligned}
P(r, t) &= \frac{\Sigma_r(r)}{\Sigma_{r1}} P_0(r, t) \\
&\quad r - r' \quad 2 \\
&\left(3\sigma^2 - 1 + \frac{\sigma_0 \delta(x'-a)}{3} \frac{(x-x')}{\sigma_0} \right) + \left(1 - \frac{\Sigma_r}{\Sigma_{r1}} \right) \\
&P_0(r - r', t - t') P(r', t') dr' dt' \\
&\quad r - r' \quad 2 \\
&\left(3\sigma^2 - 1 + \frac{\sigma_0 \delta(x'-a)}{3} \frac{(x-x')}{\sigma_0} \right) + \left(1 - \frac{\Sigma_r}{\Sigma_{r1}} \right) \\
&P_0(r - r', t - t') \\
&\quad r' - r'' \quad 2 \\
&\left(3\sigma^2 - 1 + \frac{\sigma_0 \delta(x''-a)}{3} \frac{(x'-x'')}{\sigma_0} \right) + \left(1 - \frac{\Sigma_r}{\Sigma_{r1}} \right) \\
&P_0(r' - r'', t' - t'') P_0(r'', t'') dr'' dt'' \\
&\quad \frac{3(D_2 - D_1)}{\sigma^2 \Sigma_{r1}} \\
&\quad \frac{3(D_2 - D_1)}{\sigma^2 \Sigma_{r1}} \\
&\quad \frac{3(D_2 - D_1)}{\sigma^2 \Sigma_{r1}} \\
&\quad \frac{+\Sigma_r(r)}{\Sigma_{r1}} \int_2
\end{aligned}$$

(4.30)

where again clubbed the delta function and distributed source contributions for compactness is clubbed.

Numerical modeling of the above case is more complicated, since several distributions are involved. Moreover some negative terms are present and also there is a delta function in one of the distributions. The sampling scheme would therefore have to admit negative particle weights which means analog MC is not possible. Assuming if this requirement is given up, let us see what kind of MC scheme is required.

The first thing to do is to factorise the kernel into a "transport part" and a "collision part". The transport part gives the probability that the particle starting at a point \mathbf{r}' at time t' will have its next significant event ("collision") at point \mathbf{r} at time t . This must be normalised to unity. The collision part then gives the weight of the re-emitted particle which will be then either transported or if the weight is below the Russian Roulette threshold may be killed or transported with an enhanced weight. The natural choice (but by no means the only one) for the "transport part" is the Green's function defined above (infinite medium kernel with the shorter lifetime (larger absorption cross section) and diffusion co-efficient D_1). In the above discussion it is assumed that this region is to the

$$r - r' \ll \lambda$$

left of the interface. The multiplying factors such as for example $\frac{3(D_2 - D_1)}{\sigma^2 \Sigma_{r1}}$ are then part of the

"collision kernel" and can be used to adjust the particle weight. As regards tallying, tally the entire weight if the particle "collides" on the left but on the right, tally the weight fraction $\frac{\Sigma_{r2}}{\Sigma_{r1}}$.

Negative and positive weight particles will have to be transported separately. A point to be noted is that the terms arising due to different diffusion coefficients in the two regions have positive and negative contributions which add up to zero. On the other hand the one due to different absorption in the two regions causes a net positive weight to be emitted from sites in the second medium which is exactly equal to the difference between the weight entering the collision and the weight absorbed at the collision site. Thus the difference in the diffusion coefficients causes only the weights to be re-distributed in space and time.

The first "collision" point is sampled from the distribution $P_0(\vec{r}, t)$ for the variables y, z and t . With

$$2\pi^{-1/2}$$

probability $1 + \frac{1}{-1}$ sample x using the same Gaussian ($P_0(\vec{r}, t)$) and set its weight equal to $1/p$.

$$p =$$

With probability $1 - p$ set $x=a$ and set its weight equal to $(1-p)/p$. This is done to take care of the

delta function. In the former case transportation is done according to the usual transport kernel and a weight

$$r - r' = \frac{3(D_2 - D_1)}{\sigma^2 \Sigma_{r1}} \left(1 - \frac{\Sigma_r}{\Sigma_{r1}} \right)$$

is assigned. In the latter case transport the particle using the distribution $P(\vec{r} - \vec{r}', t - t')$ with $x'=a$ and assign a weight equal to $\frac{3(D_2 - D_1)}{\sigma^2 \Sigma_{r1}} \frac{(x-a)}{\sigma}$. In either case the particle may be absorbed fully at the new location or it may be re transported according to the same procedure. On an average the weights (positive or negative) keep reducing in magnitude. As mentioned above, a Russian Roulette has to be played to terminate the process once the weight falls below a certain magnitude.

Alternative approach for analog games

The approach described above is not suitable for analog MC. However, it is possible to model this problem with transport theory type MC methods (Rana et. al, 2013). It is noted that the diffusion kernels are Gaussians, and that diffusion theory is the limiting situation of transport theory when the neutron undergoes a very large number of collisions before absorption and the mean free paths are short compared to other lengths. This is another statement of the Central limit theorem. In practice, however, a few random numbers when added together show a distribution closely resembling a Gaussian. So the only thing that is necessary is to preserve the parameters.

The total distance traveled by a particle is vt (t is the removal time of neutron) while the average distance traveled in each collision is (in medium I) $3D_1$, the mean free path. The number of collisions is thus $vt/3D_1$. This could be very large (let us say 100). If this is to be scaled down to let us say 4, all is needed to do is to scale up the mean free path (diffusion coefficient) in medium I by $\sqrt{(vt/3D_1)}/4$. Likewise, while traveling in medium II, scale up the mean free path in medium II

by $\sqrt{(vt/3D_2)}/4$. This prescription will correctly give the (RMS) distance traveled by the neutron from its starting point before removal and also the (approximately) correct spatial distribution for the sampled value of t . Finally whether the removal point is to be accepted or not is decided by the rejection technique described in 4.3.1.1.

Numerical Validation

Consider a two region infinite medium with a boundary at 2 cm away from the origin. The source is located at the origin. Medium 1 has absorption cross section of $\Sigma_{r1} = 0.01 \text{ cm}^{-1}$ and mean free path of 0.04545 cm. Medium 2 has absorption cross section of $\Sigma_{r2} = 0.005$ and mean free path of 0.99 cm. Here, Transport MC method based on Coleman's Method or pseudo collision method (Cloeman W. A., 1968) is used for estimating the absorption rate in the two mediums. Accept the point with a probability equal to the ratio of the actual removal cross section of the region in which the selected point lies and the maximum removal cross section. Else the point is rejected. In the latter case particle is displaced to a new point in the same direction with distance equals to the mean free path of the particle assuming it has suffered a pseudo collision. The process is repeated till a point is accepted. Other details are same as described in section 4.3.1.1

A plot of the time integrated absorption rate for the recipe suggested above is given in Fig 4.6. 10^7 particles are simulated. Fitted values of absorption rate obtained by increased mean free path differs by about a maximum of 8% with that of original mean free path while the associated statistical error is $\pm 1\%$ and $\pm 3\%$ respectively. It is seen that near the source, deviations are larger due to the presence of residual transients but at distance away from the source, deviations are within statistical error. In Fig. 4.7 a comparison of the absorption at different time in the two media is shown. Maximum deviation of 10% is observed in absorption rate for time bin of 0-0.1 msec.

4.4 Transport Corrections to Diffusion MC

It was mentioned earlier that diffusion theory is not valid (a) close to localized sources (b) close to vacuum boundary (c) inside and close to strong absorbers (d) highly anisotropic scattering. In this section each of these conditions is examined one by one and will develop methods to extend the applications of Diffusion Theory MC to such regimes.

The solution of the transport equation for a point source in an infinite homogeneous medium can be obtained by the Fourier Laplace transforms similar to that of the diffusion equation. The flux splits into a sum of a transient flux which dominates close to the source and an asymptotic flux which has a form similar to the diffusion flux and is important far away from the source. These facts are used in this section to show that it is possible to extend the diffusion theory MC method to situations where diffusion theory is not valid, viz., close to localized sources, strong absorbers, boundaries and anisotropic scattering.

4.4.1 Transient Flux Close to a Localized Source

Expression for the flux for a point source placed at the origin in the infinite medium is given by (Bell and Glasstone, 1970),

$$\varphi(r) = \varphi_{As}(r) + \varphi_{transient}(r) \quad (4.31)$$

where,

$$\varphi_{As}(r) = \frac{S_0 \beta}{4\pi D r} \exp(-\kappa r)$$

$$\varphi_{transient}(r) \approx (S_0/4\pi r^2) \exp(-\Sigma' r)$$

With $\kappa = \sqrt{\Sigma' / D}$, $\beta = 1 - \Sigma_a / \Sigma'$ and $\Sigma' = 5 \Sigma / 4$

The flux near a localized source is not well described by diffusion theory even in a diffusive medium i.e. one in which scattering is large compared to removal. This is due to the presence of a transient flux. Since it is also known that most of the transient flux is simply the un-collided flux while the asymptotic flux is due to neutrons that have undergone collisions. The difference between

diffusing and non diffusing (absorbing) media is simply the relative contribution of the transient and asymptotic components.

A recipe for transport correction to Diffusion MC is proposed using the approximations available for the transient flux given in equation (4.31). Sample the absorption event using the expression for the transient flux with a probability proportional to the transient component while rest of the times it will be sampled using the asymptotic flux expression. A more accurate expression for the transient flux is available (A. M. Weinberg, 1958) but sampling the relevant distribution is not easy.

Numerical Validation

Numerical Simulations were carried out using the usual transport MC method as described in section 4.4.1. Transport Corrected Diffusion MC simulation was carried out using equation (4.31). Total cross section of the medium is 2.2 cm^{-1} , while the absorption and scattering cross sections are 0.01 cm^{-1} and 2.19 cm^{-1} respectively. Fig. 4.8 shows the time averaged neutron flux due to a source in a mildly absorbing medium with a point source located at the origin, obtained by the above method. Also the flux distribution by infinite diffusion kernel is plotted. The latter represents the asymptotic flux which obeys the diffusion equation. The relaxation length estimated by fitting the asymptotic flux agrees well with the theoretical value. It can be seen from the plot that Diffusion MC flux near the source is lower than the Transport MC flux since diffusion theory fails in this region, but the transport corrected Diffusion MC flux estimates same flux as obtained by transport theory. Flux estimated by Transport corrected Diffusion MC differs from that estimated by Transport MC by about a maximum of 2%. The corresponding time dependent fluxes at different times are compared in Fig. 4.9. It is seen that the flux decreases with the distance away from the source and this rate of decrease becomes less effective with longer collision time. Maximum deviation of 3% is observed in absorption rate for time bin of 0-0.1 msec.

4.4.2 Transport in a strongly absorbing medium

This case is related to the one discussed in the previous section. In a weakly absorbing medium, a neutron undergoes a large number of collisions before absorption and therefore the asymptotic flux is the dominant term except very close to the source. In case of a strong absorber there are few collisions before absorption and hence the transient flux is dominant near the source but there are not many collisions and hence the asymptotic component is small.

Numerical Validation

The results of calculations by the transport MC and transport corrected diffusion MC are shown in Fig. 4.10. The total cross Section of the medium is 2.2 cm^{-1} , the absorption cross section is 1.2 cm^{-1} and the scattering cross section is 1.0 cm^{-1} . It can be seen near the source, there is large difference of 40% in the asymptotic flux and the flux estimated by the Transport MC. With transport correction applied to the asymptotic flux, this difference is considerably reduced to 10%. The agreement is quite good showing that the recipe is valid even for strongly absorbing media. The only difference is that savings in computer time are small as the neutron history is anyway not too long. On the other hand the savings in case of a weak absorber are much larger.

4.4.3 Transients Close to a Vacuum Boundary

Transients close to a vacuum boundary are due the negative source of the neutrons directed outwards.

Numerical Validation

Fig. 4.11 shows the flux distribution due to a source in a finite isotropic medium with boundary at 4.5 cm from the point source placed at the origin. Transport flux is obtained using a MC algorithm using the last event absorption estimator described in section 4.4.2. In case the particle leaks out, the event is stopped and goes for the next neutron history. It is seen from Fig. 4.11 that asymptotic flux obtained by Diffusion MC Method compares well with the analytical expression for the flux distribution for symmetric boundary given below.

$$\phi(x) = -LS/2D(1/1 + e^{(2X/L)})e^{(x/L)} + LS/2D(e^{(2X/L)}/1 + e^{(2X/L)})e^{(-X/L)} \quad (4.32)$$

where, L , D , S and X are the neutron diffusion length, diffusion coefficient, source strength and extrapolation distance respectively.

It is also seen that the flux estimated by transport and diffusion MC are nearly the same at the boundary which implies that the transient flux near the boundary is small compared to that near the source. This is probably due to the fact that by Placzek's Lemma, the transients at a boundary are caused by a negative source of neutrons directed outwards, which produces smaller transients inside the region of interest. Flux estimated by Diffusion MC differs from that estimated by Transport MC by about a maximum of 0.5%.

4.4.4 Transport Effects with Anisotropic Scattering

In all the examples given above, it is assumed that the scattering is isotropic in the laboratory system. The general case involving anisotropic scattering requires a transformation of coordinate system from the one in which the scattering law is given, to the fixed coordinate system in which the particle is tracked (Stephen Dupree et. al., 2001; MCNP Guide 1987; Paul et. al., 2013). While the transformation is elementary, but for clarity and better understanding a detailed derivation of the transformation and a description of the algorithm is presented in Appendix A.

Numerical Validation

Using the above algorithm calculations for a hydrogenous medium in which the scattering is strongly anisotropic in the laboratory system is carried out. Fig. 4.12 gives the flux distribution obtained using transport MC and the transport corrected diffusion MC for a mildly absorbing medium. Transport cross section was used for estimating the diffusion coefficient to account for anisotropic scattering. Flux estimated by Transport corrected Diffusion MC differs from that estimated by Transport MC within statistical error. The good agreement shows that the above recipe is valid in a medium with anisotropic scattering.

4.5 Conclusions

Analytical Green's function based Diffusion MC methods have been applied earlier for by Rana et. al. for simulation of reactor noise experiments in experimental reactors for measuring the degree of sub-criticality in accelerator driven systems. Although this approach has several advantages such as speed, elegance and exactitude, but it was applicable to a rather restricted class of problems, such as the bare rectangular parallel piped homogeneous reactor. Here, the analytical Greens function based Diffusion MC methods is developed further, to demonstrate its utility in a wider class of problems such as in finite homogeneous and heterogeneous media. Mathematical and numerical proofs of the recipes proposed for applying diffusion kernel of infinite homogeneous medium to heterogeneous medium with same or different diffusion coefficient developed.

For a heterogeneous medium consisting of two regions having different diffusion coefficients, the mathematical proof goes through but the resulting sampling functions are more complicated and hence the method may be difficult particularly for analog MC but would be usable with non analog MC. However, a different recipe suggested for this situation in Rana et. al., 2013 which is more appropriate for analog MC has been demonstrated to work successfully. It has been also shown that by a transport correction based on incorporating the transient flux kernel in addition to the diffusion kernel, the method can be applied to the situations where diffusion theory is otherwise inapplicable.

Computational time for Diffusion MC is about 10 times less than that by Transport MC. In addition to its use as a fast analog method for simulating noise by MC, the present work could find application in devising mesh less methods in time dependent diffusion theory, particularly in situations involving moving media where meshes tend to get distorted. Another application could be to study various aspects of MC such as variance reduction techniques, and speeding up convergence to the fundamental mode of criticality calculations. In this context, it may be mentioned that besides

the advantage of speed, the diffusion MC has the advantage that analytical results are available in diffusion theory for the purpose of making comparisons.

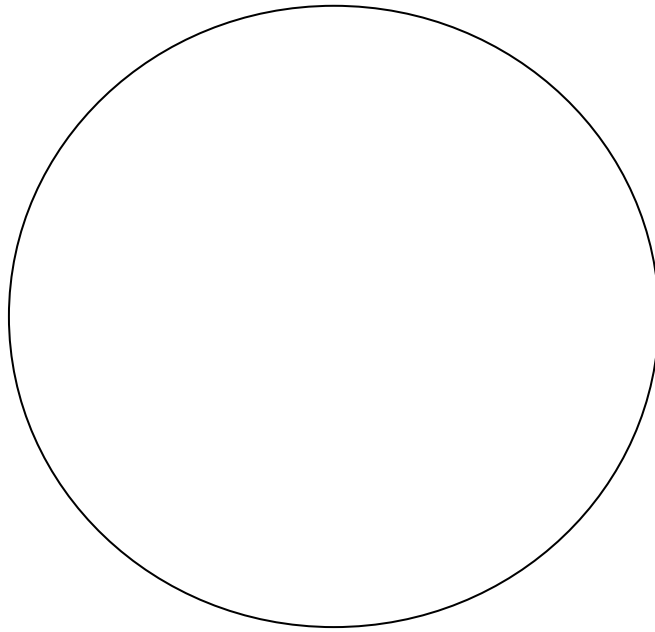


Fig. 4.1 Diagrammatic representation of the source and image point locations and the coordinates used in the estimation of the reduction in extrapolation distance for a bare homogeneous cylindrical reactor by method of images

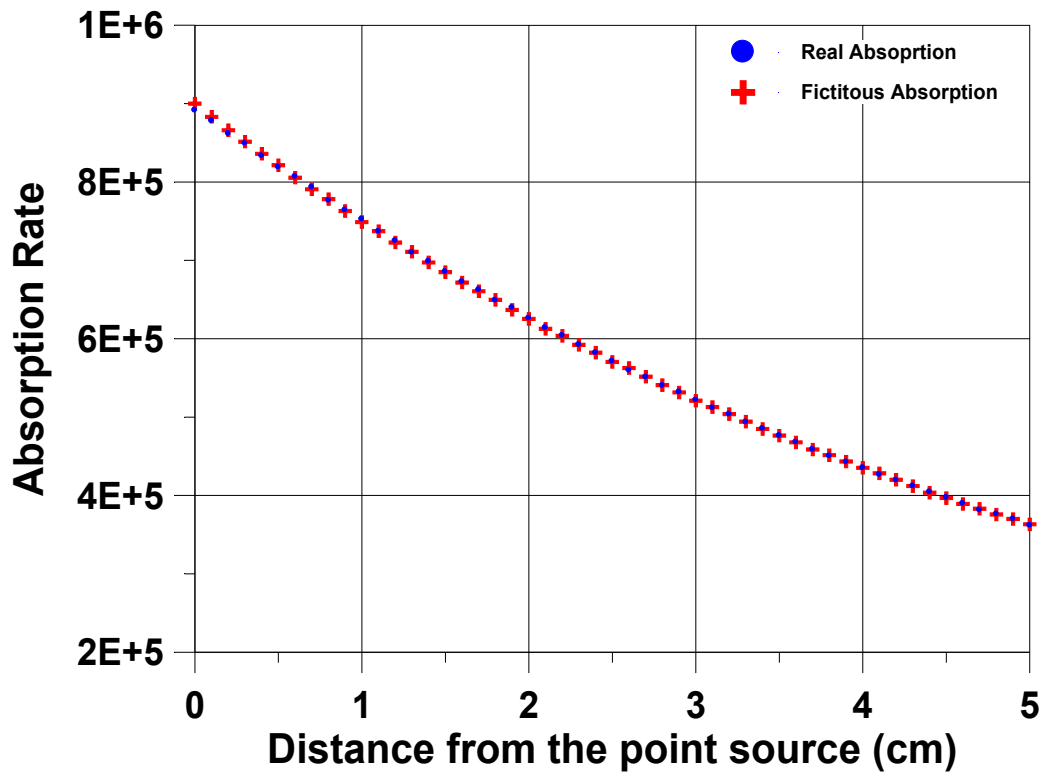


Fig. 4.2 Variation of the time integrated neutron absorption rate with distance from a point source placed at the origin in single region medium. The blue dots indicate the absorption rate obtained using the real absorption cross section $\Sigma_{ar} = 0.005 \text{ cm}^{-1}$ while the red cross indicate the absorption rate calculated with a fictitious absorption $\Sigma_{af} = 0.01 \text{ cm}^{-1}$ followed by a rejection with a 50% probability.

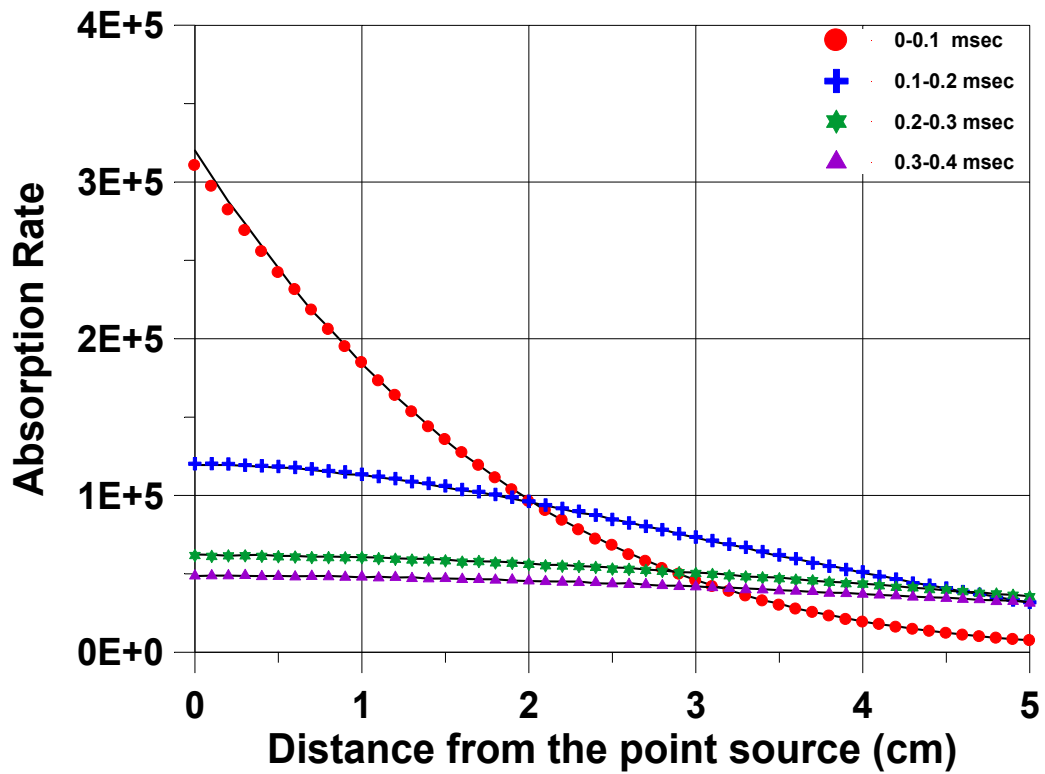


Fig. 4.3 Variation of the time dependent neutron absorption rate with distance from a point source placed at the origin in single region medium. The various markers indicate the absorption rate obtained using the real absorption cross section $\Sigma_{ar} = 0.005 \text{ cm}^{-1}$ while the solid lines indicate the absorption rate calculated with a fictitious absorption $\Sigma_{af} = 0.01 \text{ cm}^{-1}$ followed by a rejection with a 50% probability.

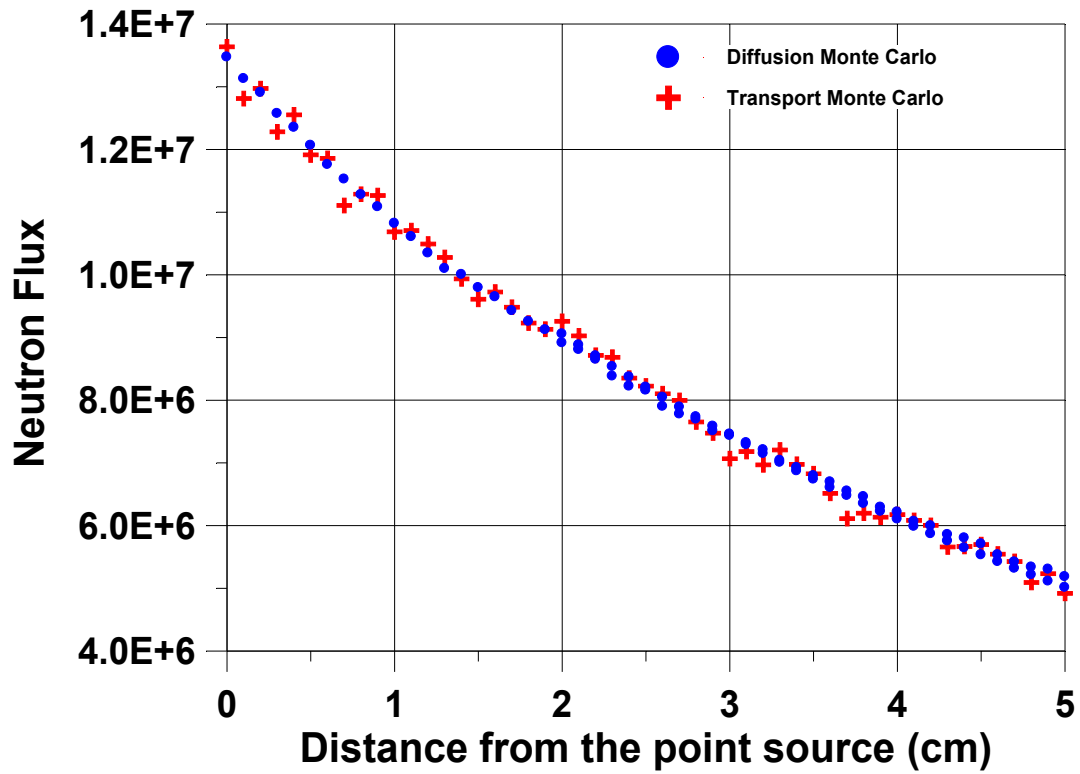


Fig. 4.4 Variation of the time integrated neutron flux with distance from a point source placed at the origin in a two region medium with same diffusion coefficients but different absorption cross sections viz. $\Sigma_{ar} = 0.005 \text{ cm}^{-1}$ to the left of $x=2$ and $\Sigma_{ar} = 0.01 \text{ cm}^{-1}$ to the right of the plane $x=2$. The red crosses indicate the exact results by Transport MC while the blue stands for diffusion MC.

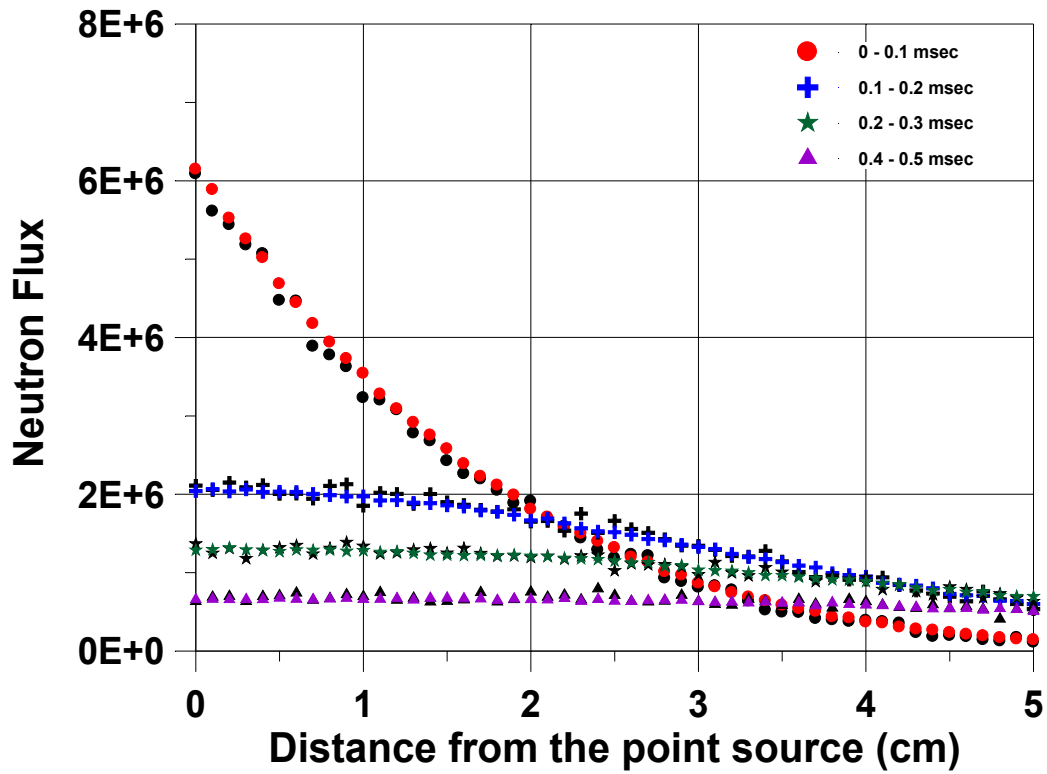


Fig. 4.5 Variation of the time dependent neutron flux with distance from a point source placed at the origin in a two region medium with same diffusion coefficients but different absorption cross sections viz. $\Sigma_{al} = 0.005 \text{ cm}^{-1}$ to the left of $x=2$ and $\Sigma_{ar} = 0.01 \text{ cm}^{-1}$ to the right of the plane $x=2$. The various markers indicate the flux obtained using the Diffusion MC while the corresponding black markers indicate the flux calculated with Transport MC using the rejection technique.

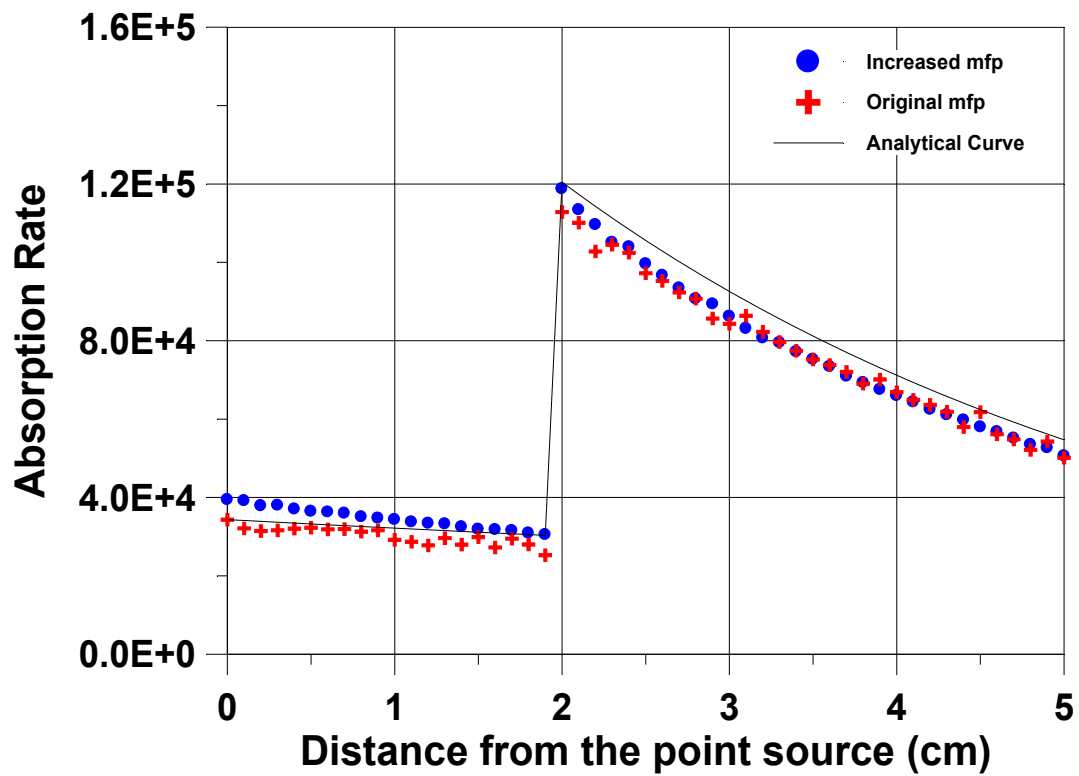


Fig.4.6 Variation of time averaged neutron absorption rate with distance from the point source placed at the origin in two region medium with boundary at $x=2$. $\Sigma_{r1} = 0.01 \text{ cm}^{-1}$ and $D_1=0.1515$ to the left of the boundary while $\Sigma_{r2} = 0.005 \text{ cm}^{-1}$ and $D_2=0.33$ to the right. The figure shows a comparison of the absorption rate obtained with actual mean free path (mfp) and that with 4 times higher mfp. Solid curve corresponds to analytically computed neutron absorption rate.

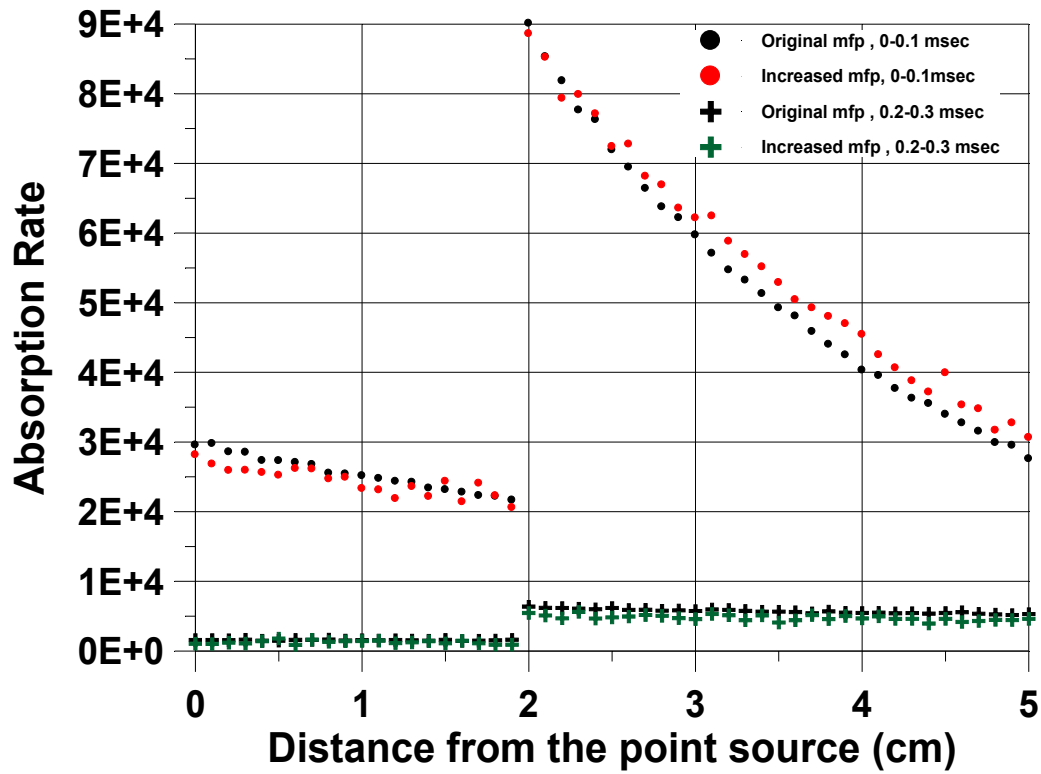


Fig. 4.7 Variation of time dependent neutron absorption rate with distance from the point source placed at the origin in two region medium with boundary at $x=2$. $\Sigma_{r1} = 0.01 \text{ cm}^{-1}$ and $D_1=0.1515$ to the left of the boundary while $\Sigma_{r2} = 0.005 \text{ cm}^{-1}$ and $D_2=0.33$ to the right. The figure shows a comparison of the absorption rate obtained with actual mean free path (mfp) and that with 4 times higher mfp.

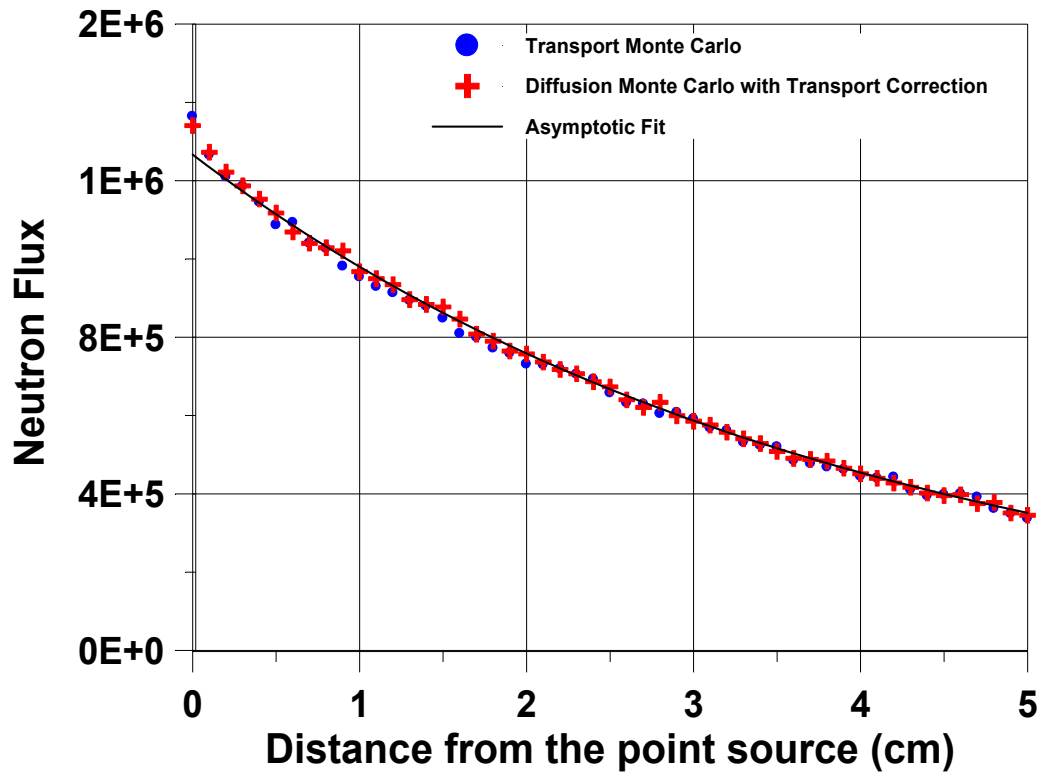


Fig. 4.8 Variation of the time averaged neutron flux with distance from a point source located at the origin in a mildly absorbing medium. The figure compares the results using transport MC and transport corrected diffusion MC.

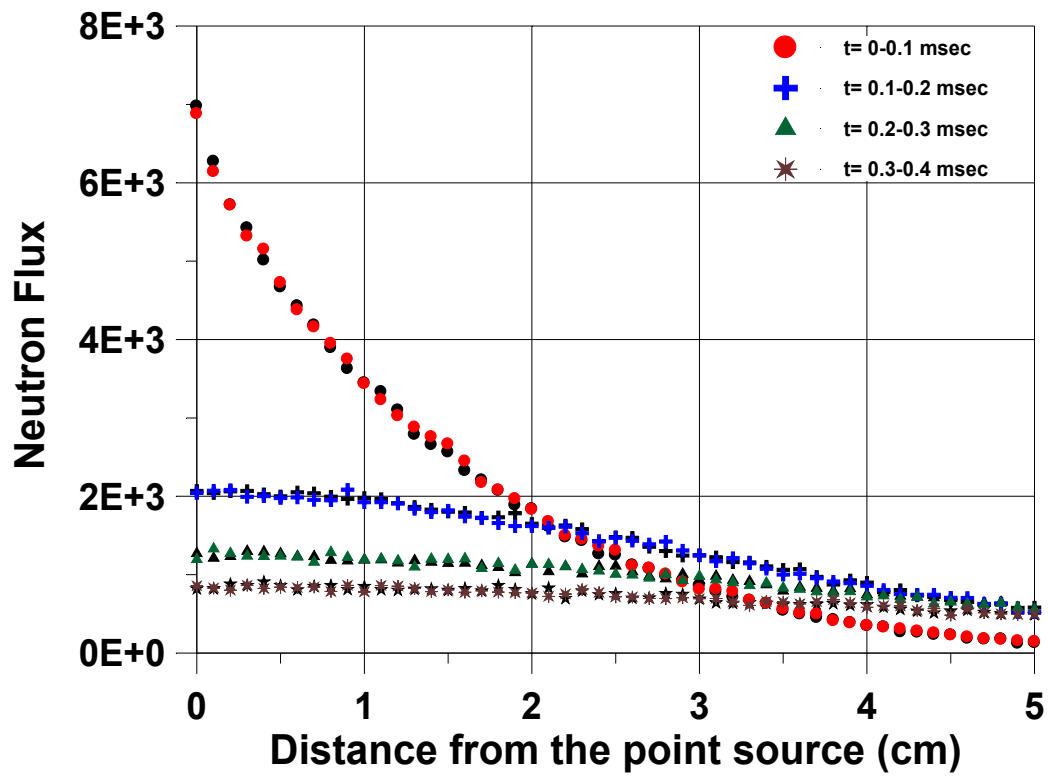


Fig. 4.9 Variation of the time dependent neutron flux with distance from a point source located at the origin in a mildly absorbing medium. The figure compares the results using transport MC and transport corrected diffusion MC.

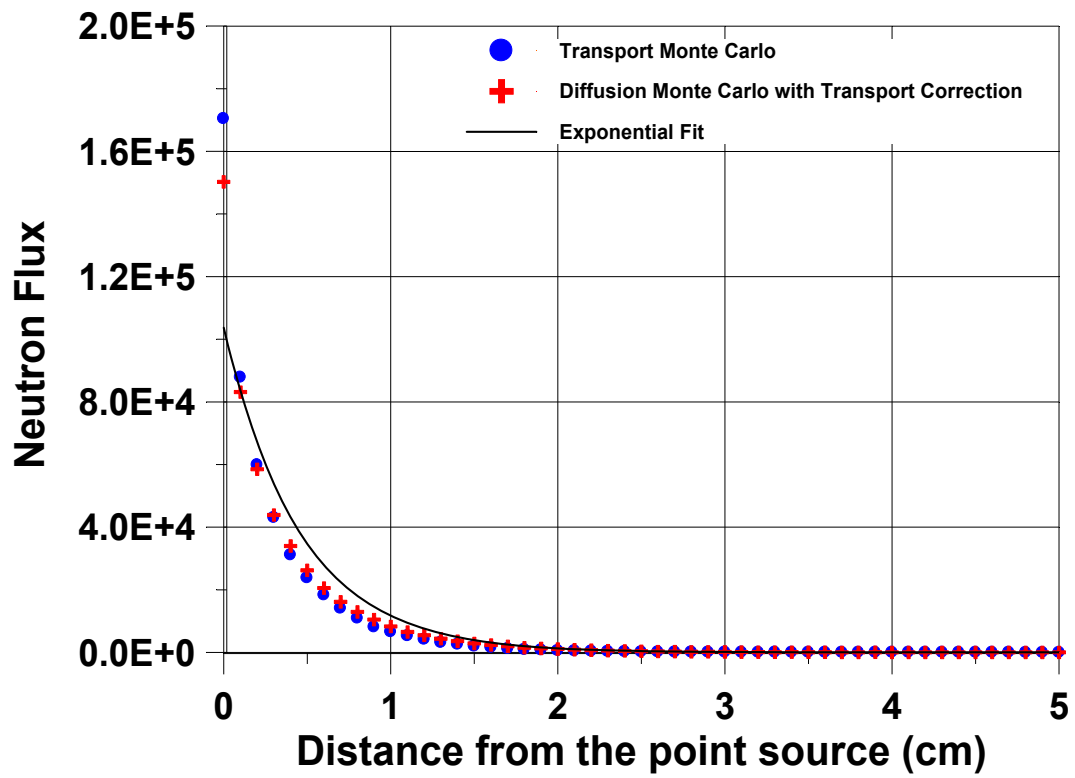


Fig. 4.10 Variation of the time averaged neutron flux with distance from a point source located at the origin in a strongly absorbing medium. The figure compares the results using transport MC and transport corrected diffusion MC.

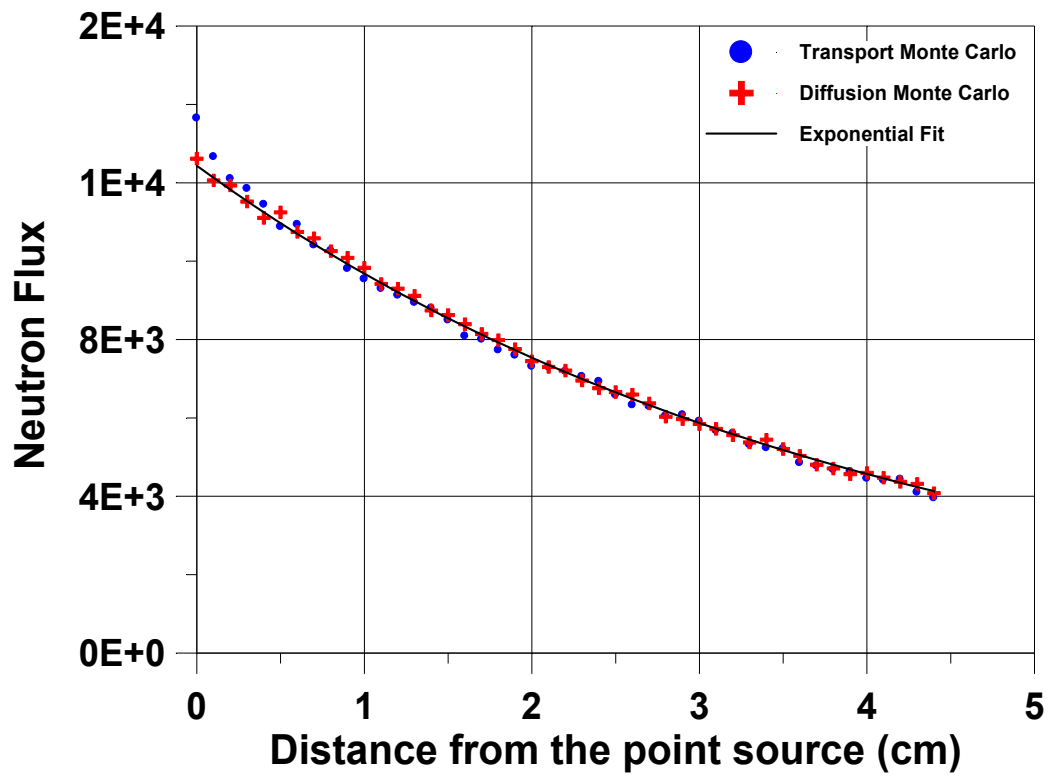


Fig. 4.11 Variation of the neutron flux (time averaged) with distance from the point source in a semi infinite homogeneous medium. The point source is placed at the origin and the medium-vacuum boundary is located at $x=4.5$ cm from the source. The figure shows a comparison of results based on transport and diffusion MC and the analytical fit.

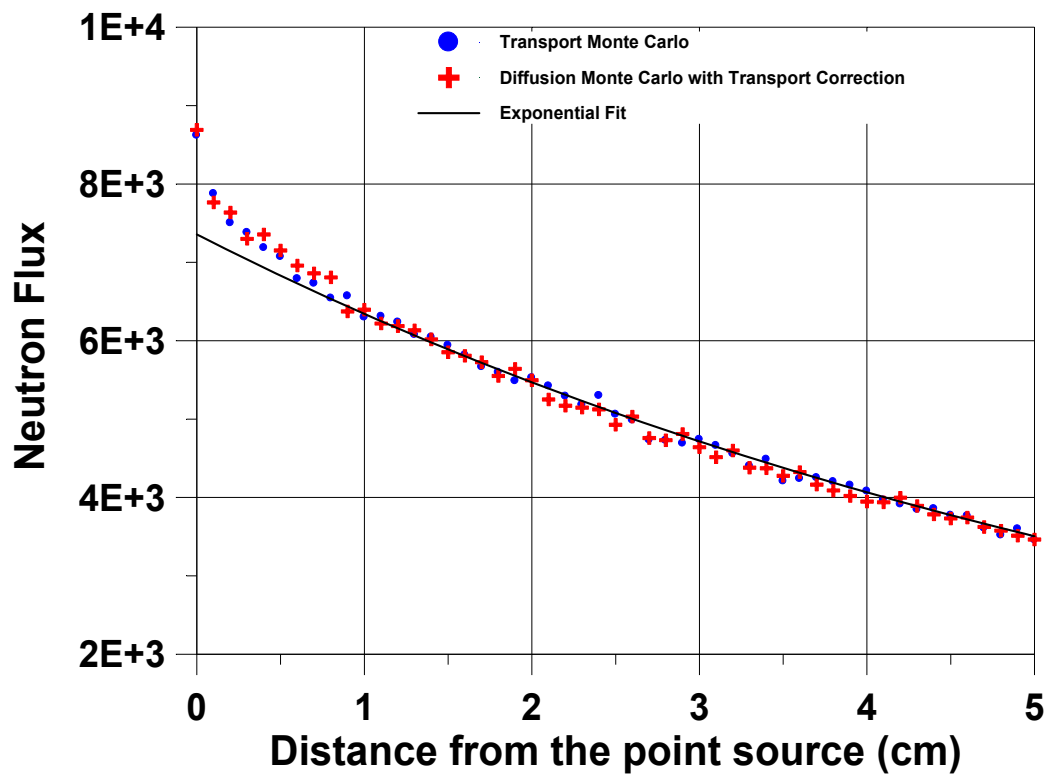


Fig. 4.12 Neutron Flux due to a source in an infinite homogeneous medium with mild absorption and anisotropic scattering - comparison of results obtained using transport MC and transport corrected diffusion MC.

**Table 4.1 Reduction in extrapolation distance d_{ex} as function of radius of the cylinder
(Diffusion Length, $L= 6$ cm)**

<i>Radius R (cm)</i>	<i>d_{ex} required to give correct k_{eff} using a single image</i>	<i>$d_{ex} = L^2/R$ as given by eq. (4)</i>	<i>d_{ex}, as given by eq. (6) with $a=1.2$</i>	<i>d_{ex}, as given by eq. (5)</i>
30	0.94	1.20	0.92	0.91
40	0.88	0.90	0.75	0.73
50	0.64	0.72	0.63	0.61
60	0.52	0.60	0.55	0.53

Diffusion Theory Monte Carlo: Model Description and Extension

In the previous Chapter the application of some of the ideas regarding Monte Carlo Kinetics to the simplest model viz. the point kinetics model is discussed. In this chapter another model for studying Monte Carlo space time kinetics viz. the Diffusion theory Monte Carlo Model is introduced.

Monte Carlo Methods for solving problems in Diffusion Theory have been studied by Booth, 1981; Sadiku, 2006. Rana and Degweker, 2013 developed the analytical Green's function approach as well as the finite difference based numerical approach for diffusion theory Monte Carlo. The present chapter is based on and is an extension of their work..

For full Space-Time Space Time Monte Carlo Simulations, both spatial as well as temporal variation of the neutron and precursor concentrations has to be modeled. The model discussed in this chapter allows to apply the schemes for modeling the spatial variation of neutrons and precursors. Besides providing a simple model for testing these ideas regarding Monte Carlo space time Kinetics, the diffusion theory MC model permits an exact comparison of the results of MC simulation with the large number of kinetics benchmarks that have been solved using deterministic diffusion theory methods. This is particularly important since there are very few 'exact' benchmarks that are based on transport theory MC

There is another reason for interest in the study of this model. MC calculations are mostly performed by the non analog technique for the purpose of computational efficiency. However, for simulation of noise experiments for measurement of reactor kinetics parameters such as reactivity, the analog MC is more appropriate. There has been a lot of theoretical and experimental interest (Pazsit et. al., 2005; Degweker et. al., 2003; Munoz Cobo et. al. 2001) in recent times in the noise methods for sub criticality measurement of accelerator driven systems. This also includes noise simulation using standard MC codes after removing all non analog features (Yamamoto et. al., 2011). While there have been suggestions (Szeiberth et. al., 2010) that non analog methods can be

used for this purpose, they will have limitations such as being applicable for the specific stochastic descriptor for which the tallies have been corrected and would certainly not be suitable for estimating errors due to statistics or dead time effects. Since analog MC is highly computational time consuming, the concept of the diffusion theory based analog MC technique to reduce the computing time was proposed by Rana and Degweker, 2013. This is based on the observation that in a variety of situations, diffusion theory, an approximate form of transport theory is very successful in giving quick results which may be fairly close to transport theory. It was shown that the methods of Diffusion MC developed are quite successful in simulating noise experiments.

Two approaches - viz., the analytical Green's function method and the finite difference method - were developed by Rana and Degweker, 2013. In analytical Green's function method they use analytical solutions of diffusion equation to construct probability distribution function for neutron absorption in a medium. The analytical Greens function approach has several advantages such as speed and exactitude, but was applicable to a rather restricted class of problems, such as the bare homogeneous reactor. A number of developments in this approach have been carried out and these form the subject of the present chapter.

With the developments discussed in this chapter the Analytical Greens Function MC becomes a useful tool of stochastic space time kinetics primarily for simulating noise experiments. On the other hand the finite difference diffusion MC is useful for exact comparison with diffusion theory benchmarks and forms the subject for the next chapter.

It was mentioned in earlier works (Rana and Degweker, 2013) that analytical Greens function method can be used for (a) infinite homogeneous medium and (b) bare homogeneous reactor of the rectangular geometry. Some recipes were proposed (without proof) for treating other situations like cylindrical geometry and non homogenous media.

The analytical Greens function (AGF) approach is further developed, to demonstrate its utility in a wider class of problems including homogeneous cylinders and heterogeneous reactors. In this Chapter, mathematical and numerical proofs of the validity of these recipes which were proposed

for such systems is provided. Other limitations of Diffusion MC Methods and means to overcome these are also discussed. It is well known that diffusion theory is not valid (a) close to localized sources (b) close to vacuum boundary (c) inside and close to strong absorbers (d) highly anisotropic scattering. In all such cases, the flux gradients are very sharp and the angular distribution of the flux is highly anisotropic causing the diffusion approximation to break down. Corrections to diffusion MC methods to overcome these limitations is applied.

With these developments, the Analytical Greens Function MC becomes a useful tool of stochastic space time kinetics primarily for simulating noise experiments. On the other hand, the finite difference diffusion MC is useful for exact comparison with diffusion theory benchmarks and forms the subject for the next chapter.

4.1 Earlier Work

4.1.1 Probability Distribution Function for Infinite Homogenous Medium

The probability distribution function (pdf) for simulating infinite homogeneous medium with Diffusion MC was derived by solving the one group time dependent diffusion equation using Fourier and Laplace transforms (Rana et. al., 2013).

It was shown (Rana et. al., 2013) that for a single source neutron initially (at $t=0$) located at the origin in an infinite homogeneous medium, the flux is given by

$$\varphi(\vec{r}, t) = \frac{v}{4\pi Dvt} e^{-\frac{r^2}{4Dt}} e^{-\lambda t} \quad (4.1)$$

where v is the velocity of the neutron and D is the diffusion coefficient. The neutron life-time in an infinite medium is given by $l=1/\nu\Sigma_r$. The probability that a neutron will be removed in the small space time interval $dx dy dz dt$ is obtained by multiplying the flux with the macroscopic removal cross section Σ_r to give

$$P(x, y, z, t) = \frac{1}{4\pi Dvt} \exp(-t/l) \frac{1}{l} \quad (4.2)$$

The marginal distribution for the removal time is obtained by integrating equation (4.2) over the space variables and $\int \frac{1}{l} \exp(-t/l) dt$ is obtained. The conditional distribution for the space variables for a given value of time is obtained by dividing equation (4.2) by the marginal distribution. The conditional distribution is given by

$$\frac{1}{4\pi Dvt} \exp(-t/l) \quad (4.3)$$

The conditional distribution can be written as a product of the three Gaussians for the three coordinates, each having zero mean and $\frac{2Dvt}{3}$ as variance. Therefore the position and time of absorption of a neutron in an infinite medium with Diffusion MC using pdf given in equation (4.2) with the following scheme can be sampled. First the time as an exponential distribution (with mean as l) is sampled. Then the position coordinates as three independent Gaussians, each with zero mean and $\frac{2Dvt}{3}$ as the variance (for the sampled value of time) is sampled. In what follows, variants of the above sampling scheme for finite and multi-region medium (with same or different diffusion coefficients and absorption cross-sections) is employed.

4.1.2 Bare Homogenous Reactor: Method of Images

For a point source in an infinite medium, pdf described in the previous section can be used. To use these pdfs for bare homogeneous reactor of rectangular and cylindrical geometry, the method of images was developed (Rana et. al., 2013) to reproduce zero flux boundary condition.

Rectangular Parallelepiped

Rana et. al. (2013) also showed that the zero flux boundary condition for a bare homogeneous reactor can be simulated by locating suitably placed image sources outside the reactor, for one, two

and three dimensional rectangular geometries. Unlike the case of electrostatics where an infinite number of images are required, one, three or seven images (depending upon whether the source is near a face, edge or corner) placed outside the reactor volume suffice to reproduce the zero flux boundary condition (Jackson, 1958). This makes the problem fairly tractable.

4.2 Further development & Extension of the method of images

4.2.1 Right Circular Cylinder

It is difficult to reproduce the zero flux boundary condition on the curved surface exactly using the method of images. Since the problem is not exactly solvable in terms of simple function, a simplifying argument is used. The crux of this argument is that the use of the image point at an equal distance is equivalent to using the tangent plane as the boundary. Hence, the material between the tangent plane and the curved cylindrical surface can scatter neutrons back into the cylinder (i.e. act as a reflector) and this is incorrect. To correct this we try to estimate this effect in the form of the reflector savings of this material and subtract this from the extrapolation distance (that is used for a vacuum boundary). Since the reflector material in this situation has a thickness that varies from point to point along the curved surface, (being larger for points away from the line joining the source and the image and smaller otherwise), it is not immediately clear what thickness (and corresponding reflector saving value) should be used. We proceed as follows. We obtain the reflector thickness from the geometry of the situation in the plane P' and use it to estimate the reflector saving. We use the expression for the flux in this plane due to a point source (in an infinite medium) as a weighting function to find the average reflector saving.

We place an image source in a transverse plane containing the source along the diameter joining the centre (axis) and the source point and at an equal distance outside the cylinder as shown in Fig. 4.1 and applying a small correction to the extrapolation distance. In what follows, an analytical expression for this correction is obtained.

The image causes the flux to be zero at the tangent plane rather than at the circular boundary. A reflector causes the flux to go to zero at a distance beyond the usual extrapolated boundary. To compensate for this the usual extrapolated length ($0.71 \lambda_{tr}$) by an amount which will give the correct buckling or K_{eff} is reduced. This was done numerically in works of Rana et. al, 2013. In this section an approximate analytical formula for this reduction in extrapolation distance is attempted.

Since the problem is not exactly solvable in terms of simple function, a simplifying argument is used. The crux of this argument is that the reflector thickness varies from point to point along the curved surface, being larger for points away from the line joining the source and the image and smaller otherwise. If it is assumed that the radius is large compared to a diffusion length, the extra reflector thickness can be shown to be small. This effect can be compensated by reducing the extrapolation distance by a suitable amount obtained, in a heuristic manner, below.

As shown in Fig. 4.1, an image source is placed in a transverse plane containing the source along the diameter joining the center axis and the source point and at an equal distance outside the cylinder represented by axial plane P. A vertical plane P' parallel to the axial plane P (which contains the source point) is drawn and at a distance x away from it. The total flux at the plane P' due to the source is easily calculated to be

$$\begin{aligned} \phi(x) &= \int_0^R \frac{1}{4\pi D} \frac{\exp(-\sqrt{x^2+r^2}/L)}{\sqrt{x^2+r^2}} 2\pi r dr \\ &= \frac{L}{2D} \exp(-x/L) \end{aligned} \tag{4.4}$$

where L is the diffusion length. It is not merely a coincidence that this turns out to be the same as the flux due to a plane source. In fact this would be expected on the basis of the reciprocity as well. The flux at any point Q on P' is same as the flux at the source point due to source at Q. Integrating over all points in the plane P', the flux due to source in plane P' at the original source point is obtained.

Neutrons in this plane see an extra reflector thickness (between the tangent plane T and the circle)

$$y = R - \sqrt{R^2 - x^2} \approx \frac{x^2}{2R}$$

given by . The approximation is justified since neutrons travel a distance

typically to a distance of a few diffusion lengths and since R is assumed to be small compared to L , it is clear that x is also small compared to R . For a thin reflector, this extra thickness can be treated as the added extrapolation distance (reflector saving) for neutrons at the plane P'. Using the number of neutrons (removed) absorbed at the plane P' as a weighting function, the average value of the additional extrapolation due to the extra reflector is calculated as

$$d_{ex} = \int \frac{x^2}{2RL} \exp(-x/L) dx = \frac{L^2}{R} \quad (4.5)$$

For systems with smaller radii, the assumption of a thin reflector is not correct and the expression

$$L \tanh \left(\frac{x^2}{2RL} \right)$$

for the extrapolation distance (Glasstone and Edlund, 1953) must be used. With this,

$$d_{ex} = \int_0^\infty \tanh \left(\frac{x^2}{2RL} \right) \exp(-x/L) dx \quad (4.6)$$

The integration is not easy and so it is substituted with approximation $\tanh(x) = 1 - \exp(-ax)$.

The following result is obtained as

$$d_{ex} = L \left[\sqrt{\frac{2\pi R}{aL}} \exp\left(-\frac{R}{aL}\right) - \operatorname{erf}\left(\frac{R}{aL}\right) \right] \quad (4.7)$$

In Table 4.1 a comparison is shown for d_{ex} obtained using the expressions in Eq. (4.5), (4.7) and by exact numerical integration of (4.6) with the value required to get the correct k_{eff} with diffusion MC based on infinite medium kernel and a single image. It is seen that with, $a=1.2$ practically indistinguishable result is obtained from the MC calculation down to radii about 5 times the diffusion length. Exact numerical evaluation of the integral gives similar results. Even the simple formula in equation (4.5) is in error by about 2 mm in a reactor of radius 30 cm. The corresponding error in the estimated geometrical buckling amounts to less than 2%.

This shows that, for cylindrical geometries, the approximate boundary condition described in this section can be used together with a reduction in the extrapolation distance by an amount d_{ex} . The latter is small enough (few mm up to about 1 cm) to be treated as a correction and may be obtained using the simple expressions derived above.

4.3 Extension of AGF Method to Heterogeneous Media

It might appear that the diffusion theory kernel derived for an infinite homogeneous medium could be extended to situations involving interfaces between two media through the use of the familiar interface conditions of continuity of flux and current. While the general three dimensional problems are clearly unsolvable, even the time dependent problem involving a single planar interface between two media presents insurmountable difficulties. It was suggested (Rana et. al., 2013) that the probabilities derived for the infinite homogeneous medium can be applied not only to bare homogeneous reactors but also to multi-region reactors including reflected reactors. A number of recipes were described earlier without any mathematical or numerical proof. One by one these recipes are examined and the necessary mathematical and numerical justification is provided in this section.

4.3.1 Heterogeneous media with uniform diffusion coefficient

Two different cases of heterogeneous media with uniform diffusion coefficient is considered. First case is a single region medium with actual absorption cross section and a fictitious absorption cross section. In the second case, two regions medium with different absorption cross sections but with same diffusion coefficient is considered. In the following section the recipes to simulate these cases with Diffusion MC Methods and provide mathematical and numerical proofs for the recipes is described.

4.3.1.1 Single Region Medium with Fictitious Absorption

Consider a single region with actual absorption cross section. Introduce a fictitious absorption in the medium, fictitious absorption being larger than the actual one. The time of removal neutron using the usual probability distribution function of the infinite homogeneous medium [as given eq. (4.2)] is sampled but with a 'fictitious' removal cross section (lifetime) which is the highest (shortest) among the two. Then the position using the Gaussian corresponding to this time is sampled and

accept the point with a probability equal to the ratio of the actual absorption cross section of the region in which the selected point lies and the maximum absorption cross section. Else the point is rejected. In the latter case another point is selected starting from the rejected point. The process is repeated till a point is accepted.

Mathematical proof of the recipe goes as follows. The demonstration given below shows that if there is a single medium having some absorption cross section and sampling from infinite medium kernels is chosen but with a fictitious absorption cross section which is larger than the actual absorption cross section, the above recipe gives the same results as that with the actual cross section.

Start with a neutron at the origin at time $t=0$. Let $P(\vec{r}, t)$ be the probability of real absorption at point \vec{r} and time t . Then $P(\vec{r}, t)$ in terms of infinite medium diffusion kernel as given by (4.2), is given by

$$P(\vec{r}, t) = \frac{1}{4\pi Dvt} \exp\left(-\frac{r^2}{4Dt} - \frac{t}{l}\right) \quad (4.8)$$

Where,

D- Diffusion coefficient of the medium

l- Neutron lifetime

t- Time of absorption

Consider a fictitious absorption in the medium. Let Σ_{ar} be the absorption cross section of the medium, called the real absorption cross section, such that $l = 1/\nu\Sigma_{ar}$. Let Σ_{af} ($>\Sigma_{ar}$) denote a fictitious absorption cross section and define a corresponding fictitious neutron lifetime $l_0 = 1/\nu\Sigma_{af}$. Then, the probability (p) of non absorption event following (or after) one fictitious absorption and the probability ($1-p$) of real absorption event following one fictitious absorption, are given by

$$1 - p = \frac{\Sigma_{ar}}{\Sigma_{af}} = \frac{l_0}{l} \quad (4.9)$$

$$p = 1 - \frac{\Sigma_{ar}}{\Sigma_{af}} = 1 - \frac{l_0}{l}$$

If $P_0(\vec{r}, t)$, is written for the probability corresponding to the fictitious absorption at point \vec{r} and time t , i.e.

$$4\pi Dvt \quad 1/2$$

$$l_0 \quad (4.10)$$

$$P_0(\vec{r}, t) = \frac{1}{l_0}$$

Then as per the above recipe, the actual probability $P(\vec{r}, t)$ for absorption at point \vec{r} and at time t can be expressed as,

$$P(\vec{r}, t) = (1-p)P_0(\vec{r}, t) + \int pP_0(\vec{r}, t)(1-p)P_0(\vec{r} - \vec{r}_1, t - t_1)d\vec{r}_1dt + \int (1-p)p^2 P_0(\vec{r}_1, t_1)P_0(\vec{r}_2 - \vec{r}_1, t_2 - t_1) \quad (4.11)$$

Where, the 1st term indicates that in the first collision itself, the neutron undergoes a real absorption, 2nd term indicates that neutron suffers in the first collision a fictitious absorption at $r-r_1$ and time $t-t_1$ and real absorption at r and time t in the 2nd collision. 3rd term is for the real absorption after 3 collisions and so on. It can be seen that each of the terms is a convolution. Hence if a Fourier transform of the equation (4.11) is performed in the position variables ' \vec{r} ' and a Laplace Transform in time ' t ' then,

$$\mathcal{P}(\vec{k}, s) = \mathcal{P}_0(\vec{k}, s)(1-p) + p\mathcal{P}_0(\vec{k}, s)(1-p)\mathcal{P}_0(\vec{k}, s) + p\mathcal{P}_0(\vec{k}, s)(1-p)\mathcal{P}_0(\vec{k}, s)p\mathcal{P}_0(\vec{k}, s) + \dots(4.12)$$

Equation (4.12) is an infinite geometric series. The sum of the series is easily written as

$$\mathcal{P}(\vec{k}, s) = \frac{(1-p)\mathcal{P}_0(\vec{k}, s)}{1-p\mathcal{P}_0(\vec{k}, s)} \quad (4.13)$$

The expression (4.13) is the (transformed) probability for real absorption as per the recipe. To proceed further, take the Fourier-Laplace transform of the expression for the probability of fictitious absorption viz. that of equation (4.10) and then

$$\int_{-\infty}^{+\infty} P_0(\vec{r}, t)\exp(-i2\pi\vec{k}\cdot\vec{r})d\vec{r} = \frac{1}{l_0}\exp\left(-\frac{t}{l_0}\right)\exp\left(-\frac{\pi^2\vec{k}^2}{a}\right) \quad (4.14)$$

Laplace Transformation of equation (4.14) over the time variable gives

$$\tilde{P}_0(\vec{k}, s) = \int_0^\infty P_0(\vec{k}, t) \exp(-st) dt = \frac{1}{1 + (4\pi^2 k^2 Dv + s)l_0} \quad (4.15)$$

Substituting equation (4.15) in (4.13)

$$\tilde{P}(\vec{k}, s) = \frac{(1-p)}{1 + (4\pi^2 k^2 Dv + s)l_0 / (1-p)} \quad (4.16)$$

Since the functional forms of $\tilde{P}(\vec{k}, s)$ and $\tilde{P}(\vec{k}, s)$, are the same it follows that $P(\vec{r}, t)$ should also have the same form as $P_0(\vec{r}, t)$ but with the increased neutron lifetime $\frac{(1-p)}{l_0}$, which is the same as the actual lifetime of the medium as given by equation (4.9). This proves the correctness of proposed recipe.

Numerical Validation

Numerical simulation of the recipe was carried out using a fictitious absorption cross section twice as large as the real absorption. Another simulation was carried out using only the real absorption cross section. For both the simulation pdfs [given in eq. (4.2)] derived for infinite homogeneous medium for Diffusion MC Method was used. A point source placed at the origin in single region medium with real absorption cross section $\Sigma_{ar} = 0.005 \text{ cm}^{-1}$ and a fictitious absorption section $\Sigma_{af} = 0.01 \text{ cm}^{-1}$ is considered. 10^7 neutrons are considered for simulation. Fig. 4.2 shows a comparison of the time integrated neutron flux for the two cases. Maximum deviation of the absorption rate estimated for the case with fictitious absorption w.r.t. case with only real absorption is about 0.5%. Associated statistical error is about $\pm 0.03 \%$.

Fig. 4.3 gives comparison of time dependent neutron absorption rate at different times. It is seen that the absorption rate decreases with the distance away from the source and this rate of decrease becomes less effective with longer collision time. Maximum deviation of 1% is observed in absorption rate for time bin of 0-0.1 msec for the case with fictitious absorption w.r.t. that with only

real absorption with statistical error of $\pm 0.2\%$. Thus, in all cases the two sets of results are found to be in good agreement confirming the correctness of the recipe for a single region.

4.3.1.2 Two Region Medium with different absorption but same Diffusion

Coefficient

Here the probabilities derived in section 4.1.1 to the two-region medium with different absorption cross sections (Σ_{r1}, Σ_{r2}) in the two regions are applied, but having a uniform diffusion coefficient. The two region medium assumed here is akin to regions having different enrichments or burn ups in different assemblies which give rise to a varying absorption cross sections but almost same diffusion coefficient throughout the core.

If a neutron is produced in a region close to the interface of the regions, it may be absorbed in one of the two regions. Assuming the larger value of the cross-sections let say in region 1 and using equations (4.1) and (4.2) to evaluate probability of absorption in an infinite medium, the probability of absorption in either of the two regions is calculated. If this event occurs in the region 2, accept it with $\frac{\Sigma_{r1}-\Sigma_{r2}}{\Sigma_{r1}}$ probability. In the region 1, the probability of the neutron absorption is always one. Σ_{r1} is called the fictitious absorption cross section as used in section 4.3.1.1

Mathematical proof of the above recipe goes as follows. Let us consider two region medium with ($x < a$ being region I and $x > a$ being region II) different absorption cross-sections (Σ_{r1}, Σ_{r2} with $\Sigma_{r1} > \Sigma_{r2}$) and a constant diffusion coefficient D . The diffusion equation can be written as

$$\nabla \cdot D \nabla \varphi - \Sigma_r \varphi + \delta(r) \delta(t) = \frac{1}{v} \frac{\partial \varphi}{\partial t} \quad (4.17)$$

where

$\Sigma_r = \Sigma_{r1} + (\Sigma - \Sigma)H(x - a)$ and the diffusion coefficient D is a constant, Hence forth referred to as D_1 . $H(x - a)$ is the Heavyside function. By substituting the above forms for the removal cross section and diffusion coefficient, rewrite the diffusion equation in the form

$$\frac{1}{v} \frac{\partial \varphi}{\partial t} - D_1 \nabla^2 \varphi + \Sigma_{r1} \varphi = \delta(r) \delta(t) - (\Sigma - \Sigma)H(x - a) \varphi \quad (4.18)$$

consider the equation

$$\frac{1}{v} \frac{\partial \varphi}{\partial t} - D_1 \nabla^2 \varphi + \Sigma_{r1} \varphi = \delta(r - r') \delta(t - t') \quad (4.19)$$

and denote its solution (the Green's function) by $G(r,t,r',t')$. Then the solution of (4.18) can be written formally as

$$\varphi(r, t) = G(r, t) + \int G(r - r', t - t') S(r', t') dr' dt'$$

where the source $S(r', t') = (\Sigma - \Sigma) H(x - a) \varphi$. Inserting this expression for the source we get

$$\varphi(r, t) = G(r, t) + \int G(r - r', t - t') [(\Sigma - \Sigma) H(x - a) \varphi] dr' dt' + \int_2 G(r - r', t - t') [(\Sigma - \Sigma) \varphi(r')] dr' dt' \quad (4.20)$$

Expanding in a Von Neumann series we get,

$$\begin{aligned} \varphi(r, t) = & G(r, t) + \int_2 G(r - r', t - t') [(\Sigma - \Sigma) \varphi(r', t')] dr' dt' \\ & G(r, t) + (\Sigma - \Sigma) \int_2 G(r - r', t - t') G(r', t') dr' dt' \quad (4.21) \\ & \Sigma - \Sigma \int_2 \int_2 G(r - r', t - t') G(r' - r'', t' - t'') G(r'', t'') dr'' dt'' dr' dt' + \dots \\ & + \end{aligned}$$

Rewrite the above equation in terms of the probability of absorption instead of flux. Using the same notation as before write $P(\vec{r}, t) = \Sigma_r \varphi(\vec{r}, t)$ and $P_0(\vec{r} - \vec{r}', t - t') = \Sigma_{r1} G(\vec{r} - \vec{r}', t - t')$ Then the above equation becomes

$$\begin{aligned} P(r, t) = & \frac{\Sigma}{\Sigma} P_0(r, t) + \frac{\Sigma}{\Sigma} \left(1 - \frac{\Sigma}{\Sigma}\right) \int_2 P_0(r - r', t - t') P_0(r', t') dr' dt' \quad (4.22) \\ & \frac{+\Sigma}{\Sigma} \left(1 - \frac{\Sigma}{\Sigma}\right)^2 \int_2 \int_2 P_0(r - r', t - t') P_0(r' - r'', t' - t'') P_0(r'', t'') dr'' dt'' dr' dt' + \dots \end{aligned}$$

The Von Neumann series on the RHS of the above equation can be interpreted as being equivalent to the MC recipe described above.

Numerical Validation

A Diffusion MC simulation based on the above recipe was carried out using the pdf of the infinite medium [as given in eq. (4.2)]. Consider a two region infinite medium with the inter region boundary 2 cm away from the origin at $x=2$, and a source placed at the origin. The total cross sections and diffusion coefficient in the two regions are 2.2 cm^{-1} and 0.1515 . Absorption cross

sections are $\Sigma_{al} = 0.005 \text{ cm}^{-1}$ to the left of $x=2$ and $\Sigma_{ar} = 0.01 \text{ cm}^{-1}$ to the right of the plane $x=2$. 10^7 neutrons are used in the simulation.

Transport MC was also carried out for the same problem for the purpose of comparison with Diffusion MC. In Transport MC method each particle is tracked collision by collision through the problem geometry. The flight of the particle is along + X axis and a first collision point is sampled using the equation, $\lambda = -1/\Sigma_t \ln(\xi)$ (where ξ is a random number and λ is the mean free path). Direction of flight of the particle is sampled using the random number. The random point is found by first calculating a random cosine for the polar angle over the range (0, 1) assuming forward scattering, after which a random azimuthal angle φ is selected over the range (0, 2π). Following this collision direction for the second flight path is obtained by selecting fresh random number. The length of this second flight is obtained and by equation, $x = x_0 + \lambda \Omega$, (λ is sampled with new random number for every collision) the second collision point is determined.

Each collision is scored by testing the distance of the collision point from the source, finding the spatial bin (with bin width of 0.1 cm) that contains this point and incrementing a counter for that bin. Flux of the particle for each bin is obtained by dividing by the total cross sections. First collision of the particle is not tallied to remove the transient due to source.

The neutron flux distribution obtained by the Diffusion MC is compared with exact transport MC. Fig. 4.4 shows a comparison of the time integrated flux by the two methods. Flux distribution obtained by Diffusion MC agrees with that obtained by Transport MC within statistical error of $\pm 2\%$. Fig. 4.5 shows a comparison of the flux distributions at different times. Maximum deviation of 1% is observed in absorption rate for time bin of 0-0.1 msec which is within the statistical error. First collision was neglected in Transport MC to mitigate the effect of transients. Deviation of 1% shows that transients are not fully eliminated in the 0-0.1 msec interval. It was found that to simulate 10^7 particles with Transport MC, CPU time is ~ 6 min while for the same simulation, Diffusion MC takes only ~ 6 sec.

4.3.1.3 Two Region Medium with different Diffusion Coefficient

Consider a two region medium as before but with significantly different diffusion coefficients

$D_1 \neq D_2$ and removal cross sections $\Sigma_{r1} \neq \Sigma_{r2}$

In this case, the diffusion co-efficient D and the absorption cross sections can be written in terms of Heaviside function as follows

$$\Sigma_r = \Sigma_{r1} + (\Sigma - \Sigma_{r1})H(x - a)$$

$$D = D_1 + (D_2 - D_1)H(x - a)$$

The diffusion equation

$$\nabla \cdot D \nabla \varphi - \Sigma_r \varphi + \delta(r) \delta(t) - \frac{1}{v} \frac{\partial \varphi}{\partial t} = 0 \quad (4.23)$$

can be written as

$$\begin{aligned} \frac{1}{v} \frac{\partial \varphi}{\partial t} - D_1 \nabla^2 \varphi + \Sigma_{r1} \varphi &= \nabla \cdot (D \nabla \varphi) - D_1 \nabla^2 \varphi + (\Sigma_{r1} - \Sigma) \varphi + \delta(r) \delta(t) \\ \nabla D \cdot \nabla \varphi + (D - D_1) \nabla^2 \varphi + (\Sigma_{r1} - \Sigma) \varphi + \delta(r) \delta(t) & \end{aligned} \quad (4.24)$$

and the equation for the Green's Function is

$$\frac{1}{v} \frac{\partial G}{\partial t} - D_1 \nabla^2 G + \Sigma_{r1} G = \delta(r - r') \delta(t - t')$$

By the method of Green's function, solution of the above equation is

$$G(r - r', t - t') [\nabla D \cdot \nabla \varphi(r', t') + (D - D_1) \nabla^2 \varphi(r', t') + (\Sigma_{r1} - \Sigma_r) \varphi(r', t')] dr' dt'$$

$$\varphi(r, t) = G(r, t) + \int G(r - r', t - t') [\nabla D \cdot \nabla \varphi(r', t') + (D_2 - D_1) \nabla^2 \varphi(r', t') + (\Sigma_{r1} - \Sigma_{r2}) \varphi(r', t')] dr' dt' \quad (4.25)$$

Since, $\nabla \cdot D \nabla \varphi = D \nabla^2 \varphi + \nabla D \cdot \nabla \varphi$, so equation (4.25) becomes

$$\begin{aligned} & (D_2 - D_1) \\ [& \nabla^2 G(r - r', t - t') - \nabla D \cdot \nabla G(r - r', t - t') + (\Sigma_{r1} - \Sigma_{r2}) \varphi(r', t') dr' dt' \\ & \varphi(r, t) = G(r, t) + \int \end{aligned} \quad (4.26)$$

By explicitly evaluating the $\nabla D \cdot \nabla G$ term, equation (4.25) is further simplified as

$$\begin{aligned}
& r - r' \quad ^2 \\
& +(\Sigma_{r1} - \Sigma_{r2}) \\
& \text{righ} \quad (4.27)
\end{aligned}$$

$$\frac{(D_2 - D_1)}{\sigma^2}$$

Rewrite the above equation so that the contributions of the delta function and the distributed sources are seen distinctly.

$$\begin{aligned}
& r - r' \quad ^2 \\
& (\sigma^2 - 3| \) + (\Sigma_{r1} - \Sigma_{r2}) \\
& G(r - r', t - t')\varphi(r', t') \\
& \frac{+(x-x')}{\sigma} G(r - r', t - t')\sigma\delta(x' - a)\varphi(r', t') \quad (4.28) \\
& \text{righ}
\end{aligned}$$

$$\frac{(D_2 - D_1)}{\sigma^2}$$

$$\varphi(r, t) = G(r, t) +$$

$$\text{where } \sigma^2 = \frac{1}{2D_1 v(t-t')}$$

Like before rewrite the equation in terms of the probability of absorption $P(\vec{r}, t) = \Sigma_r \varphi(\vec{r}, t)$ and

$$P_0(\vec{r} - \vec{r}', t - t') = \Sigma_{r1} G(\vec{r} - \vec{r}', t - t'), \text{ rather than the fluxes, to get}$$

$$r - r' \quad 2$$

$$(\sigma^2 - 3| \) + (\Sigma_{r1} - \Sigma_{r2})$$

$$P_0(r - r', t - t')P'(r', t')$$

$$\frac{+(D_2 - D_1)(x - x')}{\sigma^2 \Sigma_r} \frac{1}{\sigma} P_0(r - r', t - t') \sigma \delta(x' - a) P(r', t') \quad (4.29)$$

ri gh

$$\frac{(D_2 - D_1)}{\sigma^2 \Sigma_r}$$

$$P(r, t) = \frac{\Sigma_r}{\Sigma_{r1}} P_0(r, t) +$$

Finally the solution of the integral equation in a Neuman series is developed to obtain

$$\begin{aligned}
P(r, t) &= \frac{\Sigma_r(r)}{\Sigma_{r1}} P_0(r, t) \\
&\quad r - r' \quad 2 \\
&\left(3\sigma^2 - 1 + \frac{\sigma_0 \delta(x'-a)}{3} \frac{(x-x')}{\sigma_0} \right) + \left(1 - \frac{\Sigma_r}{\Sigma_{r1}} \right) \\
&P_0(r - r', t - t') P(r', t') dr' dt' \\
&\quad r - r' \quad 2 \\
&\left(3\sigma^2 - 1 + \frac{\sigma_0 \delta(x'-a)}{3} \frac{(x-x')}{\sigma_0} \right) + \left(1 - \frac{\Sigma_r}{\Sigma_{r1}} \right) \\
&P_0(r - r', t - t') \\
&\quad r' - r'' \quad 2 \\
&\left(3\sigma^2 - 1 + \frac{\sigma_0 \delta(x''-a)}{3} \frac{(x'-x'')}{\sigma_0} \right) + \left(1 - \frac{\Sigma_r}{\Sigma_{r1}} \right) \\
&P_0(r' - r'', t' - t'') P_0(r'', t'') dr'' dt'' \\
&\quad \frac{3(D_2 - D_1)}{\sigma^2 \Sigma_{r1}} \\
&\quad \frac{3(D_2 - D_1)}{\sigma^2 \Sigma_{r1}} \\
&\quad \frac{3(D_2 - D_1)}{\sigma^2 \Sigma_{r1}} \\
&\quad \frac{+\Sigma_r(r)}{\Sigma_{r1}} \int_2
\end{aligned}$$

(4.30)

where again clubbed the delta function and distributed source contributions for compactness is clubbed.

Numerical modeling of the above case is more complicated, since several distributions are involved. Moreover some negative terms are present and also there is a delta function in one of the distributions. The sampling scheme would therefore have to admit negative particle weights which means analog MC is not possible. Assuming if this requirement is given up, let us see what kind of MC scheme is required.

The first thing to do is to factorise the kernel into a "transport part" and a "collision part". The transport part gives the probability that the particle starting at a point \mathbf{r}' at time t' will have its next significant event ("collision") at point \mathbf{r} at time t . This must be normalised to unity. The collision part then gives the weight of the re-emitted particle which will be then either transported or if the weight is below the Russian Roulette threshold may be killed or transported with an enhanced weight. The natural choice (but by no means the only one) for the "transport part" is the Green's function defined above (infinite medium kernel with the shorter lifetime (larger absorption cross section) and diffusion co-efficient D_1). In the above discussion it is assumed that this region is to the

$$r - r' \ll \lambda$$

left of the interface. The multiplying factors such as for example $\frac{3(D_2 - D_1)}{\sigma^2 \Sigma_{r1}}$ are then part of the

"collision kernel" and can be used to adjust the particle weight. As regards tallying, tally the entire weight if the particle "collides" on the left but on the right, tally the weight fraction $\frac{\Sigma_{r2}}{\Sigma_{r1}}$.

Negative and positive weight particles will have to be transported separately. A point to be noted is that the terms arising due to different diffusion coefficients in the two regions have positive and negative contributions which add up to zero. On the other hand the one due to different absorption in the two regions causes a net positive weight to be emitted from sites in the second medium which is exactly equal to the difference between the weight entering the collision and the weight absorbed at the collision site. Thus the difference in the diffusion coefficients causes only the weights to be re-distributed in space and time.

The first "collision" point is sampled from the distribution $P_0(\vec{r}, t)$ for the variables y, z and t . With

$$2\pi^{-1/2}$$

probability $1 + \frac{1}{-1}$ sample x using the same Gaussian ($P_0(\vec{r}, t)$) and set its weight equal to $1/p$.

$$p =$$

With probability $1 - p$ set $x=a$ and set its weight equal to $(1-p)/p$. This is done to take care of the

delta function. In the former case transportation is done according to the usual transport kernel and a weight

$$r - r' = \frac{3(D_2 - D_1)}{\sigma^2 \Sigma_{r1}} \left(1 - \frac{\Sigma_r}{\Sigma_{r1}} \right)$$

is assigned. In the latter case transport the particle using the distribution $P(\vec{r} - \vec{r}', t - t')$ with $x'=a$ and assign a weight equal to $\frac{3(D_2 - D_1)}{\sigma^2 \Sigma_{r1}} \frac{(x-a)}{\sigma}$. In either case the particle may be absorbed fully at the new location or it may be re transported according to the same procedure. On an average the weights (positive or negative) keep reducing in magnitude. As mentioned above, a Russian Roulette has to be played to terminate the process once the weight falls below a certain magnitude.

Alternative approach for analog games

The approach described above is not suitable for analog MC. However, it is possible to model this problem with transport theory type MC methods (Rana et. al, 2013). It is noted that the diffusion kernels are Gaussians, and that diffusion theory is the limiting situation of transport theory when the neutron undergoes a very large number of collisions before absorption and the mean free paths are short compared to other lengths. This is another statement of the Central limit theorem. In practice, however, a few random numbers when added together show a distribution closely resembling a Gaussian. So the only thing that is necessary is to preserve the parameters.

The total distance traveled by a particle is vt (t is the removal time of neutron) while the average distance traveled in each collision is (in medium I) $3D_1$, the mean free path. The number of collisions is thus $vt/3D_1$. This could be very large (let us say 100). If this is to be scaled down to let us say 4, all is needed to do is to scale up the mean free path (diffusion coefficient) in medium I by $\sqrt{(vt/3D_1)}/4$. Likewise, while traveling in medium II, scale up the mean free path in medium II

by $\sqrt{(vt/3D_2)}/4$. This prescription will correctly give the (RMS) distance traveled by the neutron from its starting point before removal and also the (approximately) correct spatial distribution for the sampled value of t . Finally whether the removal point is to be accepted or not is decided by the rejection technique described in 4.3.1.1.

Numerical Validation

Consider a two region infinite medium with a boundary at 2 cm away from the origin. The source is located at the origin. Medium 1 has absorption cross section of $\Sigma_{r1} = 0.01 \text{ cm}^{-1}$ and mean free path of 0.04545 cm. Medium 2 has absorption cross section of $\Sigma_{r2} = 0.005$ and mean free path of 0.99 cm. Here, Transport MC method based on Coleman's Method or pseudo collision method (Cloeman W. A., 1968) is used for estimating the absorption rate in the two mediums. Accept the point with a probability equal to the ratio of the actual removal cross section of the region in which the selected point lies and the maximum removal cross section. Else the point is rejected. In the latter case particle is displaced to a new point in the same direction with distance equals to the mean free path of the particle assuming it has suffered a pseudo collision. The process is repeated till a point is accepted. Other details are same as described in section 4.3.1.1

A plot of the time integrated absorption rate for the recipe suggested above is given in Fig 4.6. 10^7 particles are simulated. Fitted values of absorption rate obtained by increased mean free path differs by about a maximum of 8% with that of original mean free path while the associated statistical error is $\pm 1 \%$ and $\pm 3\%$ respectively. It is seen that near the source, deviations are larger due to the presence of residual transients but at distance away from the source, deviations are within statistical error. In Fig. 4.7 a comparison of the absorption at different time in the two media is shown. Maximum deviation of 10% is observed in absorption rate for time bin of 0-0.1 msec.

4.4 Transport Corrections to Diffusion MC

It was mentioned earlier that diffusion theory is not valid (a) close to localized sources (b) close to vacuum boundary (c) inside and close to strong absorbers (d) highly anisotropic scattering. In this section each of these conditions is examined one by one and will develop methods to extend the applications of Diffusion Theory MC to such regimes.

The solution of the transport equation for a point source in an infinite homogeneous medium can be obtained by the Fourier Laplace transforms similar to that of the diffusion equation. The flux splits into a sum of a transient flux which dominates close to the source and an asymptotic flux which has a form similar to the diffusion flux and is important far away from the source. These facts are used in this section to show that it is possible to extend the diffusion theory MC method to situations where diffusion theory is not valid, viz., close to localized sources, strong absorbers, boundaries and anisotropic scattering.

4.4.1 Transient Flux Close to a Localized Source

Expression for the flux for a point source placed at the origin in the infinite medium is given by (Bell and Glasstone, 1970),

$$\varphi(r) = \varphi_{As}(r) + \varphi_{transient}(r) \quad (4.31)$$

where,

$$\varphi_{As}(r) = \frac{S_0 \beta}{4\pi D r} \exp(-\kappa r)$$

$$\varphi_{transient}(r) \approx (S_0/4\pi r^2) \exp(-\Sigma' r)$$

With $\kappa = \sqrt{\Sigma' / D}$, $\beta = 1 - \Sigma_a / \Sigma'$ and $\Sigma' = 5 \Sigma / 4$

The flux near a localized source is not well described by diffusion theory even in a diffusive medium i.e. one in which scattering is large compared to removal. This is due to the presence of a transient flux. Since it is also known that most of the transient flux is simply the un-collided flux while the asymptotic flux is due to neutrons that have undergone collisions. The difference between

diffusing and non diffusing (absorbing) media is simply the relative contribution of the transient and asymptotic components.

A recipe for transport correction to Diffusion MC is proposed using the approximations available for the transient flux given in equation (4.31). Sample the absorption event using the expression for the transient flux with a probability proportional to the transient component while rest of the times it will be sampled using the asymptotic flux expression. A more accurate expression for the transient flux is available (A. M. Weinberg, 1958) but sampling the relevant distribution is not easy.

Numerical Validation

Numerical Simulations were carried out using the usual transport MC method as described in section 4.4.1. Transport Corrected Diffusion MC simulation was carried out using equation (4.31). Total cross section of the medium is 2.2 cm^{-1} , while the absorption and scattering cross sections are 0.01 cm^{-1} and 2.19 cm^{-1} respectively. Fig. 4.8 shows the time averaged neutron flux due to a source in a mildly absorbing medium with a point source located at the origin, obtained by the above method. Also the flux distribution by infinite diffusion kernel is plotted. The latter represents the asymptotic flux which obeys the diffusion equation. The relaxation length estimated by fitting the asymptotic flux agrees well with the theoretical value. It can be seen from the plot that Diffusion MC flux near the source is lower than the Transport MC flux since diffusion theory fails in this region, but the transport corrected Diffusion MC flux estimates same flux as obtained by transport theory. Flux estimated by Transport corrected Diffusion MC differs from that estimated by Transport MC by about a maximum of 2%. The corresponding time dependent fluxes at different times are compared in Fig. 4.9. It is seen that the flux decreases with the distance away from the source and this rate of decrease becomes less effective with longer collision time. Maximum deviation of 3% is observed in absorption rate for time bin of 0-0.1 msec.

4.4.2 Transport in a strongly absorbing medium

This case is related to the one discussed in the previous section. In a weakly absorbing medium, a neutron undergoes a large number of collisions before absorption and therefore the asymptotic flux is the dominant term except very close to the source. In case of a strong absorber there are few collisions before absorption and hence the transient flux is dominant near the source but there are not many collisions and hence the asymptotic component is small.

Numerical Validation

The results of calculations by the transport MC and transport corrected diffusion MC are shown in Fig. 4.10. The total cross Section of the medium is 2.2 cm^{-1} , the absorption cross section is 1.2 cm^{-1} and the scattering cross section is 1.0 cm^{-1} . It can be seen near the source, there is large difference of 40% in the asymptotic flux and the flux estimated by the Transport MC. With transport correction applied to the asymptotic flux, this difference is considerably reduced to 10%. The agreement is quite good showing that the recipe is valid even for strongly absorbing media. The only difference is that savings in computer time are small as the neutron history is anyway not too long. On the other hand the savings in case of a weak absorber are much larger.

4.4.3 Transients Close to a Vacuum Boundary

Transients close to a vacuum boundary are due the negative source of the neutrons directed outwards.

Numerical Validation

Fig. 4.11 shows the flux distribution due to a source in a finite isotropic medium with boundary at 4.5 cm from the point source placed at the origin. Transport flux is obtained using a MC algorithm using the last event absorption estimator described in section 4.4.2. In case the particle leaks out, the event is stopped and goes for the next neutron history. It is seen from Fig. 4.11 that asymptotic flux obtained by Diffusion MC Method compares well with the analytical expression for the flux distribution for symmetric boundary given below.

$$\phi(x) = -LS/2D(1/1+e^{(2X/L)})e^{(x/L)} + LS/2D(e^{2X/L}/1+e^{(2X/L)})e^{(-X/L)} \quad (4.32)$$

where, L , D , S and X are the neutron diffusion length, diffusion coefficient, source strength and extrapolation distance respectively.

It is also seen that the flux estimated by transport and diffusion MC are nearly the same at the boundary which implies that the transient flux near the boundary is small compared to that near the source. This is probably due to the fact that by Placzek's Lemma, the transients at a boundary are caused by a negative source of neutrons directed outwards, which produces smaller transients inside the region of interest. Flux estimated by Diffusion MC differs from that estimated by Transport MC by about a maximum of 0.5%.

4.4.4 Transport Effects with Anisotropic Scattering

In all the examples given above, it is assumed that the scattering is isotropic in the laboratory system. The general case involving anisotropic scattering requires a transformation of coordinate system from the one in which the scattering law is given, to the fixed coordinate system in which the particle is tracked (Stephen Dupree et. al., 2001; MCNP Guide 1987; Paul et. al., 2013). While the transformation is elementary, but for clarity and better understanding a detailed derivation of the transformation and a description of the algorithm is presented in Appendix A.

Numerical Validation

Using the above algorithm calculations for a hydrogenous medium in which the scattering is strongly anisotropic in the laboratory system is carried out. Fig. 4.12 gives the flux distribution obtained using transport MC and the transport corrected diffusion MC for a mildly absorbing medium. Transport cross section was used for estimating the diffusion coefficient to account for anisotropic scattering. Flux estimated by Transport corrected Diffusion MC differs from that estimated by Transport MC within statistical error. The good agreement shows that the above recipe is valid in a medium with anisotropic scattering.

4.5 Conclusions

Analytical Green's function based Diffusion MC methods have been applied earlier for by Rana et. al. for simulation of reactor noise experiments in experimental reactors for measuring the degree of sub-criticality in accelerator driven systems. Although this approach has several advantages such as speed, elegance and exactitude, but it was applicable to a rather restricted class of problems, such as the bare rectangular parallel piped homogeneous reactor. Here, the analytical Greens function based Diffusion MC methods is developed further, to demonstrate its utility in a wider class of problems such as in finite homogeneous and heterogeneous media. Mathematical and numerical proofs of the recipes proposed for applying diffusion kernel of infinite homogeneous medium to heterogeneous medium with same or different diffusion coefficient developed.

For a heterogeneous medium consisting of two regions having different diffusion coefficients, the mathematical proof goes through but the resulting sampling functions are more complicated and hence the method may be difficult particularly for analog MC but would be usable with non analog MC. However, a different recipe suggested for this situation in Rana et. al., 2013 which is more appropriate for analog MC has been demonstrated to work successfully. It has been also shown that by a transport correction based on incorporating the transient flux kernel in addition to the diffusion kernel, the method can be applied to the situations where diffusion theory is otherwise inapplicable.

Computational time for Diffusion MC is about 10 times less than that by Transport MC. In addition to its use as a fast analog method for simulating noise by MC, the present work could find application in devising mesh less methods in time dependent diffusion theory, particularly in situations involving moving media where meshes tend to get distorted. Another application could be to study various aspects of MC such as variance reduction techniques, and speeding up convergence to the fundamental mode of criticality calculations. In this context, it may be mentioned that besides

the advantage of speed, the diffusion MC has the advantage that analytical results are available in diffusion theory for the purpose of making comparisons.

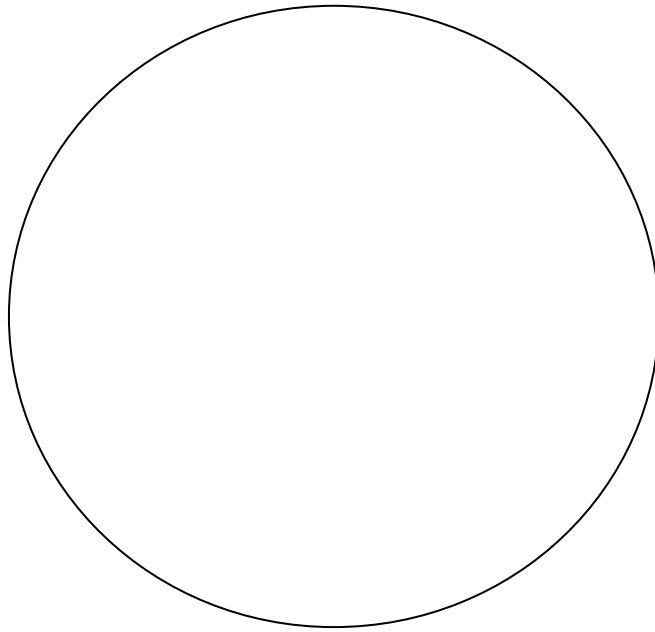


Fig. 4.1 Diagrammatic representation of the source and image point locations and the coordinates used in the estimation of the reduction in extrapolation distance for a bare homogeneous cylindrical reactor by method of images

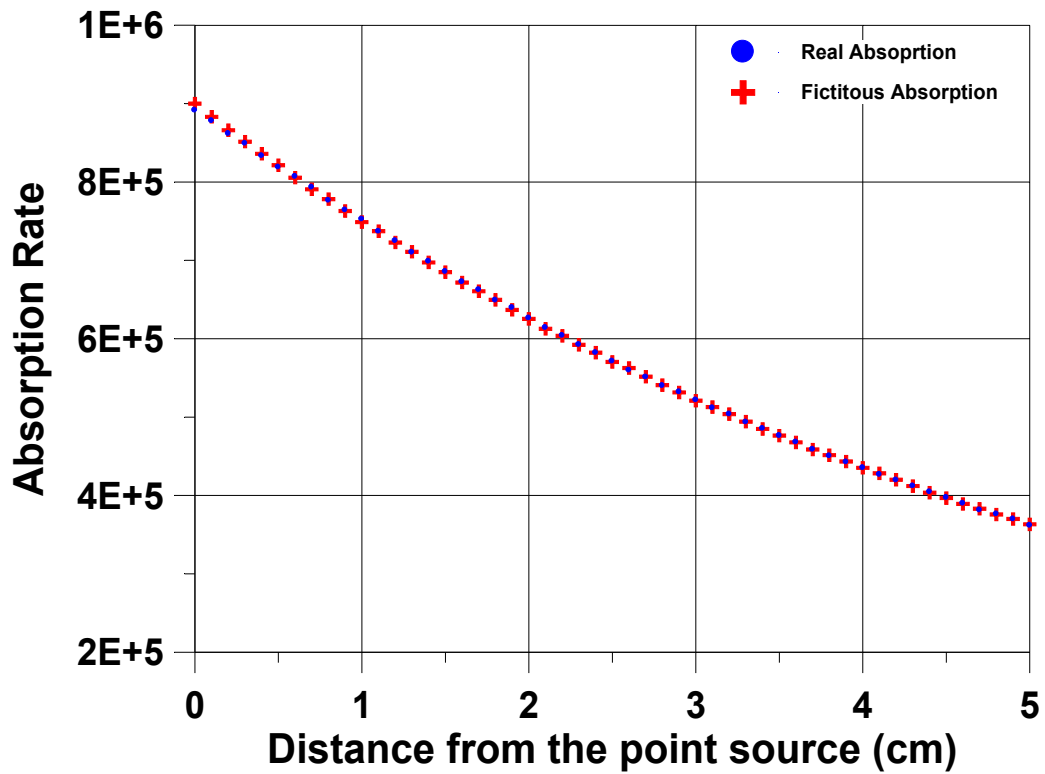


Fig. 4.2 Variation of the time integrated neutron absorption rate with distance from a point source placed at the origin in single region medium. The blue dots indicate the absorption rate obtained using the real absorption cross section $\Sigma_{ar} = 0.005 \text{ cm}^{-1}$ while the red cross indicate the absorption rate calculated with a fictitious absorption $\Sigma_{af} = 0.01 \text{ cm}^{-1}$ followed by a rejection with a 50% probability.

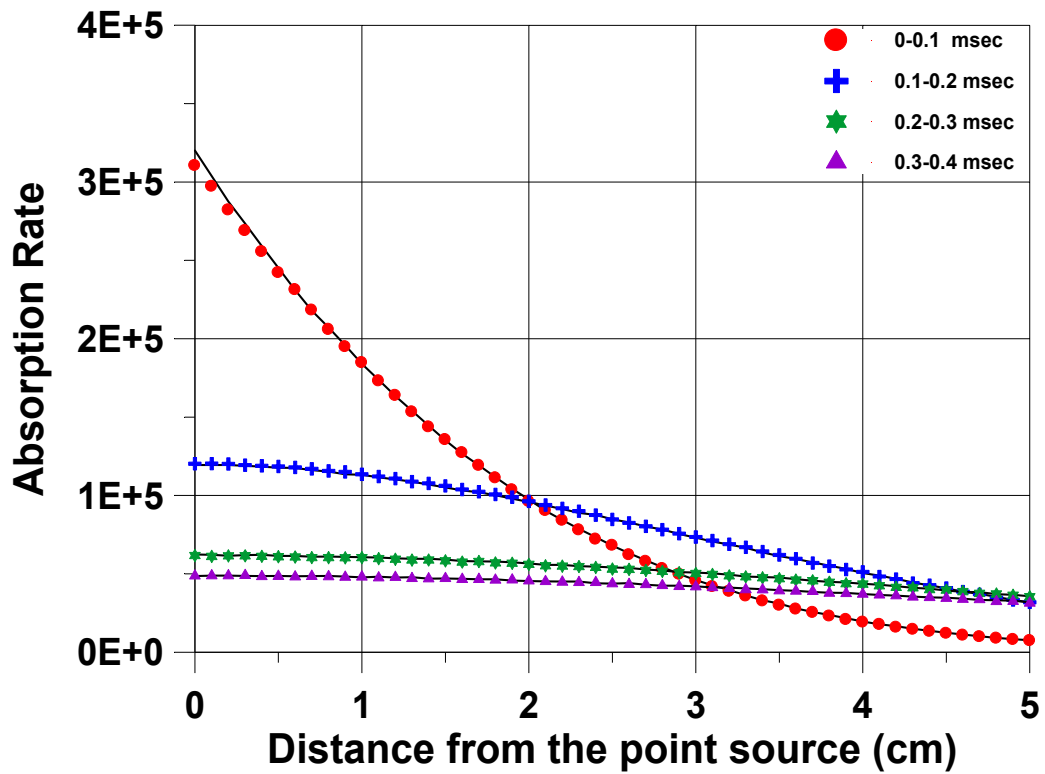


Fig. 4.3 Variation of the time dependent neutron absorption rate with distance from a point source placed at the origin in single region medium. The various markers indicate the absorption rate obtained using the real absorption cross section $\Sigma_{ar} = 0.005 \text{ cm}^{-1}$ while the solid lines indicate the absorption rate calculated with a fictitious absorption $\Sigma_{af} = 0.01 \text{ cm}^{-1}$ followed by a rejection with a 50% probability.

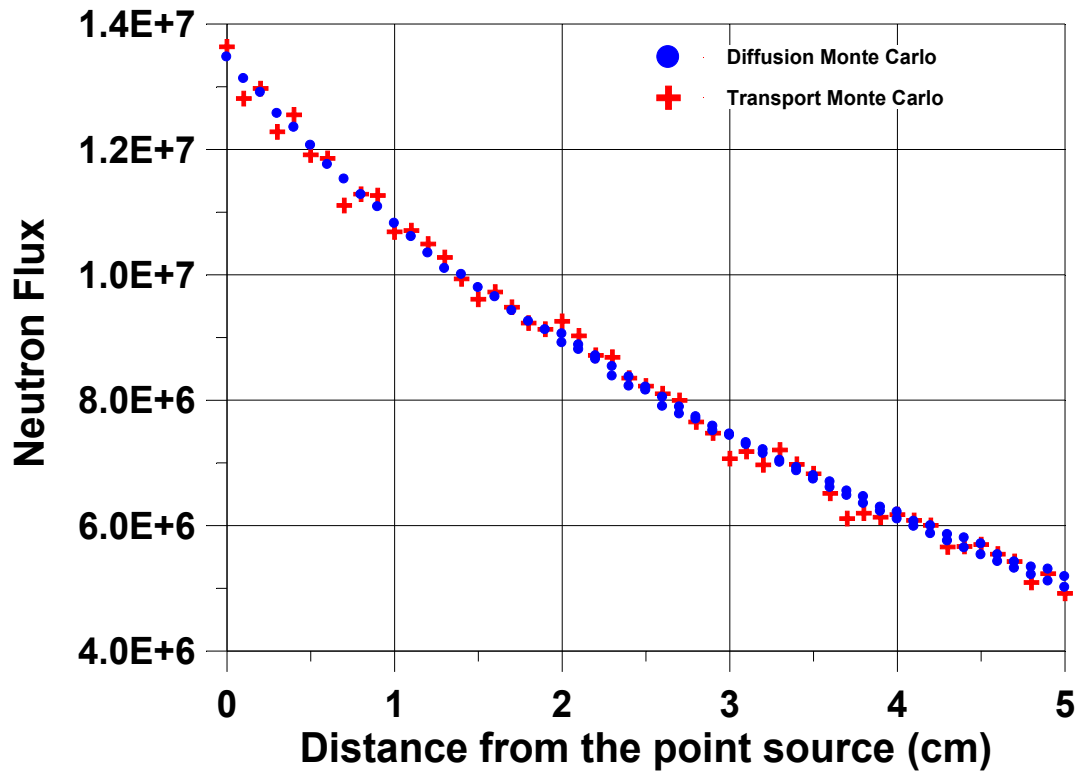


Fig. 4.4 Variation of the time integrated neutron flux with distance from a point source placed at the origin in a two region medium with same diffusion coefficients but different absorption cross sections viz. $\Sigma_{ar} = 0.005 \text{ cm}^{-1}$ to the left of $x=2$ and $\Sigma_{ar} = 0.01 \text{ cm}^{-1}$ to the right of the plane $x=2$. The red crosses indicate the exact results by Transport MC while the blue stands for diffusion MC.

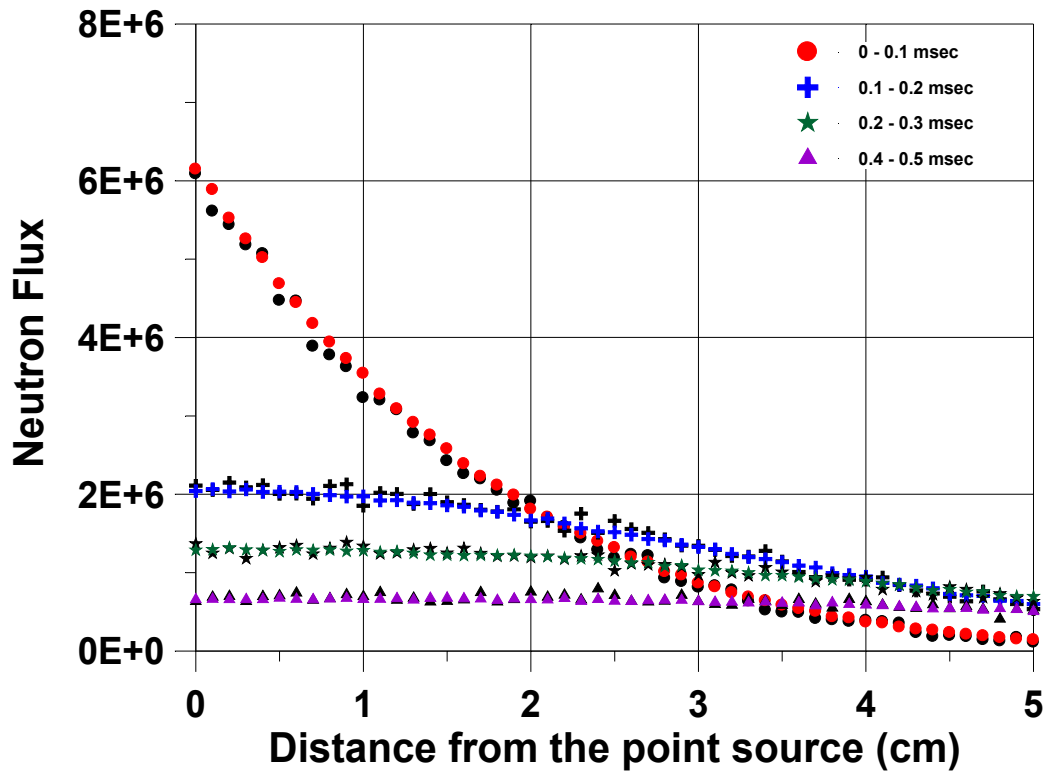


Fig. 4.5 Variation of the time dependent neutron flux with distance from a point source placed at the origin in a two region medium with same diffusion coefficients but different absorption cross sections viz. $\Sigma_{al} = 0.005 \text{ cm}^{-1}$ to the left of $x=2$ and $\Sigma_{ar} = 0.01 \text{ cm}^{-1}$ to the right of the plane $x=2$. The various markers indicate the flux obtained using the Diffusion MC while the corresponding black markers indicate the flux calculated with Transport MC using the rejection technique.

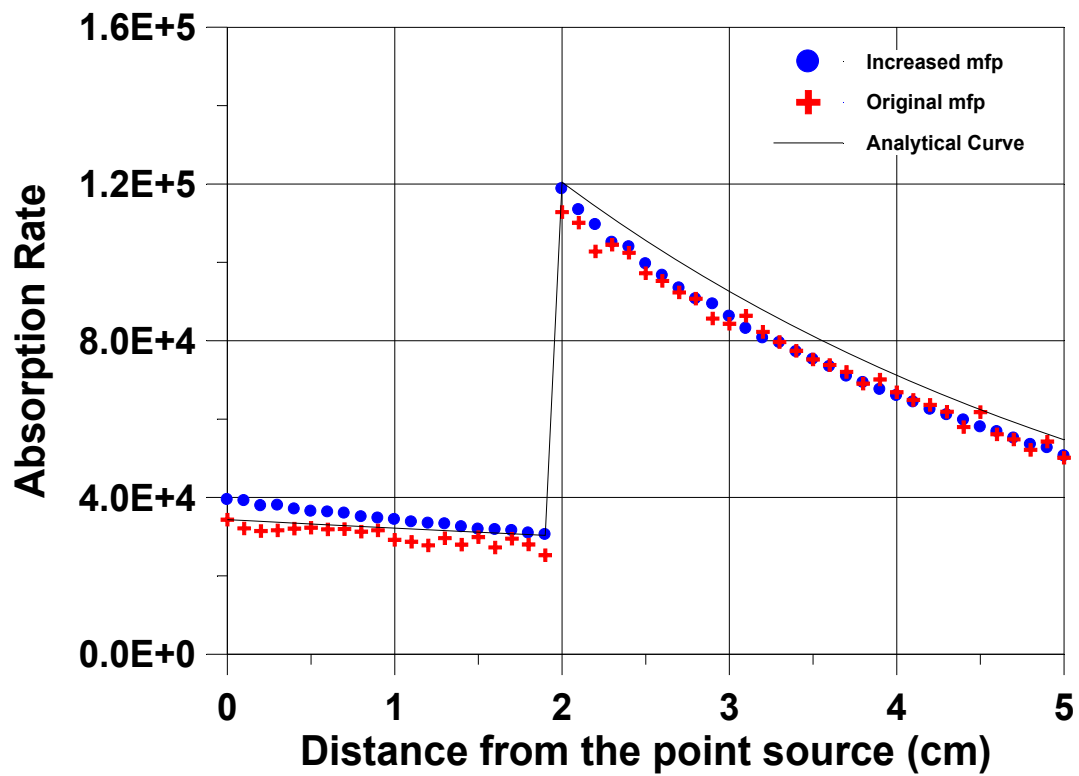


Fig.4.6 Variation of time averaged neutron absorption rate with distance from the point source placed at the origin in two region medium with boundary at $x=2$. $\Sigma_{r1} = 0.01 \text{ cm}^{-1}$ and $D_1=0.1515$ to the left of the boundary while $\Sigma_{r2} = 0.005 \text{ cm}^{-1}$ and $D_2=0.33$ to the right. The figure shows a comparison of the absorption rate obtained with actual mean free path (mfp) and that with 4 times higher mfp. Solid curve corresponds to analytically computed neutron absorption rate.

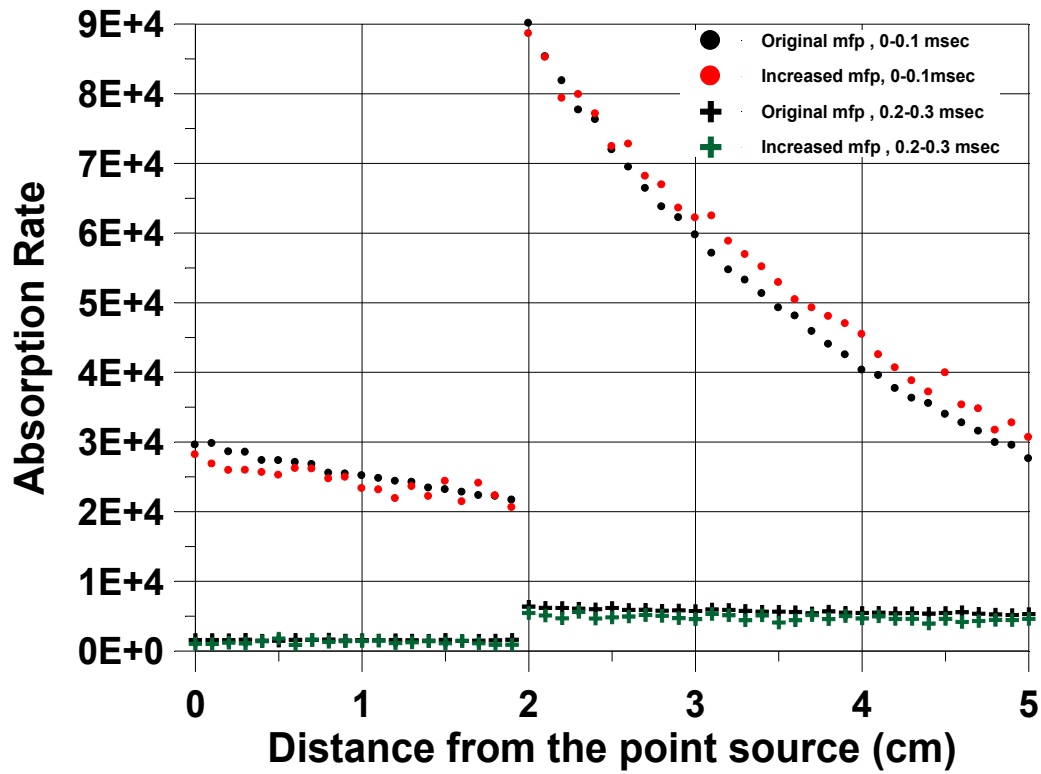


Fig. 4.7 Variation of time dependent neutron absorption rate with distance from the point source placed at the origin in two region medium with boundary at $x=2$. $\Sigma_{r1} = 0.01 \text{ cm}^{-1}$ and $D_1=0.1515$ to the left of the boundary while $\Sigma_{r2} = 0.005 \text{ cm}^{-1}$ and $D_2=0.33$ to the right. The figure shows a comparison of the absorption rate obtained with actual mean free path (mfp) and that with 4 times higher mfp.

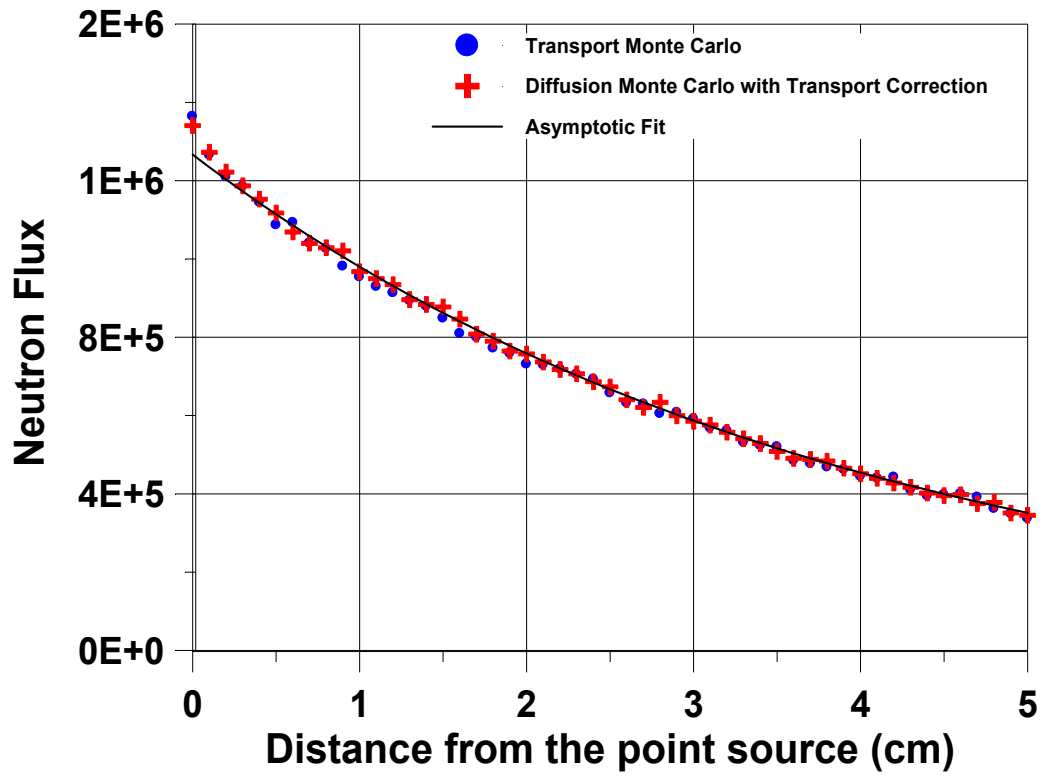


Fig. 4.8 Variation of the time averaged neutron flux with distance from a point source located at the origin in a mildly absorbing medium. The figure compares the results using transport MC and transport corrected diffusion MC.

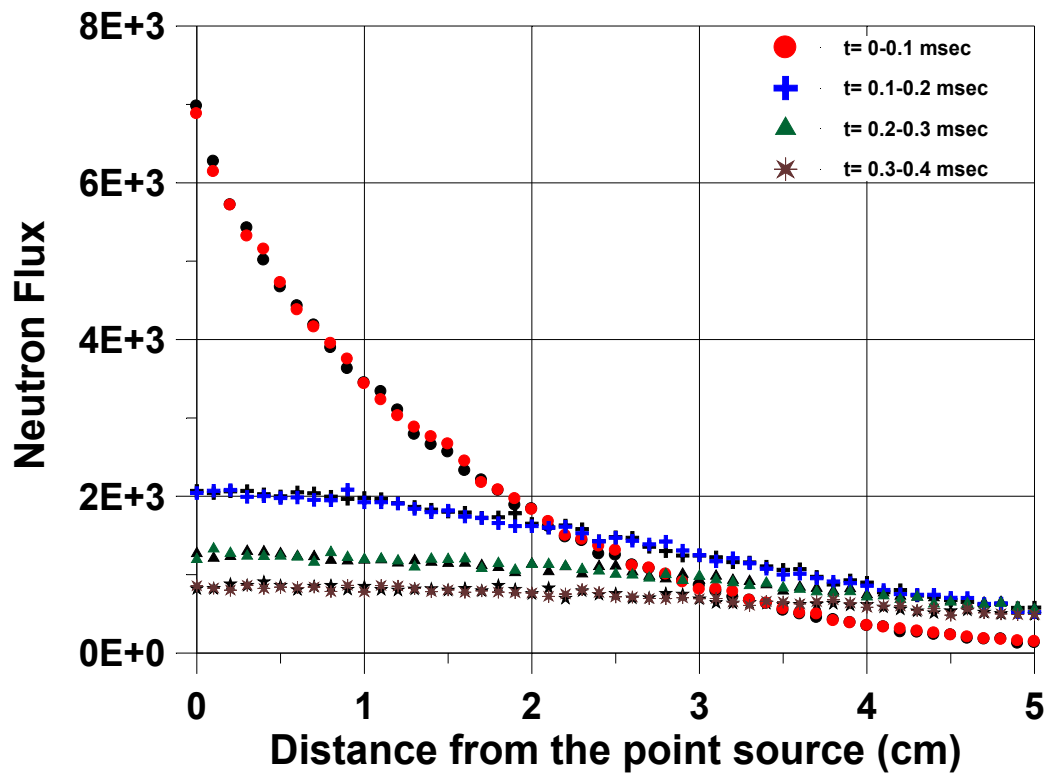


Fig. 4.9 Variation of the time dependent neutron flux with distance from a point source located at the origin in a mildly absorbing medium. The figure compares the results using transport MC and transport corrected diffusion MC.

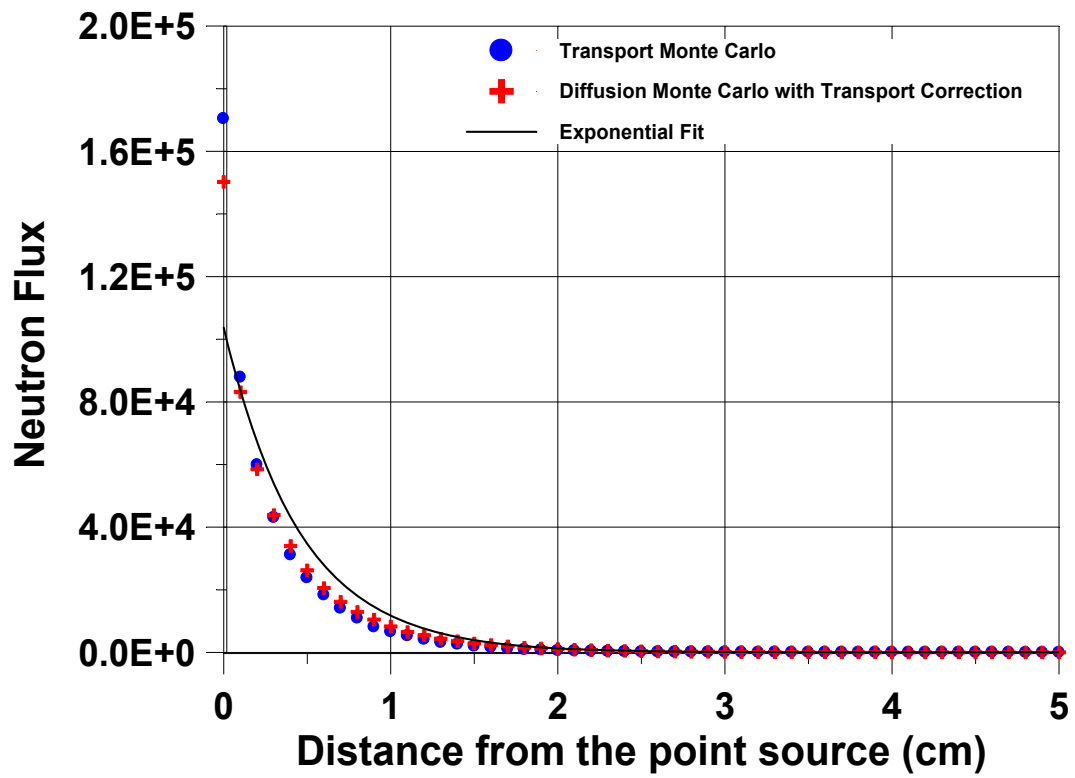


Fig. 4.10 Variation of the time averaged neutron flux with distance from a point source located at the origin in a strongly absorbing medium. The figure compares the results using transport MC and transport corrected diffusion MC.

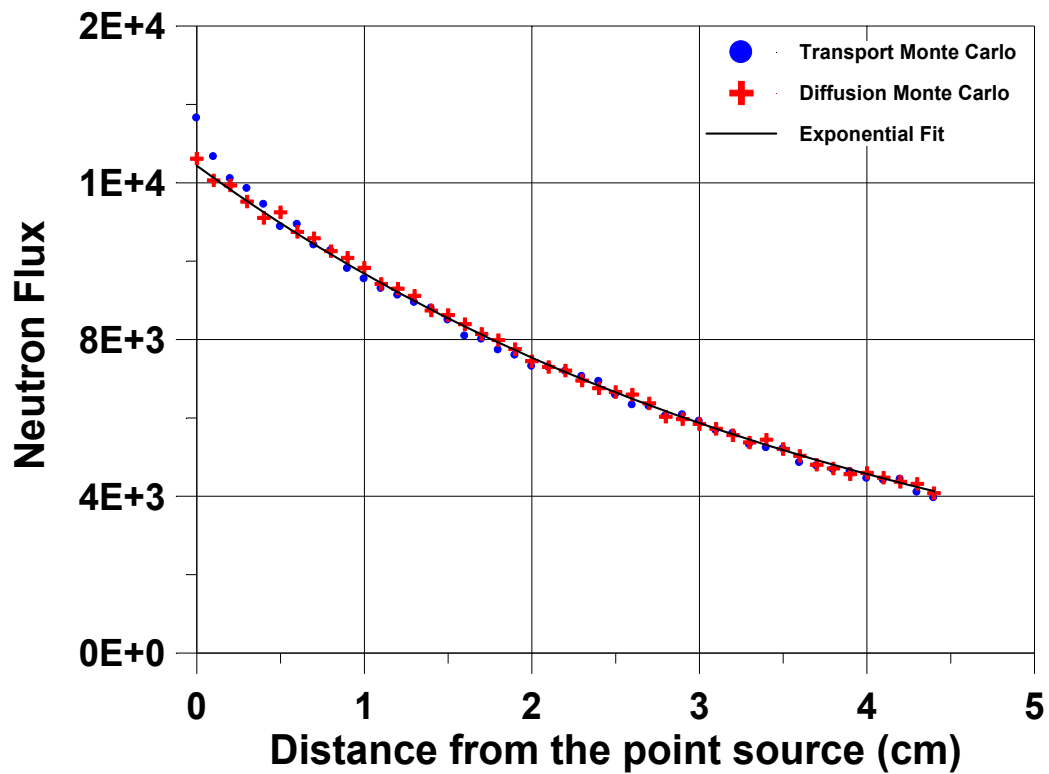


Fig. 4.11 Variation of the neutron flux (time averaged) with distance from the point source in a semi infinite homogeneous medium. The point source is placed at the origin and the medium-vacuum boundary is located at $x=4.5$ cm from the source. The figure shows a comparison of results based on transport and diffusion MC and the analytical fit.

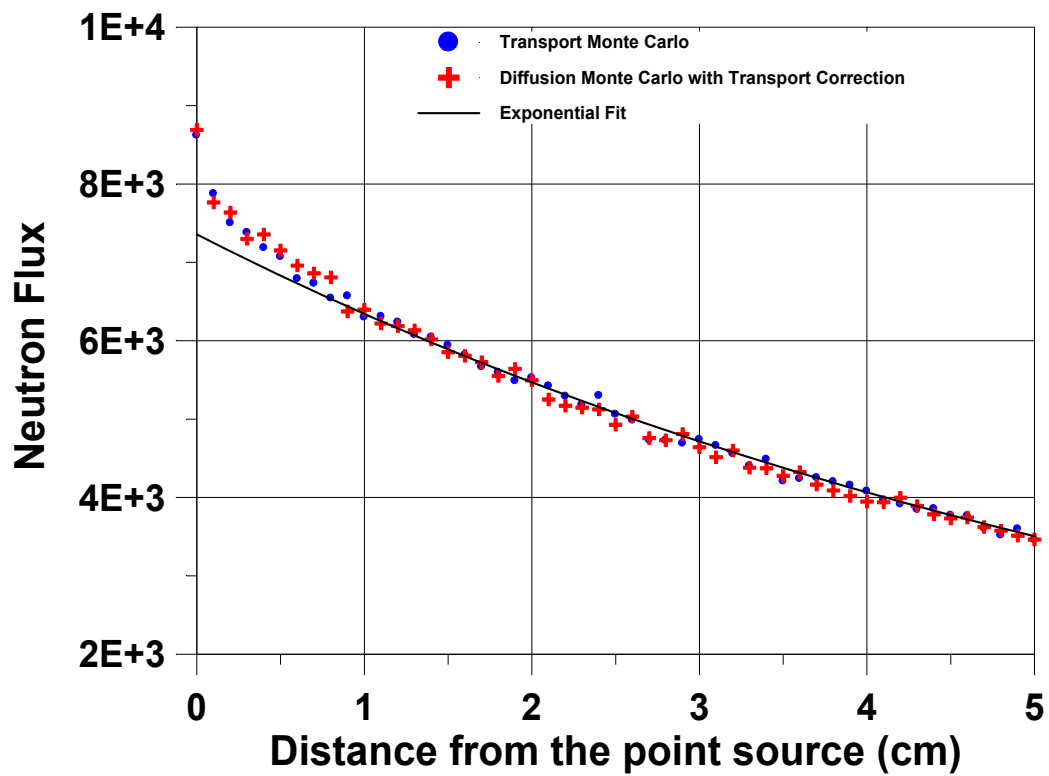


Fig. 4.12 Neutron Flux due to a source in an infinite homogeneous medium with mild absorption and anisotropic scattering - comparison of results obtained using transport MC and transport corrected diffusion MC.

**Table 4.1 Reduction in extrapolation distance d_{ex} as function of radius of the cylinder
(Diffusion Length, $L= 6$ cm)**

<i>Radius R (cm)</i>	<i>d_{ex} required to give correct k_{eff} using a single image</i>	<i>$d_{ex} = L^2/R$ as given by eq. (4)</i>	<i>d_{ex}, as given by eq. (6) with $a=1.2$</i>	<i>d_{ex}, as given by eq. (5)</i>
30	0.94	1.20	0.92	0.91
40	0.88	0.90	0.75	0.73
50	0.64	0.72	0.63	0.61
60	0.52	0.60	0.55	0.53

A Diffusion Monte Carlo Based Algorithm for Estimation of Higher Modes of a Reactor

In the Chapter 2 some schemes for developing Monte Carlo kinetics capability is discussed. Application of these schemes to simple point kinetics and diffusion based space time kinetics were discussed in subsequent chapters. Another important problem that is of interest in both statics and kinetics relates to the calculation of higher modes. While most often this problem has been solved using deterministic diffusion theory, in recent years there has been interest in obtaining higher modes using Monte Carlo methods. The present chapter discusses the problem of obtaining higher modes using Monte Carlo.

The K and α or time eigenvalue problems are basic to the subject of nuclear reactor physics. While the fundamental modes are most often computed as they decide the multiplication factor and power distribution of a critical reactor, some of the dominant higher modes of these problems are often useful as basis functions for expanding the flux (Singh et. al., 2009; Pfeiffer, 1971, 1972). The eigenvalue problem is usually solved by deterministic neutron transport theory and most often using the diffusion theory approximation. In recent years the use of the MC method has expanded in scope to solve an increasingly larger variety of Reactor Physics problems due to its exactitude. In this spirit, there have been efforts at solving the problem of obtaining higher modes using the MC Method.

Estimation of higher modes of the neutron transport equation by MC methods has been developed earlier (Booth et. al., 2003; 2006; 2009; Modak et. al. 2007; Lathouwers, 2003; Kophazi et. al., 2012). The Modified Power Iteration method suggested by Booth et. al., 2003 is used to reduce the error associated with higher eigenfunctions. Another technique to obtain the higher order eigenfunctions in MC criticality calculations was proposed by (Yamamoto et. al., 2003; Yamamoto et. al., 2011). Yamamoto estimated the higher order α mode eigenvalues by the MC Power

Iteration. Estimation of higher order eigenvalues for deep sub criticality is difficult due to large negative weights. Yamamoto introduced a pseudo absorption term to reduce negative weights. Korneich et. al., 2005 used Greens function method to calculate higher time eigenvalues in multi region Cartesian geometry. Dufek and Gudowski et.al., 2009, Wenner and Haghghat et. al., 2011 have also tried the Fission Matrix approach for eigenvalue calculations. Carney et. al., 2012 and Carney et. al., 2013 and Urbatsch, 1995 has included the fission matrix method in a modified version of the MCNP Code. Sub space iteration techniques have also been tried for efficient MC solutions of K eigenvalue problem (Gupta et. al., 2013).

Estimation of higher eigenvalues of the neutron transport equation by various MC methods presents a number of challenges that continue to be the subject of research. Thus, for example, Arnoldi's method requires orthogonalization and normalization of the fission source which inevitably leads to negative fission source in some regions. Some recipes are required to tackle sampling from such a fission source. Similarly, the modified power method also introduces negative weights and hence needs recipes for cancellation of positive and negative weights.

The main issue with the fission matrix is the uncertainty on its elements. This is related to the size of the zones (which must be judiciously chosen) for obtaining the fission matrix. The zone size must be kept small, so that there is little variation in the fission source distribution within a zone. However, if the zones are made very small, not only does the fission matrix increase (due to increase in number of zones) but the elements of fission matrix contain larger statistical errors, since the number of starting neutrons per zone decrease with a decrease in the zone size. Another problem of fission matrix methods (transition rate matrix methods for alpha eigenvalues) is that of estimating the statistical uncertainty of the eigenvalues obtained by these methods (Betzler and Kiedrowski et. al., 2018; Betzler and Martin et. al., 2014; Betzler and Kiedrowski et. al., 2015)

The suitability and adequacy of various recipes used in these methods for computing higher eigenmode cannot be decided only from theoretical principles, and therefore require intense numerical studies for their validation. The study of simpler models may be expected to provide

better insights into some of these problems. The issues involved in sampling fission matrix and effect of these recipes can be studied more easily using simpler and faster MC scheme based on diffusion theory.

In this Chapter, a simple model based on Diffusion theory MC to estimate the higher K eigenvalues of the neutron transport equation is studied. The Diffusion MC method (Rana et. al., 2013) was developed for quick simulation of ADS noise experiments that must be done using analog MC and therefore requires rather long computational time by the usual transport MC route. The method was expanded in scope (Srivastava and Degweker., 2015) and subsequently used to study space time kinetics by the Monte Carlo (Srivastava et. al., 2018) approach as discussed in Chapters 4 and 5 respectively.

This Chapter is focused on the calculation of the higher λ modes based on Diffusion MC. A MC Algorithm is developed for estimating higher eigenvalues and eigenvector using Fission Matrix. Numerical testing of the algorithm so developed is carried out by considering a PHWR benchmark in super critical and deep sub critical conditions. A first order perturbation approach is developed to estimate the variance in higher eigenvalues from the deviations of the matrix elements [in successive iteration cycle] from the mean.

6.1 Methodology

6.1.1 Computation of the Fission Matrix

In the algorithm developed, eigenvalues of the system by the Fission Matrix Method is estimated. The Fission Matrix (FM) of a system contains information about the number of neutrons produced in one region of the core from one neutron born in another region. The order of the FM is simply the number of spatial regions the core is divided into. The eigenpairs of the fission matrix are estimates of the k-eigenvalues and eigenvectors of the core that are limited by the resolution of the discretised phase space. An estimate of the FM matrix is obtained using the neutron histories data. At first, the region containing fuel (the core) is divided into a number of meshes. These meshes are

superimposed on the geometry description used for neutron tracking. Starting from an initial spatial distribution of fission neutrons across the meshes, these neutrons are tracked one by one till they are absorbed (capture or fission) or leak out. The neutrons produced as a result of fission caused by these initial neutrons are assigned to the mesh in which they are produced and form the starting neutrons for the next cycle. The number of neutrons in each cycle are maintained the same as in the algorithm for k_{eff} estimation.

Tallying of the fission matrix is carried out using the following procedure after a user decided number of cycles have been discarded, so that the distribution of fission neutrons becomes stationary in the statistical sense. After making a check to find out the mesh (j) from which the particle is starting, the tally (N_j) of the number of neutrons starting from mesh j is updated by adding one to it. The neutron is then tracked for its movement from the mesh into its neighboring meshes or for slowing down to lower energy groups or absorption using the relative probabilities of these events described in detail as discussed in Chapter 5. The tracking is continued till it is absorbed (capture or fission) or it escapes from the system. If it terminates in fission, the mesh number (i) in which fission occurred and the number of fission neutrons emitted (ν) are recorded. The fission matrix element tally F_{ij} is updated by adding an amount equal to ν to it. A schematic of the process is shown in Fig. 6.1.

At the end of a cycle, the fission matrix elements are normalized (to obtain the value per particle) i.e. the ratio F_{ij}/N_j computed and these are simply the elements of FM. That is to say that (i, j)th element of this matrix is the average number of fission neutrons generated in zone i per unit neutron starting from mesh j . The above described process to obtain FM is by using tallying whenever fission occurs. At each cycle then a FM (we call it the *cycle* FM) is obtained. At the end of all the cycles the individual FMs are combined together to get an average FM.

6.1.2 Eigenvalues and Eigenvectors of the Fission Matrix

It is clear from the definition of the fission matrix, that the number of fission neutrons generated in the mesh in the $(n+1)^{\text{th}}$ generation is related to the number produced in j in the n^{th} generation as follows

$$\phi_i^{(n+1)} = \sum_j F_{ij} \phi_j^{(n)} \quad (6.1)$$

For a stationary situation, the distribution does not change from generation to generation, but may change in magnitude. This gives rise to the lambda or k eigenvalue problem defined by the equation $\sum_j F_{ij} \phi_j = \lambda \phi_i$

Or,

$$F\phi = \lambda\phi \quad (6.2)$$

Hotelling's Deflation method is incorporated along with the Power method to obtain higher eigenmodes. The process of obtaining higher eigenmodes is as follows. At first, the largest (fundamental) eigenpair is obtained using the power method. The FM is then deflated of its fundamental eigenpair. Deflation means removing the eigenmode from the matrix. That is, after deflation of fundamental mode, the power method applied on the deflated matrix gives the 2nd eigenpairs (of the original matrix), as *this* is the fundamental mode of the deflated matrix (Mallick et. al., 2014). The above process may be repeated by deflating the last deflated matrix for 2nd eigenpair to obtain 3rd eigenpairs and so on. The method and algorithm to obtain higher eigenmodes is described below briefly.

Let λ_1 be the highest eigenvalues and ϕ_1 the corresponding eigenvector of the matrix, F as obtained using Power method. The matrix, F is then deflated of the eigenpair (λ_1, ϕ_1) as follows

$$F_{d1} = F - \lambda_1 \phi_1 \phi_1^T \quad (6.3)$$

Where F_{d1} stands for the fission matrix deflated of the pair (λ_1, ϕ_1)

Next, the power method is applied to the deflated matrix F_{d1} to obtain its largest eigenvalue and the corresponding eigenvector. This eigenpair is the 2nd eigenpair of the original matrix^F. The last deflated matrix F_{d1} is then again deflated of the *newly* obtained eigenpair, to obtain F_{d2} , the matrix deflated of the first two eigenpairs

$$F_{d2} = F_{d1} - \lambda_2 \phi_2 \phi_2^T \quad (6.4)$$

This process is repeated till all the desired eigenpairs are obtained.

6.1.3 Estimation of Error in the Eigenvalues of the Fission Matrix

MC calculations involve statistical uncertainties in the estimated quantities. Estimation of these uncertainties is important to get an idea of the statistical error in the computed quantities. This is usually done by calculating the same quantity using several batches and estimating the standard error of the mean of all batches from the standard deviation of the batches. This is not easily possible in the fission matrix method. In this section it is shown how perturbation theory may be used to obtain the error estimate. Let us say that the estimated average fission matrix is F while the matrix computed in the n^{th} cycle is $F + f^{(n)}$, where $f^{(n)}$ is assumed to be small and may be treated as a perturbation.

The matrix $f^{(n)}$ represents the deviation from the mean estimate of the fission matrix and leads to a corresponding deviation $\Delta\lambda_\mu^{(n)}$ in the estimation of the μ^{th} eigenvalue in the n^{th} cycle. It is well known from perturbation theory that to the first order in $f^{(n)}$,

$$\begin{aligned} & +, f^{(n)} \phi_\mu \\ & \phi_\mu \\ & +, \phi_\mu \quad (6.5) \\ & \phi_\mu \end{aligned}$$

$$\Delta\lambda_\mu^{(n)} =$$

where $\Delta\lambda_\mu^{(n)}$, ϕ_μ and $+ \phi_\mu$ respectively stand for the deviation in the estimate of the μ^{th} eigenvalue in the n^{th} cycle, and the μ^{th} eigenvectors of the forward and adjoint (transpose) estimated mean fission matrix F .

On writing this formula out explicitly in terms of components of the eigenvectors and matrix elements, we have

$$\frac{\sum_i \phi_{i\mu} + \phi_{i\mu}}{\sum_{i,j} \phi_{i\mu} + \phi_{j\mu} f_{ij}^{(n)}} \quad (6.6)$$

$$\Delta\lambda_{\mu}^{(n)} =$$

The error in the estimation of the μ th eigenvalue is obtained as follows:

1. First the components of the deviation matrix $f_{ij}^{(n)}$ are estimated. To do this, the fission matrix $F + f^{(n)}$ that is computed in each cycle is stored for all the cycles. The mean matrix F is obtained at the end of all the cycles by averaging $F + f^{(n)}$ over all the cycles. $f_{ij}^{(n)}$ are obtained by subtracting the ij^{th} components of $F + f^{(n)}$ from the corresponding components of F .
2. The mean fission matrix F generated in step 1 is also used to generate estimates of the eigenvalues and the direct (ϕ_{μ}) and adjoint ($+\phi_{\mu}$) eigenvectors as described in Section 6.1.2. Thus all quantities required for estimating the deviation in the eigenvalues in the n th cycle $\Delta\lambda_{\mu}^{(n)}$ are available. The deviation in the eigenvalues for each of the cycles may therefore be obtained by substituting $f_{ij}^{(n)}$ in step 1 and ϕ_{μ} and $+\phi_{\mu}$ in step 2 in the above equation.
3. The variance of $\Delta\lambda_{\mu}^{(n)}$ is estimated in the usual way (the mean is expected to be zero since the mean of $f_{ij}^{(n)}$ is zero by definition and $\Delta\lambda_{\mu}^{(n)}$ is linearly related to the $f_{ij}^{(n)}$), viz.,

$$\sigma^2 = \frac{1}{N-1} \sum_n [\Delta\lambda_{\mu}^{(n)}]^2 \quad (6.7)$$

where N is the number of cycles used for averaging.

4. The result is finally divided by the number of cycles N to get the variance of mean. The square root of this gives us the required error in the estimate of the eigenvalue.

While there is a cycle to cycle correlation in the fission source and this introduces a corresponding correlation in the estimates of k_{eff} and the error in the k_{eff} , this is not the case in the present method.

The reason is that individual matrix elements F_{ij} are estimated by tallying the number of fission neutrons generated in the i^{th} mesh due to fission neutrons starting from the j^{th} mesh and dividing by the total number of fission neutrons starting from the j^{th} mesh. Thus even if there are cycle to cycle correlations in the number of neutrons starting from the j^{th} mesh these are not reflected in the fission matrix generated. The only effect the iteration method has on the elements is that the most important ones are computed with the lowest error which is beneficial. The present process does cause correlations among different matrix elements within a cycle. However, since it is not assumed that these elements are independent in the above procedure for estimating errors in the eigenvalues, this has no consequence. Since tallying commences after the distribution has reached the fundamental mode, the deviation in the eigenvalues are not only independent, but also drawn (sampled) from the same population.

Storage of a large number of matrix elements may seem to pose a problem. These however need not be stored in the computer memory. It is enough that they are stored on a file. They are required to be accessed only once while calculating the deviations (the mean matrix can be computed during the cycles and not necessarily at the end of all cycles). If the fission matrix is approximately symmetric, the ϕ_{μ} and $+\phi_{\mu}$ eigenvectors are not expected to be very different and it may not be necessary to separately calculate $+\phi_{\mu}$.

6.2 Test Problem and Results

6.2.1 A Problem Description

The λ eigenvalues and eigenfunctions of a 3-D realistic PHWR model given by Judd and Rouben, 1981 are studied using proposed MC method. This test-problem consists of two radial fuel zones in the XY plane surrounded by reflector (Fig. 6.2). In the axial Z direction, the reactor extends up to 600 cm and has uniform material properties. There is no reflector in axial Z direction. The two-group cross-sections and other data for two fuel zones and reflector and the spatial discretization

scheme are exactly as given by Judd and Rouben. The cross sections are listed in Table 6.1. The neutron velocities in fast and thermal groups are 10^7 cm/s and 3×10^5 cm/s, respectively. The two group fission spectrum is χ_1 is 1 and χ_2 is 0. The spatial discretisation is carried out by using a total of 3240 meshes in XYZ geometry. Only one type of mesh structure (18 x 18 x 10) has been considered.

6.2.2 Results

6.2.1.1 Standard Benchmark (near-critical case)

The fundamental eigenvalue estimated by fission matrix is 1.003537 ± 0.000181 . To estimate the passive cycles for fission source convergence, Shannon entropy is estimated and is shown in Fig.

6.3. Shannon Entropy is defined as

$$H = - \sum_{i=1}^{\text{no.ofzones}} S(i) * \log_2 (S(i))$$

Where, $S(i)$ denotes the normalized source in the i^{th} zone and is given by the fraction of source particles starting from the i^{th} zone for the cycle under consideration.

MC cycles from -100 to 0 refer to passive cycles. It can be seen from the Fig. 6.3 that within 100 passive cycles, the Shannon entropy estimated by KINMC converges to the asymptotic value of entropy estimated by deterministic diffusion based code KINFIN. Shannon Entropy estimated by transport MC code PATMOC (Mallick et. al., 2012) agrees well with KINMC. A total of six dominant λ eigenvalues were calculated for the above model by the MC Method. All the computed lambda eigenvalues are given in Table 6.2. All the six λ values computed in these studies agree with those given by KINFIN Code by Singh et al., 2009. The λ eigenvalues computed by the MC method are in the agreement with reference values given by Modak and Gupta, 2007 and Verdu, 1994. The shapes of thermal flux in first, third and sixth alpha modes in mid XY plane of the PHWR model have been plotted and are shown in Figs. 6.4–6.7. The computational time for this simulation with I7 processor is about is about 60 minutes.

6.2.2.2 Standard Benchmark (deep sub-critical case)

A case study for estimation of λ eigenvalues for a highly sub-critical reactor was also performed. The PHWR test-case was modified to make it highly sub-critical by reducing the value of fission spectrum χ_1 from 1.0 to 0.7. The χ_2 was kept 0.0 as before. Six dominant λ modes for this highly sub-critical reactor are evaluated. The entire computed lambda eigenvalues are given in Table 6.3. The fundamental λ eigenvalue computed in these studies agrees with those given by KINFIN code by Singh et. al, 2009. The shapes of thermal flux in fundamental modes in mid XY plane of the PHWR model have been plotted and are shown in Fig. 6.8.

6.3 Conclusions

The study of higher modes is of interest in reactor statics as well as reactor kinetics. In recent years there have been efforts to obtain higher modes using Monte Carlo methods. The development of a MC algorithm, based on the diffusion theory model, for estimation of higher eigenvalues and eigenvectors has been discussed in this Chapter. The discussion includes a method based on first order perturbation theory to estimate variance in the eigenvalues for the higher modes. The algorithm has been implemented in the Space Time Kinetics MC Code KINMC. The algorithm was verified by comparing the higher eigenvalues and eigenvectors by MC Method with other deterministic methods for a 3D Benchmark. The fundamental and higher order eigenvalues obtained by the MC algorithm and that by deterministic codes are in good agreement.

The objective of this development was to have a simplified MC model to study some of the problems associated with calculation of higher modes using MC. One of the developments carried out in this regard is a method to estimate errors in the higher eigenvalues using perturbation theory.

	i^{th} mesh	Diffusion of the neutron in the left mesh from j^{th} mesh
	 fission	 Diffusion of the neutron in the down mesh from j^{th} mesh
Diffusion of neutron in the upward mesh	Diffusion of the neutron in the right mesh	

Fig. 6.1 Schematic representation of the Finite Difference Diffusion MC model for estimation of the Fission Matrix

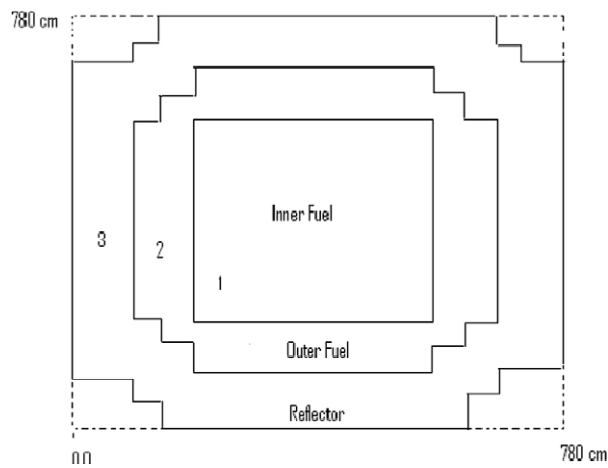


Fig. 6.2 XY representation of PHWR test reactor

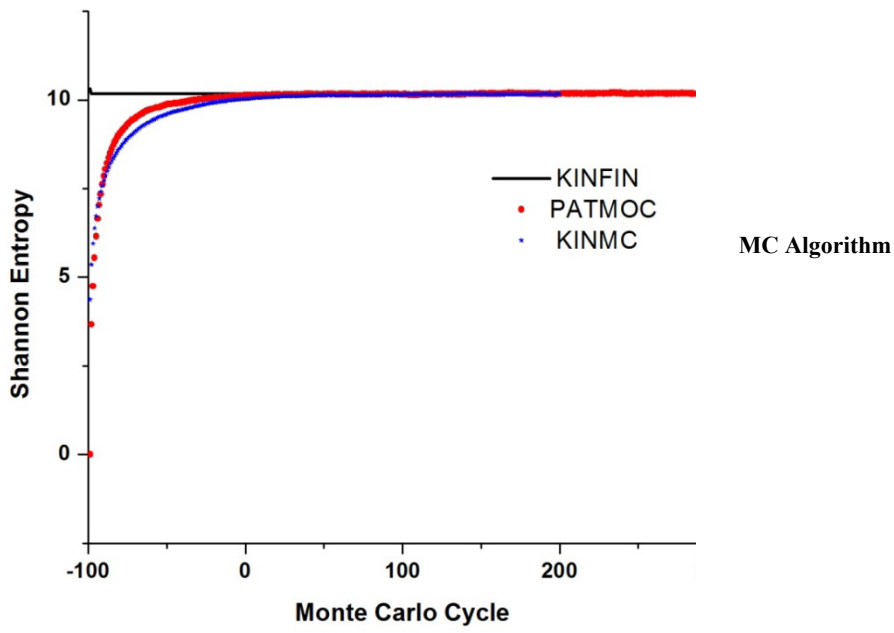


Fig 6.3 Shanon entropy with cycle for 3D PHWR Benchmark

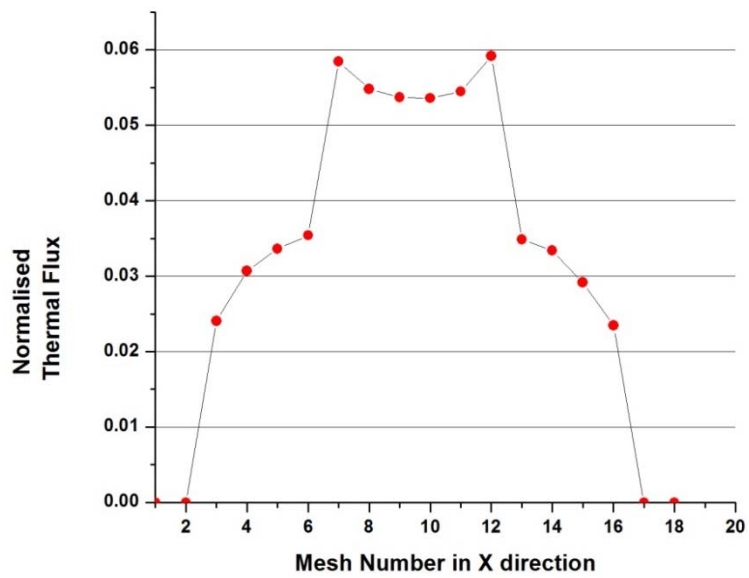


Fig. 6.4 Fundamental λ mode for PHWR Core (critical case) along X direction

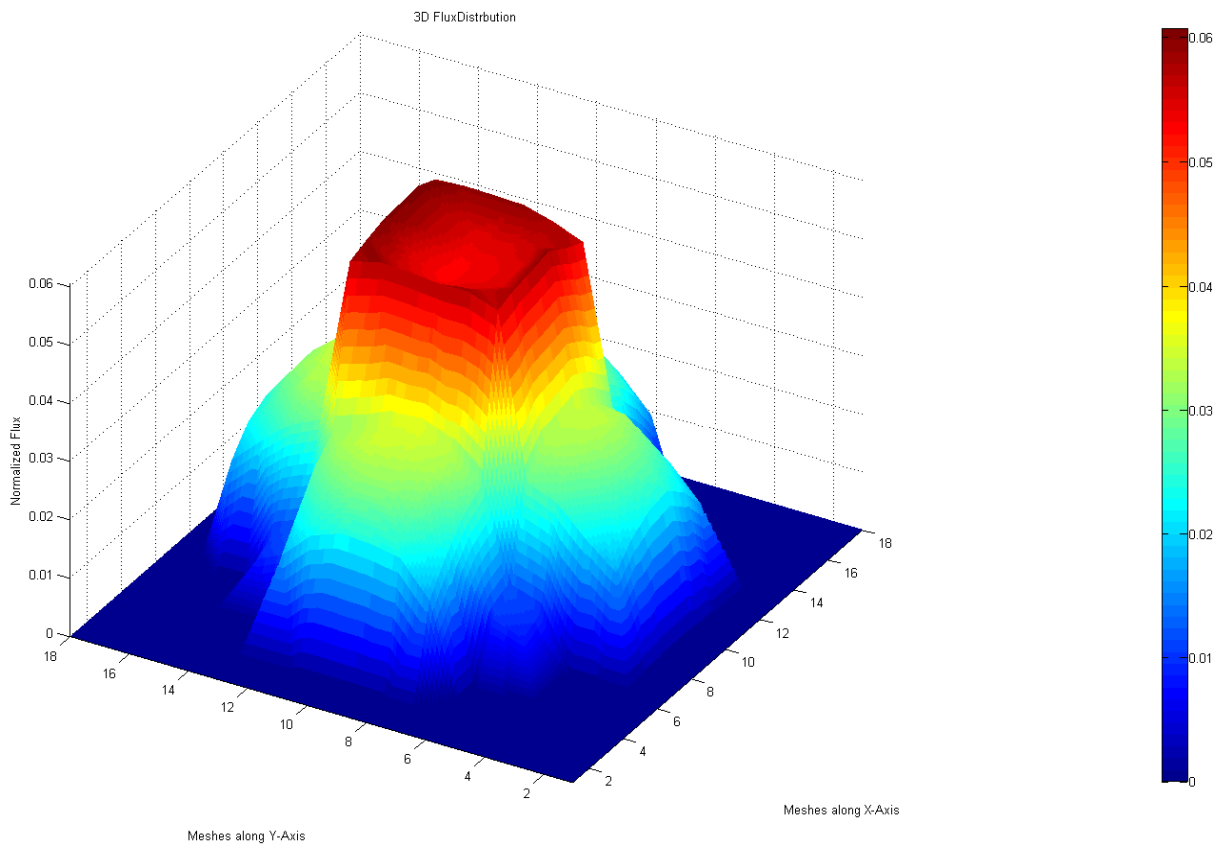


Fig. 6.5 Variation of thermal flux in fundamental λ mode obtained by MC algorithm for PHWR Core (near critical case)

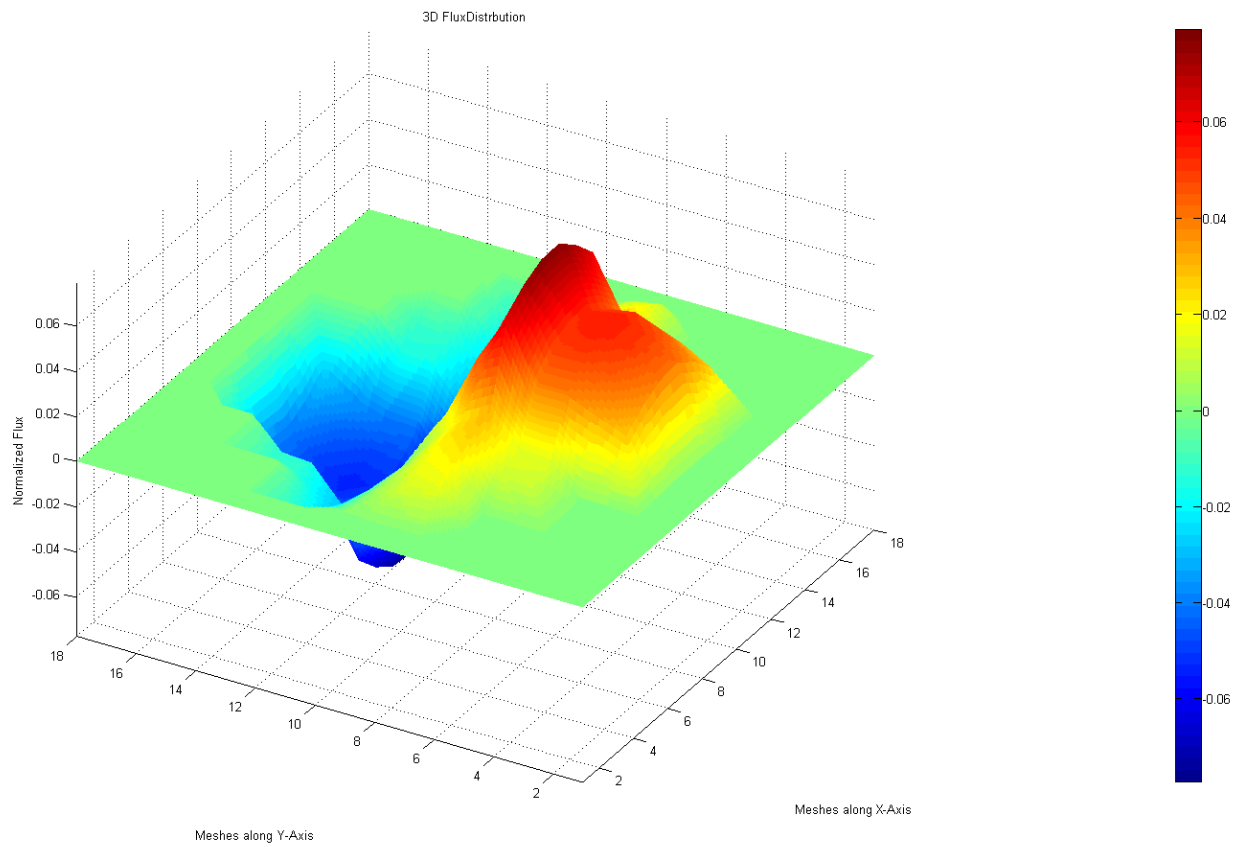


Fig. 6.6 Variation of thermal flux in second λ mode obtained by MC algorithm for PHWR Core (near critical case)

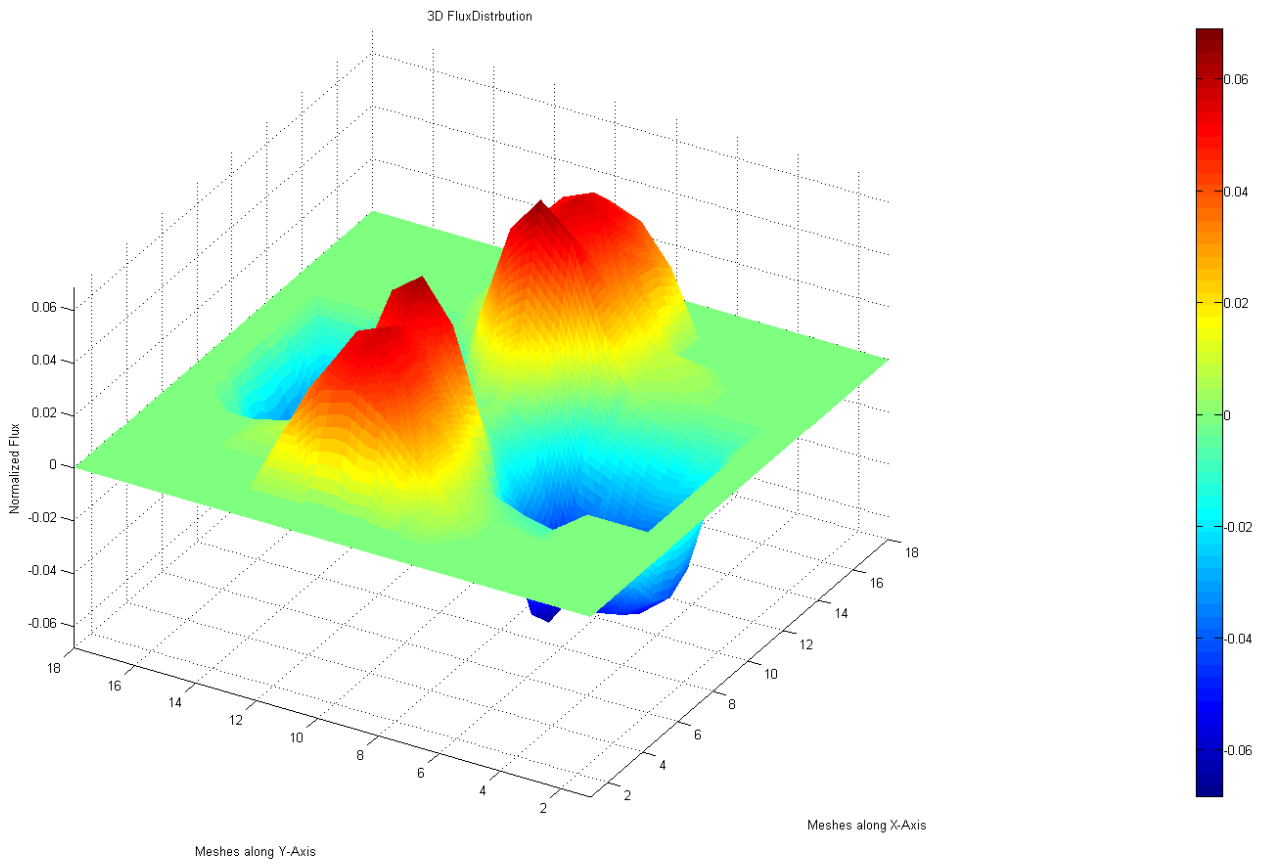


Fig. 6.7 Variation of thermal flux in sixth λ mode obtained by MC algorithm for PHWR Core (near critical case)

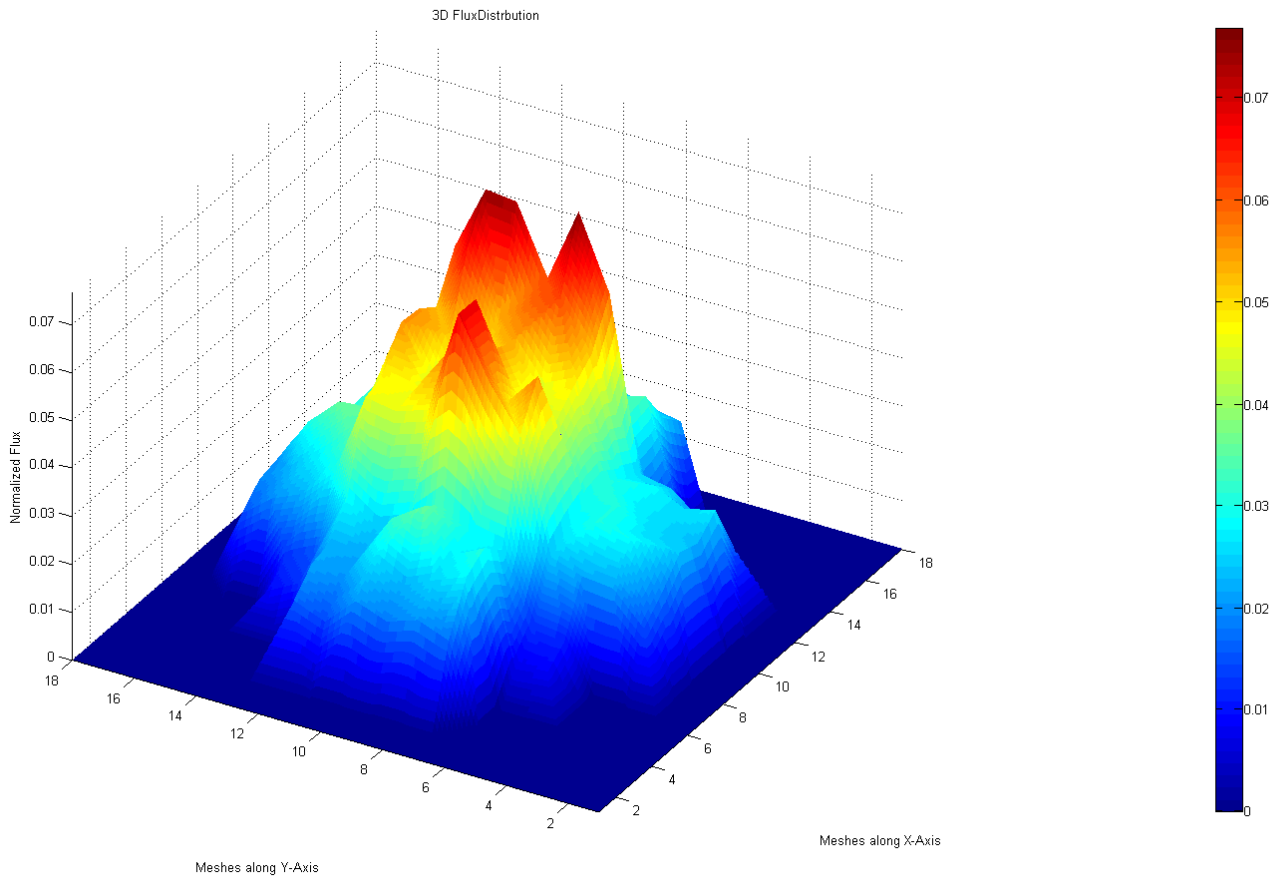


Fig. 6.8 Variation of thermal flux in fundamental λ mode obtained by MC algorithm for PHWR Core (deep subcritical case)

Table 6.1

Two group nuclear data Cross-section for PHWR test-case.

	Cross Section (cm^{-1})						
	D1	D2	$\nu \Sigma$	$\nu \Sigma$	Σ_{r1}	Σ_{r2}	$\Sigma_{s1 \rightarrow 2}$
Region No.							
1 (Core)	1.264E-00	9.3280E-01	0.000	4.5620E-03	8.1540E-03	4.1000E-03	7.3680E-03
2 (Region)	1.264E-00	9.3280E-01	0.000	4.7230E-03	8.1540E-03	4.0140E-03	7.3680E-03
3 (Region)	1.264E-00	8.6950E-01	0.000	0.0000E-00	1.0180E-02	2.1170E-04	1.0180E-02

Table 6.2**Values of λ in different modes for PHWR Core (near critical case)**

Mode No.	Stochastic Code	Deterministic Codes		
	MC	KINFIN	VERDU	MODAK's
1	1.0035370 ± 0.00034	1.00355	1.0035	1.0036
2	0.9899201 ± 0.00031	0.9901	0.9898	0.9901
3	0.9900391 ± 0.00031	0.9901	0.9898	0.9901
4	0.9733015 ± 0.00038	0.9732	0.9717	0.9732
5	0.9499810 ± 0.00020	0.9669	0.9657	
6	0.9664798 ± 0.00019	0.9649	0.9636	

Table 6.3**Values of λ in different modes for PHWR Core (deep subcritical case)**

Mode No.	λ	
	MC	KINFIN
1	0.7033128 ± 0.00028	0.702488
2	0.6940681 ± 0.00024	
3	0.6941299 ± 0.00026	
4	0.6821770 ± 0.00028	
5	0.6774225 ± 0.00025	
6	0.6771322 ± 0.00025	

Transport based Space Time Monte Carlo Code KINMC

In this Chapter the development of a multi-region multi-group MC Kinetics code is presented. Having tested the recipes on simpler models i.e. on Point Kinetics and Diffusion Theory MC Models as discussed in Chapters 3, 4 and 5, they are finally implemented in Transport theory MC resulting in the Space Time MC Kinetics Code KINMC, developed in the course of the research work.

KINMC code uses the Delta Neutron Tracking method (Leppanen et. al., 2010; Coleman, 1968) for neutron transport. The code explicitly treats the six groups of precursors and uses population and weight control of precursors and neutrons. It also employs the concept of mean number of secondaries in a collision for variance reduction. It has the capability of solving multi group space time transients. The efficacy of this code is tested by comparison with results of realistic space-time kinetics benchmarks involving multi-region reactors and energy dependence.

7.1 Methodology

7.1.1. The delta tracking algorithm

To begin with, the maximum total macroscopic cross-section of all materials in the geometry at the particle energy is found. If this is called as Σ_m , then the distance to the next collision (irrespective of the cross section of the medium in which the particle is located) is sampled using

$$s = -\frac{1}{\Sigma_m} \ln \xi (7.1)$$

If Σ_t is the actual cross section at the point of collision, the point is accepted as a collision site with a probability Σ_t/Σ_m and rejected with a probability $1-\Sigma_t/\Sigma_m$. In case of rejection, the neutron flight is continued from this point with the same direction and energy. The method requires the program to only determine the medium at any given point which is much simpler than ray tracing. The geometry modeling is done by using a geometry modeler based on combinatorial geometry logic.

Combinatorial geometry describes general three-dimensional (3-D) material configurations by considering unions, differences, and intersections of simple bodies such as spheres, boxes, cylinders, etc. This method allows space to be subdivided into unique zones of arbitrary shape. In the algorithm the task of assigning three-dimensional material configuration of the problem is accomplished in three distinct steps. First the regular body shapes to be used - rectangular parallelepiped, cylinder, sphere, etc. - their dimensions, location and orientation are defined. For a rectangular parallelepiped whose six plane surfaces are perpendicular to the co-ordinate axes, the minimum and maximum values of x, y and z coordinates of the planes perpendicular to the corresponding axis is specified. A sphere is defined by radius and co-ordinates of centre. For a right circular cylinder, the radius, the centre and the projection of its height on x, y and z axes are specified. After defining the necessary geometrical bodies, entire problem geometry is segmented into zones and materials are assigned to these zones.

7.1.2 Flow of the Simulation

At $t=0$ sec, for steady state distribution, start with thermal neutrons, fast neutrons and precursors at steady state. At the steady state condition, slowing down events and fission events are tallied along with that slowing down sites and fission sites are also stored. Total number of thermal neutron at the steady state is estimated by dividing the number of fission events with the product of the fission cross section and the velocity of the neutron in that group. Similarly, total number of fast neutrons at the steady state is estimated by dividing the number of slowing down events with the product of the slowing down cross section and the velocity of the neutron in that group. This way we can obtain the ratio of thermal to fast neutrons in the system at $t=0$ sec.

In the simulation, at $t=0$ sec, 10^5 thermal neutrons are considered and fast neutrons are considered in the ratio mentioned above. 10^5 fission sites are randomly selected from the stored fission sites which are the sites for the thermal neutrons at $t=0$ sec. Similarly, the randomly selected slowing down sites acts as sites for fast neutrons. In the problem domain having multiple regions denoted by

x, having different fission cross sections, $\Sigma_f(x)$, in each region the number of fission sites $n_2(x)$ are counted. Then the number of precursors in the steady state is given by,

$$C_{i0x} = \sum_x \frac{\beta_i}{\nu \Sigma_f(x) V / \lambda_i} n_2(x) \quad (7.2)$$

Where, summation is over total number of regions in the problem domain. β_i is the delayed neutron precursor of the i^{th} group, ν is the number neutrons produced per fission, Σ_f is the fission cross section, λ_i is the decay constant of the each precursor group, $n_2(x)$ is the thermal neutrons in the region x and V is the neutron velocity. Thus, for a population of 10^5 neutrons, there will be 10^9 precursors. This poses the first challenge population of 10^5 neutrons is probably the minimum that would be required to get any statistically meaningful results whereas modeling more than 10^9 precursors explicitly is virtually impossible on current desktops. Hence, we lump these precursors into a more manageable number say 10^5 and assign a weight

$$W_p = \sum_i \sum_x C_{i0x} / 10^5 \quad (7.3)$$

and the sites of these precursors are randomly selected from the fission sites. Now, all 10^5 precursors are allowed to decay in each time bin. Weights of the decayed and undecayed precursor are $\frac{1 - e^{-\lambda \Delta t}}{W_p}$ and $W_p e^{-\lambda \Delta t}$ respectively. Precursors which are produced by fission caused by neutrons (both by initial and delayed) are assigned weight of the decayed precursor i.e. $W_p (1 - e^{-\lambda \Delta t})$. The modeling of precursors is similar to what was done for Diffusion MC discussed in Chapter 4.

The neutrons are tracked one by one. In the case of space dependent transport MC simulations the next event is a collision event, for which the coordinates of the collision point are also sampled in addition to the time and a check is made whether the particle has leaked out of the system, in which case the history is terminated. Time of the event of the neutron is estimated by

$$t = -t_i + \frac{s}{v} \quad (7.4)$$

$$s = -\frac{1}{\Sigma_m} \ln \xi \quad (7.5)$$

Where, t_i is the initial time, s is the distance travelled to the collision, v is the velocity of the neutron, Σ_m is the maximum total cross section of all materials of the medium and ξ is a random number. The new (pseudo) collision point is obtained from the direction and the above sampled distance. The collision point is accepted as a real collision with a probability Σ_t/Σ_m . Else the point is rejected and treated as a pseudo collision. If the neutron lies within the time boundary and if the particle has suffered a pseudo collision then it is tracked in the same direction. If the event is recorded as a real collision, it is checked if the neutron has suffered scattering/ fission taking it into the same group or out of the group. The new weight of the neutron and its group (and direction from an isotropic distribution because both fission and scattering are assumed isotropic) are determined as per the prescription given in Eqs. (2.21- 2.24) using prompt ν for the number of secondaries in fission. If the neutron remains in the same group then the particle is tracked in the same group. If the neutron goes out of the energy group, then the particle is further tracked with the corresponding cross sections of that group.

New precursors are produced with probability proportional to $\nu\beta$. Delayed neutrons are then tracked in a similar way as the initial neutrons. To reduce the variance in power, the weight fluctuation of the neutron is controlled by restricting to lie within a window using splitting or Russian roulette.

If the neutron crosses the boundary of the time bin, it is stopped midway in its flight and therefore its position is moved back from its actual collision point to the position where the time bin boundary was crossed. Likewise all the thermal neutrons, fast neutrons and delayed neutrons are tracked. At the end of the each of the time boundary, weights of the all the neutrons that crossed the time boundary are tallied as follows to give the instantaneous neutron power at that time given by

$$P(t) = \varepsilon \sum_i w_i V_i \Sigma_{fi} \quad (7.6)$$

where ε is the energy per fission, w_i is the neutron weight of the i^{th} neutron, V_i is velocity of neutrons and Σ_{fi} is the fission cross section.

Neutron population control scheme is applied to reduce the variance in power and time for computation. At the time boundary thermal neutrons population are normalized to value of 10^5 and the weights of the precursors are readjusted to normalize their numbers to the value of 10^5

7.2 Test Problem and Results

7.2.1 1D Benchmark

The standard problem described by Sjenitzer and Hoogenboom, 2013 was analyzed to test the transport MC technique discussed in Section 7.1. This is a one velocity neutron transport problem within a rectangular material region of dimensions 10 x 12 x 24 cm placed in vacuum. The material cross sections and delayed neutron data are given in Table 7.1.

Initially i.e. at $t=0$, the system is in the critical state with the precursors in equilibrium with the neutrons. At $t=1$ sec, a positive step reactivity of 2.1 mk is introduced by decreasing Σ_a of the system from 0.5882 cm^{-1} to 0.5870 cm^{-1} . Σ_t of the system is kept constant by adjusting Σ_s . At $t=2$ sec, the system is brought back to the critical state.

The concentration of the precursors, as calculated using equation (7.2) for this system, is about 10^9 . The initial neutron and precursor spatial distributions (corresponding to the critical state) is generated from a criticality calculation and has an approximately cosine distribution as shown in Fig. 7.1. For 10^5 neutrons and 10^5 precursors are used for the simulation. The precursors are distributed in the 6 groups in ratio of β_i/β , where β_i is the delayed neutron fraction of the i^{th} group. The initial weight of the neutrons is taken to be 1.0, while that of the precursors is 10000. All the precursors are forced to decay within each time bin. The bin width considered for the simulation is adjusted to keep the weights of the delayed neutrons about the same as that of the initial neutrons (i.e. about 1.0) and works out to be ~ 0.01 sec. The steady state K_{eff} at $t=0$ sec estimated by MC is 0.9999 ± 0.0004 . The neutron power at the end of the time bin was estimated using equation (7.6).

The variation of neutron power with time obtained by simulation using transport MC is compared with the results of Hoogenboom et. al., 2013 in Fig. 7.2. The estimated absolute standard deviation

in the power is about 0.05. The computing time for the simulation with this level of precision is about 30 CPU hrs for a single processor. The figure also shows the results obtained using the deterministic point kinetics code. The close agreement with the two MC results shows that this benchmark is essentially a point kinetics problem and the flux distribution probably changes little or not at all with time. To test the capability of the MC method developed by us, it is important to test it on space- time problems that involve significant change in the flux shape during the transient. This is done in the next sub-section. Fig. 7.3 shows the variation of the weights of each group of the precursors with time. It indicates the variation of the precursor concentration with time.

7.2.2 TWIGL Transient Problem

The TWIGL reactor (Hoffman, 2013) is a 2D seed-and-blanket geometry 1.6 m along each side. It is surrounded by a vacuum and typically modeled with one-quarter or one-eighth core symmetry. The problem geometry is displayed in Figure 7.4. The problem specifies one delayed neutron group and cross sections for two energy groups within three different material regions: Regions 1 and 2 are seed regions while Region 3 is the blanket region. The transient was driven by varying the thermal absorption cross section in Region 1. Table 7.2 gives both the TWIGL reactor macroscopic cross sections by region and the kinetics parameters. The arrows in the table indicate the cross sections that are linearly-ramped or step-changed in the TWIGL transients.

TWIGL reactor is modeled with quarter-core symmetry with 100 square “assemblies” that are 32 cm on each side. These assemblies contained 4×4 cells that were 2 cm long and contained 25 square flat-source regions each. The transient evaluated is the TWIGL linear ramp. In this transient, the thermal absorption cross section in Region 1 is linearly decreased from 0.15 cm^{-1} to 0.1465 cm^{-1} over a 0.2 sec period. Table 7.3 gives the comparison of the steady state K_{eff} with estimated by KINMC with ANL05, 2005 and Reference Solution obtained by Time dependent MOC (Hoffman, 2013). It is found that the estimated K_{eff} values by KINMC are comparable with the deterministic values within the standard deviation. Fig. 7.5 gives the relative power estimated by KINMC. The

reference solution (Time dependent MOC) is also shown for the purpose of comparison and comparison is found to be good.

7.3 Conclusions

In this Chapter, development of a multi-region multi-group Transport based MC kinetics code KINMC is discussed. KINMC is based on Transport MC Method and has the capability of solving multi group space time transients. It explicitly treats the six groups of precursors and uses the concept of mean number of secondaries in a collision for variance reduction. The efficacy of this method is tested by comparison with results of realistic space-time kinetics benchmarks based on Transport theory methods involving multi-region reactors and energy dependence, Comparison of our results with these benchmarks show satisfactory agreement and thus provides a more complete validation of our methods. The capability of KINMC code will be extended to perform continuous energy space time simulations based on transport MC methods in future.

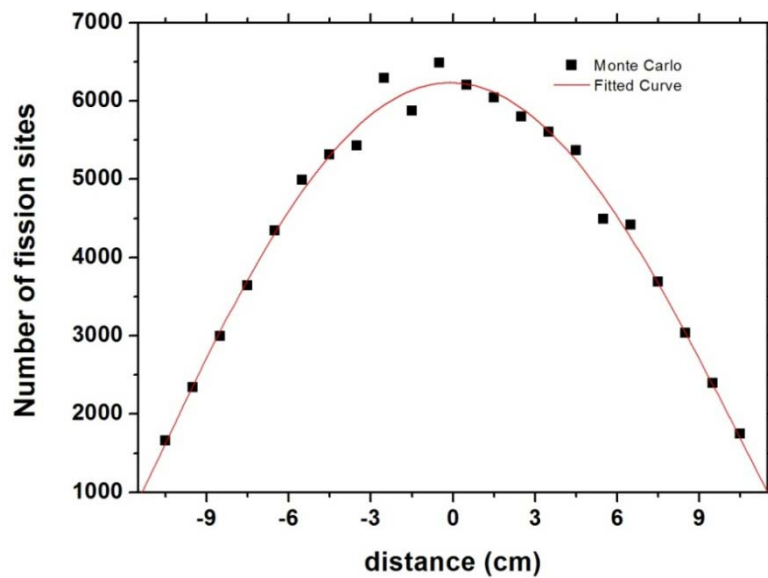


Fig. 7.1 Spatial distribution of the fission sites $t=0.0$ sec obtained for a critical state for Transport MC Benchmark.

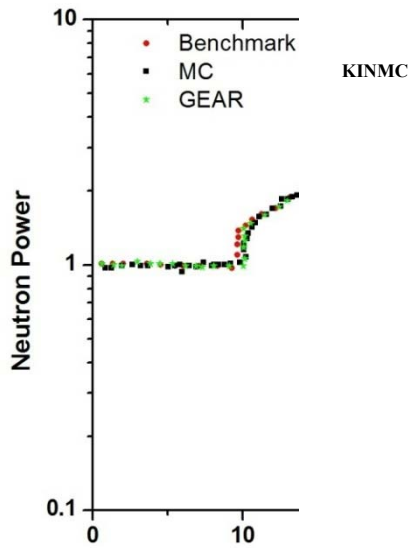


Fig. 7.2 A comparison of the neutron power estimated by MC with the Transport Monte Benchmark value. A step reactivity of 2.1 mk is added to the initially critical system at $t = 10$ sec and subsequently the system is brought back to the critical state at $t = 40$ sec.

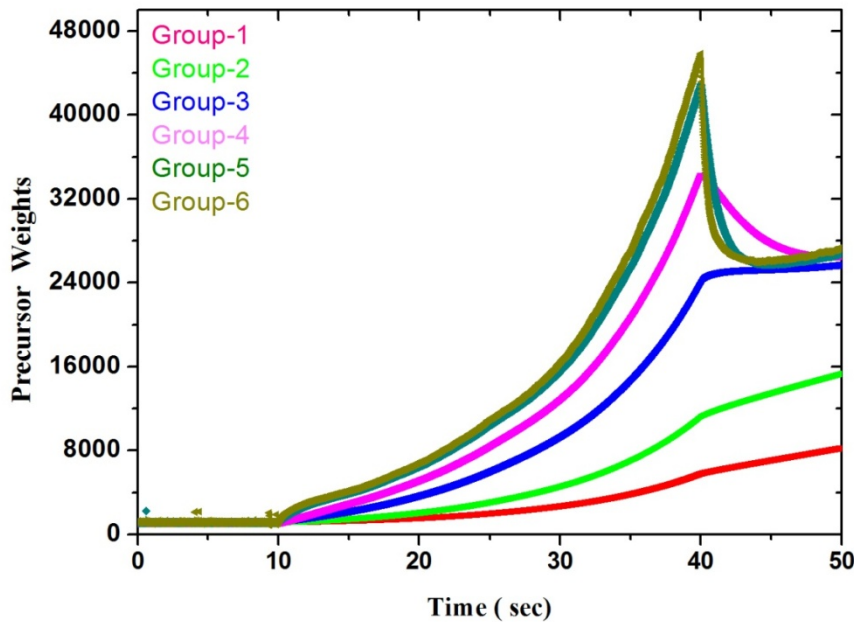


Fig. 7.3 Variation of the (6 group) precursor concentrations as a function of time in the Transport MC benchmark

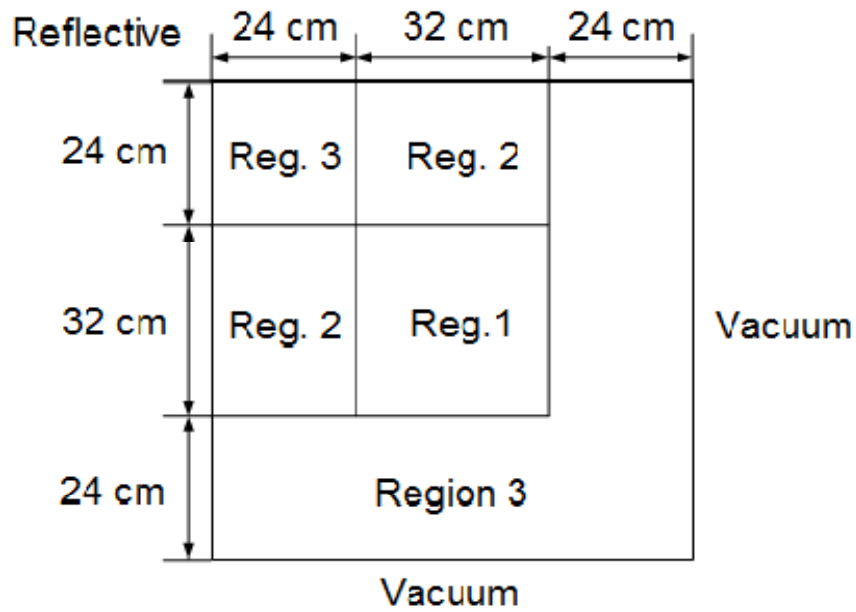


Fig. 7.4 Geometry for the south-east quadrant of TWIGL

β_i

Fig.7.5 Comparison of the Relative Power of TWIGL Transient estimated by KINMC with Reference Solution (Time Dependent Method of Characteristics)

Table7.1 Kinetics parameters and material cross sections of the Transport MC Benchmark

β_i	0.00026	0.001459	0.001288	0.002788	0.000877	0.000178
$\lambda_i(\text{sec}^{-1})$	0.0127	0.0317	0.1156	0.311	1.4	3.87
β_{eff}	0.00685					
$\lambda_{\text{avg}}(\text{sec}^{-1})$	0.0784					
ν	2.5					
$\Sigma_t(\text{cm}^{-1})$	1.0					
$\Sigma_f(\text{cm}^{-1})$	0.25					
$\Sigma_a(\text{cm}^{-1})$	0.5882					
$\Sigma_s(\text{cm}^{-1})$	0.4118					
V(cm/sec)	2.2×10^4					

Table 7.2 Cross Sections and kinetics parameters for the TWIGL Transients

Region	Group, Σ_g	Σ_a cm^{-1}	$\nu\Sigma_f$ cm^{-1}	Σ_t cm^{-1}	$\Sigma_{g \rightarrow g}$ cm^{-1}	$\Sigma_{g \rightarrow g'}$ cm^{-1}
1	1	0.01	0.007	0.238095	0.218095	0.01
	2	0.15 0.1465	0.2	0.83333 0.82983	0.68333	0.0
2	1	0.01	0.007	0.238095	0.218095	0.01
	2	0.15	0.2	0.83333	0.68333	0.0
3	1	0.08	0.003	0.25641	0.23841	0.01
	2	0.05	0.06	0.666667	0.616667	0.0

$$V_1 = 10^7 \text{ cm/sec}, V_2 = 2 \times 10^5 \text{ cm/sec}, \chi_1 = 1, \chi_2 = 0, \beta = 0.0075, \lambda = 0.08 \text{ sec}^{-1}$$

Table 7.3 Comparison of the steady state K-eff for TWIGL Benchmark

	Reference Solution (Hoffman, 2013)	ALN05 (ALN05,2005)	KINMC
K-eff	0.916051	0.916074	0.91619±0.00004

References:

- Alcouffe R. E. , Baker R. S. , Dahi J. A., S.A. Turner and Robert Ward** (2008), "PARTISN: A Time Dependent, Parallel Neutral Particle Code System," *Los Alamos National Laboratory, LA-UR-08-07258*.
- Anderson, S. L.** (1990), "Random Number Generators on Vector Supercomputers and other Advanced Architectures," *SIAM Review*, 32 (2), 221-251.
- ANL05** (2005), "The Numerical Nuclear Reactor for High Fidelity Integrated Simulation of Neutronic, Thermal-Hydraulic and Thermo-Mechanical Phenomena, Final Report," *International Nuclear Energy Research Initiative, Project Number 2002-010-K*.
- Ash M.** (1965), "Nuclear Reactor Kinetics", *New York N.Y. Mc Graw Hill Book Co.*
- Askew, J.R. et al.** (1966), "A general description of the lattice cell code WIMS", *Journal of the British Nuclear Energy Society*, 5.
- Balaraman V. and Trasi M. S.** (1981), "A Non Linear Reactor Dynamics Program", *BARC/I-639*.
- Bell and Glasstone** (1970), "Nuclear Reactor Theory", *Van Nostrand-Reinhold, New York*.
- Benjamin R. Betzler, Brian Kiedrowski C., William R. Martin & Forrest B. Brown**,(2018), "Calculating Alpha Eigenvalues and Eigenfunctions with a Markov Transition Rate Matrix Monte Carlo Method", *Nuclear Science and Engineering*, 192, 115-152.
- Betzler B. R., Martin W. R., Kiedrowski B. C., and Brown F. B.** (2014), "Calculating α Eigenvalues of One- Dimensional Media with Monte Carlo," *Journal of Computational and Theoretical Transport*, 43(1-7), 38-49.
- Betzler B. R., Kiedrowski B. C., Brown F. B., and Martin W. R.** (2015), "Calculating Infinite-medium α -eigenvalue Spectra with Monte Carlo using a Transition Rate Matrix Method," *Nuclear Engineering and Design*, 295, 639-644.
- Bielgiew F Alex** (1998), "Fundamentals of the Monte Carlo Method for Neutral and charged particle transport", *the University of Michigan, Department of Nuclear Engineering and Radiological Sciences*.
- Boer B. et al.** (2010), "Validation of the DALTON-THERMIX code system with transient analyses of the HTR-10 and application to the PBMR", *Nuclear Technology*, 170, 306, 2010.
- Booth T. E.** (2003), "Computing the higher K-Eigenfunctions by Monte Carlo Power Iteration", a conjecture, *Nucl. Sci. Eng.* 143, 291-300.
- Booth T. E.** (2006), "Power Iteration Method for the several largest Eigenvalues and Eigenfunctions", *Nucl. Sci. Eng.* 154, 48-62.
- Booth T .E. and Gubernatis J. E.** (2009), "Monte Carlo determination of multiple external Eigenpairs", *Phys. Rev. E* 80, 046704.
- Booth T.E.** (1981), "Exact Monte Carlo Solution of Elliptic Partial Differential Equations" *J. Comp Phys.* 39.

- Cacuci, D. G.** (2010), "Handbook of Nuclear Engineering", *Vol. 2: Reactor Design*, Springer.
- Carter J. C., Fischer G. J., Heames T. J., Macfarlane D.R., McNeal N. A. Sha W. T., Somnathan C. K., Youndahl,** (1970), "Sasia computer code for the analysis of fast Reactor Power and Flow Transients" ANL 7607.
- Carney, Sean E. Brown, Forrest B. Kiedrowski, Brian C. Martin, William R.** (2012), "Fission Matrix Capability for MCNP Monte Carlo," *Los Alamos National Laboratory Report LA-UR-12-24533*.
- Carney S.E., Brown F.B., Kiedrowski B.C., Martin W.R.** (2013), "Fission Matrix Capability for MCNP, Par I - Theory", *Proceedings of Mathematics & Computation 2013, Sun Valley, ID*.
- Carney S.E., Brown F.B., Kiedrowski B.C., Martin W.R.** (2013), "Fission Matrix Capability for MCNP, Part II - Applications", *Proceedings of Mathematics & Computation 2013, Sun Valley, ID*.
- Cho N. and Chang J.** (2009), "Some outstanding problems in neutron transport computation", *Nuclear Engineering and Technology, 41*.
- Coleman, W. A.** (1968), "Mathematical verification of a certain Monte Carlo sampling technique and applications of the technique to radiation transport problems", *Nuclear Science and Engineering. 32*.
- David L. Hetrick** (1993), "Dynamics of the Nuclear Reactors", The University of Chicago Press.
- Degweker S. B.** (2003), "Reactor Noise in Accelerator Driven Systems" *Annals of Nuclear Energy, 30, 223*.
- Degweker, S. B.** (1985), "BOXER3: a three dimensional integral transport code for PHWR supercell", *Report No. BARC-1295, Bhabha Atomic Research Centre, Bombay, India*.
- Denning R.S.** (1971), "One and two dimensional few group Kinetic Equations", *BMI-1911*.
- Duderstadt, J.J. and Hamilton, L.J.** (1976), "Nuclear Reactor Analysis", *Wiley, New York*.
- Dufek J., Gudowski W.** (2009), "Fission Matrix based Monte Carlo Criticality Calculations", *Annals of Nuclear Energy, 36[8], 1270-1275*.
- Dwivedi D. K., Gupta Anurag and Krishnani P. D.** (2014), "PATH: A computational code for Point kinetics Analysis with lumped Thermal-Hydraulic feedback", *RPDD/HTR/57*.
- E. D., Everett C. J.** (1959), "A practical manual on the Monte Carlo method for random walk problems".
- Glasstone S. and Edlund M. C.,** (1952), "The Elements of Nuclear Reactor Theory", *Newyork, N.Y.D.. Van Nostrand Co*.
- Glasstone Samuel and Edlund Milton C.** (1953), "Elements of Nuclear Reactor Theory" *Van Nostrand Reinhold Inc., U.S*.
- Gupta Anurag and Modak R. S.** (2013), "Efficient Monte Carlo Solutions of K-Eigenvalue problem using Sub Space Iteration Method", *ARP 2013- Advances in Reactor Physics, October 23-25*.

Gupta Anurag (2007), “Krylov Subspace Methods in Reactor Physics”, *Thesis, University of Mumbai*

Gupta Anurag (2012), "ARCH: A 3D Space–Time Analysis Code in Cartesian and Hexagonal Geometries", *Proc. of 19th National Symposium on Radiation Physics (NSRP–19)*, Dec 12–14, 2012, Mamallapuram, TN, India.

Gupta, H.C. (1991), "MONALI - Rev.1 A Monte Carlo code for analyzing fuel assemblies of nuclear reactors", *Report BARC-1543*.

Hammersley, M. and Handscomb, D. C. (1967), “Monte Carlo Methods”, *Methuen & Co. Ltd., London*.

Halsall M J (1991), “A review of the WIMS nuclear data library”, *Nuclear Energy*, 30, 285.

Hoffman A. J. (2013), “A time dependent Method of Characteristics Formulation with Time Derivative Propagation”, *Nuclear Engineering and Radiological Sciences, University of Michigan*.

Ikeda Hideaki and Takeda Toshikazu (2012), “ Development and verification of an efficient spatial neutron kinetics method for Reactivity Initiated Event Analysis”, *Journal of Nuclear Science and Technology, Volume 38, 2002 Issue 7*.

Initial MCNP6 Release Overview MCNP6 Version 1.0, *Los Alamos National Laboratory report LA-UR-13-22934*.

Jackson J. D. (1958), *Electromagnetic theory*. John Wiley & Sons.

Jagannathan, V., Jain, R. P. (2009), “EXCEL–A Combination of 1-D Transport and 2-D Diffusion Methods for Burn up Analysis of Hexagonal Lattice Assemblies”, *B.A.R.C. - Report under preparation*.

Jain V.K.andYadav R. D. S. (1989), “PointKineticsCodeMRIF-FUEL”, *B.A.R.C./I-969*.

Jain V.K.andGupta H. P. (1986), “Analysis of Super Delayed Critical Transients in Thermal Reactors using 2D and 3D Adiabatic and Improved Quasi static Models”, *Annals of Nuclear Energy* 13, 115.

Jain V. K. and Gupta H. P. (1986), “Analysis of Super Delayed Critical Transients in Thermal Reactors using 2-D and 3-D Adiabatic and improved Quasi static Models”, *Annals of Nuclear Energy, Vol. 3, No. 3, 115-124*.

Jerome Spanierand Ely M. Gelbard (1969), “Monte Carlo Principles and Neutron Transport Problems”, *Addison-Wesley Publishing Company*.

Judd R. A.and Rouben B. (1981), “Three Dimensional Kinetics Benchmark Problem in a Heavy Water Reactor”, *AECL-7236*.

Kaplan E. L.(1958), “Monte Carlo Methods for equilibrium solutions in neutron multiplication”, *UCRL-5275, Lawrence Livermore National Laboratory*.

Keepin, G. R. (1965), “Physics of Nuclear Kinetics”, *Addison-Wesley*.

Kophazi J. and Lathouwers D. (2012), "Three-dimensional Transport Calculation of Multiple Alpha Modes in Subcritical Systems," *Annals of Nuclear Energy*, vol. 50, pp. 167-174.

Kornreich D. E. and Parsons D. K. (2005), "Time-eigenvalue Calculations in Multi-region Cartesian Geometry Using Green's Functions," *Annals of Nuclear Energy*, vol. 32, 964-985.

Krishnani, P.D. (1992), "CLUB- A Multi group Transport Theory Code for Lattice Calculations of PHWR cells", *BARC/1992/E/017*.

Krishnani P. D. (1987), "Analysis of 2-D LWR Benchmarks with an Interface Current Method for Solving the Integral Transport Equation", *Ann. Nucl. Energy*, 14, 463.

Lathouwers D. (2003), "Iterative Computation of Time-eigenvalues of the Neutron Transport Equation," *Annals of Nuclear Energy*, vol. 30, 1793-1806.

Lawrence, R. D. (1986), "Progress in nodal methods for the solution of the neutron diffusion and transport equations", *Progress in Nuclear Energy, Volume 17, Issue 3*, 271-301.

Leppänen, J. et. al. (2015), "The Serpent Monte Carlo Code: Status, development and applications in 2013", *Annals of Nuclear Energy*, 82 142-150.

Leppanen. Jaakko (2010), "Performance of Woodcock delta-tracking in lattice physics applications using the Serpent Monte Carlo reactor physics burn up calculation code, *Annals of Nuclear Energy* 37:715-722, 2010.

Lewins, J.D. and Ngcobo, E.N.N. (1996), "Property Discontinuities in the Solution of Finite Difference Approximations to the Neutron Diffusion Equations", *Ann. Nucl. Energy Vol. 23, No. 1*, 29-34.

Lewis E. E. and Miller W. F. Jr. (1984), "Computational Methods of Neutron Transport", *John Wiley & Sons, New York*.

Lux, Ivan and Koblinger, Laszlo (1991), "Monte Carlo Transport Methods: Neutron and Photon Calculations", *CRC Press*.

Mallick Amod Kishore, Degweker S. B. and Krishnani P. D. (2014), "Fission Matrix and Acceleration Fission Source Convergence in Monte Carlo Neutron Transport Simulation", *RPDD/EP/99*.

Mallick Amod Kishore and Krishnani P D (2012), "PATMOC-1.0 (PARTicle Transport with MONte Carlo): A Multi-Region, Multi-Group, Isotropic, 1-Dimensional Neutron Criticality Code based on Monte Carlo Method", *RPDD/EP/65*.

Marleau G., Hébert A., Roy R. (2011), "A User Guide for DRAGON Version 4", *Institut de génie nucléaire, Département de génie mécanique, École Polytechnique de Montréal*.

Marsaglia, G. (1985), "A Current View of Random Number Generators", *Computing Science and Statistics: Proceedings of the XVIth Symposium on the Interface*, pp. 3-10.

McDonnell F. N., Baudouin A. P., Garvey P. M., and Luxat J. C. (1977), “CANDU Reactor Kinetics Benchmark Activity”, *Atomic Energy of Canada Limited, Chalk River Nuclear Laboratories, Chalk River, Ontario, Canada, Nuclear Science and Engineering: 64, Pages 95-105.*

MCUCode: (1982), *ProjectHomePage:* <http://mcuproject.ru/eabout.html>.

MCNPVersion 6.2, (2018), Release Notes, *Los Alamos National Laboratory report LA-UR-17-29981.*

MCNP (2003), “A General Monte Carlo N Particle Transport Code, Version 5”, *Volume 1: Overview and Theory, LA-UR-03-1987.*

Modak R. S. and Gupta Anurag (2007), “A scheme for the evaluation of the time Eigenvalues of nuclear reactor”, *Annals of Nuclear Energy 34, 213-221.*

Munoz-Cobo J. L. et al. (2001), “Sub-critical Reactivity Monitoring in Accelerator Driven Systems”, *Annals of Nuclear Energy, 28, 1519.*

Murthy K. P. N. (2000), “Monte Carlo Basics”, *ISRP-TD-3.*

Obaidurrahman, et.al.(2010), “ Development and validation of Coupled Dynamics Code”, *Nuclear Engineering and Technology, Vol. 42, 259-270.*

Ott, K.O. and Neuhold, R.J. (1985), “Introductory Nuclear Reactor Dynamics”, *American Nuclear Society, La Grange Park, IL, USA.*

Pal, L.(1958), "On the theory of stochastic processes in nuclear reactors", *II Nuovo Cimento 7 (Suppl.), 25-42.*

Paul K. Romano and Benoit Forget (2013), “Open MC Monte Carlo Particle Transport Code”, *Annals of Nuclear Energy 51, 274-281.*

Pazsit, Kitamura Y. Wright J. and Misawa T. (2005), “Calculation of the pulsed Feynman-Alpha Formulae and Their Experimental Verification,” *Annals of Nuclear Energy, 32, 986.*

Petit, O., Hugot, F.-X., Lee, Y.-K., Jouanne, C., Mazzolo. A. (2008), “TRIPOLI-4 Version 4 User Guide,” *Rapport CEA-R-6169.*

Pfeiffer W. (1971), "RTMODE and RZMODE - Two-Dimensional Computer Codes for Simulating Pulsed-Neutron Experiments,"*Tech. Rep. Gulf-GA-B10877, Gulf General Atomic.*

Pfeiffer W. (1972), "Computer Simulation of Pulsed-Neutron Experiments for the Fort St. Vrain HTGR,"*Tech. Rep. Gulf-GA-B10959, Gulf General Atomic.*

Podar R.S.and Trasi M.S.(1989), “An integrator for a system of stiff ordinary differential equations with application to Reactor-Kinetics Equations”, *B.A.R.C./I-581.*

Rana Y. S., Singh Arun and Degweker S. B. (2013), “Diffusion Theory Based Analogue Monte Carlo for Simulating Noise Experiments in Sub-critical Systems”, *Nuclear Science and Engg., 174, 245 – 263.*

Reuss Paul (2008), 'Neutron Physics', *Institut national des sciences et techniques nucleaires, France*.

Rineiski A. (1997), "KIN3D: A space time kinetics and perturbation theory module for TGV2 ", *CEA SPRC/LEPh, 97-203*.

Rusell L. F. (2014), "Simulation of Time Dependent Neutron Population for Reactor Physics Application using GEANT-4 Monte Carlo Toolkit", *Annals of Nuclear Energy, Volume 71, 451-461*.

Sadiku M.N.O., Akujuobi C.M., and Musa S.M. (2006), "Monte Carlo Analysis of Time Dependent Problems", *Southastcon Proceedings of the IEEE*.

Sanchez R. (1977), "Approximate Solutions of the Two-Dimensional Integral Transport Equation by Collision Probability Methods", *Nucl. Sci. Eng, 64, 384*.

Shayesteh M. and Shahriari M. (2009), "Calculation of time dependent Neutronics parameters using Monte Carlo Method", *Annals of Nuclear Energy 36, Pages 901-909*.

Singh Anmol. and Gupta H. P. (2013), "Point Reactor Kinetics Code-PEARL", *Proceedings of DAE-BRNS Symposium on Advances in Reactor Physics: Simulation Techniques and Analysis Methodologies (ARP-2013), October 23-25, 2013, BARC, INDIA*.

Singh K. P. (2013), "Theoretical developments and studies in the reactor physics of accelerator driven systems", *Homi Bhabha National Institute, Mumbai*.

Singh K. P., Modak R. S., Degweker S. B and Singh Kanchi (2009), " Iterative schemes for obtaining dominant alpha modes of the neutron diffusion equation", *Annals of Nuclear Energy, 36*.

Sjenitzer B. L. and Hoogenboom J. E. (2013), "Dynamic Monte Carlo Method for Nuclear Reactor Kinetic Calculations", *Nuclear Science and Engineering 175(1), 94-107*.

Sobol I. M. (1994), "A primer for the Monte Carlo Method", *CRC Press*.

Srivastava Argala and Degweker S. B. (2015), "Analytical Greens' Function Based Diffusion Monte Carlo with Transport Corrections", *Nuclear Science and Engineering, 179, 460-476*.

Srivastava Argala, Singh K. P. and Degweker S. B. (2018), "Monte Carlo Methods for Reactor Kinetic Simulations", *Nuclear Science and Engineering, 189, 152-170*.

Stacey W. M. (2001), "Nuclear Reactor Physics", *John Wiley & Sons, Inc*.

Stammler J. J. Rudi and Abbate J. Maximo (1983), "Method of Steady State Reactor Physics in Nuclear Design", *ISBN-13:978-0126633207*.

Stephen A. Dupree and Stanley K. Fraley (2001), 'A Monte Carlo Primer: A Practical Approach to Radiation Transport', *Kluwer Academic / Plenum Publishers, ISBN 0-036-48503-6*.

Sutton T. M. and Aviles, B. N. (1996), "Diffusion theory methods for spatial kinetics calculations," *Progress in Nuclear Energy, Vol. 30, No. 2, 119-182*.

- Szieberth Máté and Klujber Gergely** (2010), “Monte Carlo simulation of neutron noise measurements” *ADS benchmark CRP, 4th RCM, Mumbai, India*, 22-26.
- Trasi M. S., Suryanarayana P. V., Balraman V. and S.U. Kamat** (1976), “A Non Linear Reactor Dynamics Program, *BARC/I-442*.
- Urbatsch T. J.** (1995), “Iterative Acceleration Methods for Monte Carlo and Deterministic Criticality Calculation”, *LA-13052-T, Thesis UC-714*.
- Verdu et al.** (1994), “3-D lamda modes of neutron diffusion equation” *Annals Nucl Energy*, 21, 405.
- Villarino E.A., Stamm’ler R.J.J., Ferri A.A., Casal J.J.**(1992), “HELIOS: angularly dependent collision probabilities” *Nucl. Sci. Eng.* 112, 16–31.
- Wadell Jr., M.W. Dodds, H.L.**(1993), “A method for transient calculations”, *Proc. Of M & C Topical Meeting, Karlsruhe, Germany*, 633.
- Weaver Lynn E.** (1963), “System Analysis of Nuclear Dynamics”, *Rowmann and Littlefield Publishers*.
- Weinberg A. M. and Wigner E. P.** (1958), “The physical theory of neutron chain reactors”, *University of Chicago Press*.
- Wenner Michael and HaghghatAlireza** (2011), “A Fission Matrix Based Methodology for Achieving an Unbiased Solution for Eigenvalue Monte Carlo Simulations”, *Progress in Nuclear Science and Technology, Vol. 2*, 886-892.
- Williams, M. M. R.** (1974), “Random Processes in Nuclear Reactors”, Pergamon Press.
- X-5 Monte Carlo TeamMCNP** (2005), “AGeneralMonteCarloN-ParticleTransportCode”*Version 5, LA-UR-03-1987*.
- Yamamoto Toshihiro** (2011), “Applicability of non-analog Monte Carlo technique to reactor noise simulation”, *Annals of nuclear energy* 38, 647-655.
- Yamamoto Toshiro** (2011), “Higher order α Mode Eigenvalue Calculation by Monte Carlo Power Iteration”, *PNE, Vol. 2* , 826-835.
- Yamamoto T., Miyoshi Y.** (2003), “An algorithm of α and γ mode Eigenvalue calculations by Monte Carlo Method”, *Proc. 7th Int. Conf. on Nuclear Criticality Safety, ICNC 2003, Tokai Mura, Ibaraki, Japan Oct. 20-24, 2003, JAERI-Conf. 2003-019, Japan Atomic Energy Research Institute (JAERI)*.
- Yamoah S. et al.** (2013), “An accurate solution of point reactor neutron kinetics equations of multi-group of delayed neutrons”, *Annals of Nuclear Energy* 54, Pages 104–108.
- Yasinsky, J.B., Henry A.F.** (1965), “Some numerical experiments concerning space-time reactor kinetics behavior”, *Nucl. Sci. Eng.* 22, 171-181.

YuGwon Jo, Bumhee Cho, Nam Zin Cho (2016), “Nuclear Reactor Transient Analysis by continuous Energy Monte Carlo Calculation Based on Predictor Corrector Quasi-Static Method”, *Nuclear Science and Engineering* 83, 229-246.

Yun S., Kim J.W. and Cho N.Z. (2008) , “Monte Carlo Space Time Reactor Kinetics Methods and its verification with time dependent S_N method” , *International Conference on Physics of Reactors, Nuclear Power: A sustainable resource, Casino-Kursaal Conf. Center, Interlake, Switzerland, September 14-19.*

Zachary M. Prince, Jean C. Ragusa, Yaqi Wang (2016), “Implementation of the improved quastitaitc method in Rattlemak/Moose for time dependent Radiation Transport modeling”, *INC/CON-16-37879, US.*

Highlights

This thesis describes neutronic studies leading to the development of a time dependent Monte Carlo code, for use in time dependent situations such as pulsed neutron experiments and nuclear reactor transient analysis. Several new schemes have been proposed and developed to manage variance and computing time issues associated with MC based kinetics. These include measures for neutron and precursor population and weight control, forced decay of precursors without combining them together and the use of mean number of secondaries per collision. In this research work, the proposed new techniques are first applied to and tested in simpler models such as the Point Kinetics MC Model and the few group diffusion theory MC models, as it is easier to test new techniques in these simpler models. Moreover, since most space time kinetics benchmarks are based on few group diffusion equations solved by the finite difference method, the implementation in the diffusion theory MC model facilitates exact comparison with these benchmarks. A number of new developments in the theoretical basis of the diffusion MC model have been carried out. Application of Diffusion based MC has been extended for transient analysis and for the estimation of Higher Eigen modes. After testing the schemes (for reduction of variance / computing time) in these simpler models, they are implemented in a transport MC model and finally extended to the development of a multi-region multi-group MC kinetics code.